Chromatin and transcriptional regulators act in a cascade to establish a bilateral asymmetry of the *C. elegans* nervous system

by

Shunji Nakano

B.S., Biology
Nagoya University, 2001

Submitted to the Department of Biology in Partial Fulfillment of the Requirements for the Degree of

DOCTOR OF PHILOSOPHY

at the
MASSACHUSETTS INSTITUTE OF TECHNOLOGY

October 2010

Signature of author:_____
Shunji Nakano
October 31, 2010

Certified by:_____
H. Robert Horvitz
Professor of Biology
Thesis Supervisor

Accepted by:_____
Stephen P. Bell
Chair of the Graduate Committee
Department of Biology

Chromatin and transcriptional regulators act in a cascade to establish a bilateral asymmetry of the *C. elegans* nervous system

by

Shunji Nakano

Submitted to the Department of Biology in Partial Fulfillment
of the Requirements for the Degree of DOCTOR OF PHILOSOPHY

Abstract

Neuroanatomical bilateral asymmetry is a widespread feature in both vertebrates and invertebrates. Although mostly bilaterally symmetric, the nervous system of *Caenorhabditis elegans* displays bilateral asymmetry. Bilateral asymmetry in *C. elegans* arises in part from left-right asymmetric cell lineages. The single left-right unpaired MI neuron is normally generated from the right side of an otherwise left-right symmetric cell lineage that on the left gives rise to the e3D epithelial cell. We performed genetic screens and isolated mutants that displayed symmetry in this normally asymmetric cell lineage, with the MI neuron transformed into an e3D-like cell. We identified that a *C. elegans Otx* homeodomain protein CEH-36 and two basic helix-loop-helix proteins NGN-1 and HLH-2 promote the generation of the MI neuron and are required to establish the bilateral asymmetry in this cell lineage. We found that CEH-36 is asymmetrically expressed and is present in an MI precursor cell on the right but not in an e3D precursor cell on the left. This bilaterally asymmetric CEH-36 expression in turn promotes asymmetric NGN-1 and HLH-2 expression, leading to the generation of the MI neuron on the right side of the cell lineage. The *Otx/bHLH* transcriptional cascade is evolutionarily conserved, and our results suggest that this transcriptional cascade plays a role in establishing neuroanatomical bilateral asymmetry in other animals. We also discovered that a mutation in a replication-dependent histone H3 gene *his-9* transforms the MI neuron into an e3D-like cell. This mutant allele of *his-9* causes an altered-function activity that is predicted to impair the interaction of the mutant HIS-9 protein with another histone H3 molecule and inhibit the formation of a histone H3-H4 tetramer. Replication-dependent histones H3-H4 are deposited onto replicating DNA by the heterotrimeric protein complex CAF-1. We observed that loss of function of each of three genes encoding members of the *C. elegans* CAF-1 complex transformed MI into an e3D-like cell. We propose that CAF-1-mediated nucleosome formation is impaired by the presence of mutant HIS-9 proteins that are unable to form the histone H3-H4 heterotetramer. We also found that two histone-modifying enzymes SET-16 and UTX-1 are required to establish the bilateral asymmetry in this cell lineage. *set-16* encodes a protein homologous to the human MLL protein, a histone methyltransferase specific for histone H3 lysine 4, and *utx-1* encodes a protein homologous to human UTX protein, a histone demethylase specific for histone H3 lysine 27. Our results reveal a novel mechanism of establishing neuroanatomical bilateral asymmetry and suggest that nucleosome formation and histone H3 modification are required to establish this bilateral asymmetry.

Thesis Advisor: H. Robert Horvitz
Title: Professor of Biology

Acknowledgements

None of the work in this thesis would have been possible without the guidance from my advisor, Bob Horvitz. The past five years of my scientific life in the Horvitz lab have been truly precious time for me, as he allowed me to drive works purely by my scientific interests. I'd like to thank Bob for having me in his lab and giving me such a wonderful time in his lab that I would not be able to enjoy elsewhere. I also thank my committee members over the years, Peter Reddien, Chris Kaiser, Mary-Lou Pardue, Richard Hynes and Piali Sengupta for their suggestions and advices.

I am grateful to my undergraduate advisor, Kunihiro Matsumoto, for stimulating my interests in biology and genetics. I also like to thank Peter Zuber and Michiko Nakano for allowing me to explore projects independently during my time in their lab as a research technician. I am grateful to many wonderful scientists I met during this period of time, Alan Grossman, Dick Brennan, Rich Gourse, and Richard Losick. In particular, I am indebted to Alan Grossman for encouraging and supporting me, and without him I would not be able to join MIT.

I thank the past and present members of the Horvitz lab, and in particular Ron Ellis for laying the foundation of the work in this thesis, Brendan Galvin for guiding me during my rotation and supporting me when I was getting started, Niels Ringstad, Hillel Schwartz, Erik Andersen, Daniel Denning, Ezeke Alvarez-Saavedra, Kostas Boulias, David Harris, Adam Saffer and Nick Paquin for their support and discussions. I also enjoyed numerous Japanese conversations with Takashi Hirose. I have been fortunate to have Nikhil Bhatla as my baymate and friend, and I thank him for discussions about science and life. I also thank Na An, Beth Castor, Elissa Murphy, Tove Ljungars and Rita Droste for their technical support and Nick Anisimov for his administrative help.

Haruhiko Kohno accompanied me to various local cheap restaurants. I have been amazed by the similarity of the values we grew and lessons we learned from conducting science, despite the fact that we have been engaged in very different areas of science.

I thank my parents, my brothers and sisters for supporting me, allowing me to pursue my interest and redirecting me when I was lost. I have been always encouraged by the words and memory of my grandmother, Kazuko Matsubara. Without her guidance and education, I would not be able to take the path I have been taking.

Finally, I thank Mina Kato for her support, patience and having me realize the joy of a life outside the lab.

Table of contents

Chapter I

Introduction

Introduction

Lateralization of human brain function

Bilateral asymmetry of brain function is a widespread feature of humans and other animals. The discovery of lateralized human brain function came from Broca's observations on a patient named "Tan," who was not able to produce any recognizable words or phrases but could only produce a single repetitive syllable "tan." In Tan's autopsy, a lesion was found on the left frontal lobe (Broca 1865; Berker et al. 1986). Broca's careful documentation suggested the connection between speech and the inferior frontal gyrus of the left hemisphere.

That function of human brain is lateralized was further strengthened by the pioneering experiments on patients with split brains (Gazzaniga 2005). Split-brain patients are patients who have undergone corpus callosotomy, a severing of a large part of the corpus callosom that connects the two hemispheres of the brain, as a treatment for severe epilepsy (Van Wagenen and Herren 1940). Studies of the split-brain patients thus allowed researchers to gain insights into hemispheric differences and functional laterality, including the dominance of the left hemisphere for language and speech (Milner 1962).

Lateralized behaviors in vertebrates

Lateralized behaviors are observed in many vertebrate species, including birds, amphibians and fish (Bisazza et al. 1998). A variety of species show lateralized behavior

in response to predators. For example, toads are more likely to elicit escape responses when a simulated predator is presented onto their left monocular field than when it is introduced into their right monocular field (Lippolis et al. 2002). Similarly, fish display a preference in positioning themselves to inspect an image of a predator on its right side (De Santi et al. 2001). Aggressive responses are also strongly lateralized. Lizards and toads direct more aggressive responses to conspecifics on their left side than they do to those on their right side (Robins et al. 1998; Hews and Worthington 2001). Likewise, adult zebrafish preferentially uses their right eye when approaching prey, and when presented with two equivalent targets they prefer to attack the one on the right (Miklosi and Andrew 1999; Miklosi et al. 2001).

Structural asymmetries of vertebrate nervous system

Structural asymmetry is also a widespread feature in the nervous system. The human brain displays several anatomical asymmetries. The most prominent aspects of structural asymmetry are the size and position of the frontal and the occipital petalia: the left occipital pole is frequently wider and protrudes further posteriorly than the right, and the right frontal area is often wider and protrudes further anteriorly than the left (LeMay 1976). Other structural asymmetries in the human brain include the size of Heschl's gyrus, which houses the primary auditory cortex, with the left Heschl's gyrus larger than that on the right (Penhune et al. 1996).

Structural asymmetry is also observed in other vertebrate species. The habenulae are dorsal diencephalic nuclei that display bilateral asymmetry in many vertebrate

species. The habenulae are part of an evolutionarily conserved limbic-system conduction pathway that connects telencephalic nuclei to the interpeduncular nuclei of the midbrain (Sutherland 1982). The habenulae display bilateral asymmetry in size and sometimes also in neuronal organization and connectivity in most vertebrate species thus far studied (Concha and Wilson 2001), including zebrafish (Concha et al. 2000), frog (Braitenberg and Kemali 1970) and lizard (Engbretson et al. 1981). In zebrafish, the habenulae show bilateral asymmetry in neuronal organization and connectivity: the zebrafish habenular nuclei can be subdivided into medial and lateral subnuclei. The lateral subnucleus is substantially larger than the medial subnucleus on the left, whereas the medial subnucleus is larger than the lateral subnucleus on the right (Aizawa et al. 2005; Gamse et al. 2005). There is also bilateral asymmetry in connectivity in the habenula, as manifested by their innervations to the interpeduncular nucleus in the midbrain: axons from the left habenula predominantly innervate the dorsal interpeduncular nucleus, whereas those from the right habenula predominantly project to the ventral interpeduncular nucleus (Aizawa et al. 2005).

Relationship between functional and structural asymmetries

Little has been established as to whether functional asymmetry is associated with anatomical asymmetry. On one hand, Geschwind and Levitsky reported that the planum temporale, the region known to be important for language functions, display anatomical asymmetry, with the left planum temporale larger than that on the right in two-thirds of individuals (Geschwind and Levitsky 1968). Given the left-hemisphere dominance for

language functions, this observation indicated a possible relationship between anatomical asymmetry and functional asymmetry. On the other hand, Watson (1836) showed that individuals with *situs inversus,* a condition in which asymmetries of all thoracic and abdominal organs and at least some brain anatomy are reversed, are no more left-handed than the rest of the population.

A recent study of zebrafish gave insight into the relationship between structural and functional asymmetries in the brain. Barth and colleagues isolated a *frequent situs inversus (fsi)* mutant line of zebrafish that shows reversed asymmetry of viscera and neural structures, including that of habenula nuclei (Barth et al. 2005). By comparing the lateralized behaviors of *fsi* fish with those of wild-type animals, they discovered that laterality of some behaviors, including approaching a target to bite, was reversed in *fsi* mutant animals, suggesting that these behaviors are influenced by the neuroanatomical asymmetry. By contrast, laterality of other behaviors was unaffected in *fsi* animals. It remains to be determined whether these behaviors are regulated by structural asymmetries that are not affected in *fsi* mutants or are regulated independently of anatomical asymmetry. The discovery of concordant reversal of neuroanatomical and behavioral asymmetry highlights the importance of understanding developmental mechanisms by which bilateral asymmetries in nervous systems are established.

Developmental mechanisms that establish bilateral asymmetries in vertebrates

The nodal signaling pathway establishes bilateral asymmetry of visceral organs

Studies over the last decade have led to the identification of the role of cilia in determining bilateral asymmetry of visceral organs in vertebrate embryos (Levin 2005; Raya and Izpisua Belmonte 2006; Shiratori and Hamada 2006). The first observation that suggested the link between cilia and left-right determination of viscera came from the discovery of Kartagener syndrome. Patients with Kartagener syndrome show *situs inversus* and display the loss of motility of respiratory cilia and sperm flagella (Afzelius 1976). Respiratory cilia and sperm flagella of Kartagener patients were found to lack dynein arms. Subsequently, it has been observed that the *iv* mutant mouse, which displays defects in left-right patterning, also carries a mutation in one of the dynein genes (Supp et al. 1997). These observations led to the discovery that monocilia present in the mouse node, a transient midline structure located at the anterior tip of the primitive streak, rotate and generate a leftward flow of extra-embryonic fluid in the node (Nonaka et al. 1998) and that various mouse mutants in which this leftward fluid flow, referred to as nodal flow, is no longer present as a result of the immotile cilia display abnormal left-right patterning (Nonaka et al. 1998; Marszalek et al. 1999; Okada et al. 1999; Supp et al. 1999; Murcia et al. 2000). Moreover, reversal of the direction of nodal flow by the imposition of an artificial flow causes the reversal of left-right patterning (Nonaka et al. 2002). These observations demonstrate that nodal flow is important in directing subsequent left-right patterning events in mouse embryos.

The role of nodal flow in left-right patterning appears to be conserved in other vertebrate species. In rabbit embryos, monociliated cells are present in the posterior notochordal plate, and a leftward fluid flow is detectable just anterior to Hensen's node (Okada et al. 2005). In zebrafish, monocilated cells are present in the Kupffer's vesicle, a

structure equivalent to the mouse node, and it has been shown that these ciliated cells rotate and generate a leftward fluid flow (Essner et al. 2005; Kramer-Zucker et al. 2005; Okada et al. 2005). Reduction or absence of this flow results in the disruption of left-right patterning, suggesting that the role of nodal flow in left-right patterning is evolutionarily conserved in vertebrate species.

Nodal flow localizes a morphogen or morphogens asymmetrically around the node. This asymmetry is then transferred to asymmetric gene expressions in the lateral plate mesoderm, in which the gene *nodal*, a member of the transforming growth factor-β (TGF-β) family, is expressed exclusively on the left (Levin et al. 1995; Collignon et al. 1996). Establishment of left-sided *nodal* expression in the lateral plate mesoderm requires a complex regulatory network composed of both positive and negative regulators, including other TGF-β signals (Hamada et al. 2002): positive regulators include *nodal* itself (Lowe et al. 2001) and *GDF1* (Rankin et al. 2000), whereas *lefty-1* and *lefty-2* , expression of which are negatively regulated by *nodal*, exert negative effects on *nodal* expression (Meno et al. 1999; Meno et al. 2001). The concerted actions of these positive and negative regulatory loops establish the left-right asymmetry of *nodal* expression in the lateral plate mesoderm.

The left-sided expression of *nodal* in turn induces asymmetric expression of its downstream genes, including the homeodomain transcription factor *pitx2* (Piedra et al. 1998; Ryan et al. 1998; St. Amand et al. 1998; Yoshioka et al. 1998). This asymmetric expression of *pitx2* is maintained until later in development and is evident in the primodia of asymmetrical organs, such as the heart, lung and gut. Mutant mice lacking the *pitx2* gene were generated, and it was observed that whereas murine lungs normally display

bilateral asymmetry in the numbers of lobes, with a single lobe on the left and four lobes on the right, *pitx2* mutant mouse show right pulmonary isomerism, with both lungs displaying an apparent right lobular pattern (Kitamura et al. 1999; Lin et al. 1999; Lu et al. 1999), suggesting that *pitx2* drives bilaterally asymmetric organogenesis.

Developmental mechanisms that establishes bilateral asymmetry of vertebrate nervous systems

Despite the substantial knowledge of the developmental mechanisms that establish the bilateral asymmetry of visceral organs, little is known about the molecular basis of nervous system bilateral asymmetry in vertebrates. Studies focusing on the zebrafish habenula, however, have provided some insight into this problem.

The developing dorsal diencephalon of zebrafish expresses several components of the *nodal* signaling pathway, including the *nodal* ligand and the transcription factor *pitx2* (Concha et al. 2000; Liang et al. 2000). In embryos in which *nodal* signaling is activated or inactivated bilaterally, the directionality of the habenular asymmetries, including the size of medial and lateral subnuclei and connectivity to the interpeduncular nuclei, are randomized, but the asymmetries are still present (Concha et al. 2000; Aizawa et al. 2005), indicating that the *nodal* signaling pathway is not required for generating asymmetry itself but rather for superimposing laterality on such asymmetry.

A recent study suggests that the bilateral asymmetry of the size of the habenular subnuclei is generated by an asymmetry in the timing of neurogenesis (Aizawa et al. 2007). As described above, in zebrafish the medial habenular subnuclei are larger than

the lateral subnuclei on the right, while the lateral subnuclei are lager than the medial subnuclei on the left (Aizawa et al. 2005). It was observed that neural precursors for the lateral subnuclei are born at an earlier stage than those for the medial subnuclei, leading to the hypothesis that left-right differences in the ratio of lateral and medial subnuclei involve asymmetry in the timing of the activation of neurogenesis on the two sides (Aizawa et al. 2007). Consistent with this hypothesis, alteration of the timing of neurogenesis by means of genetic hyperactivation and repression of Notch signaling results in the loss of bilateral asymmetry in the relative sizes of the habenular subnuclei.

Abnormal brain asymmetries and disease

Abnormality in brain asymmetry has been implicated in several neuropathologies. Reduced asymmetry in the size of the planum temporale has been reported in patients with schizophrenia (Rossi et al. 1992; Petty et al. 1995), although there are controversial studies reporting normal planar anatomical asymmetry in patients with schizophrenia (Kulynych et al. 1995; Frangou et al. 1997). A functional study using fMRI reports the loss of functional language lateralization in patients with schizophrenia (Li et al. 2007), supporting the notion that schizophrenia is associated with abnormal brain asymmetry. Likewise, patients with persistent developmental stuttering display reduced asymmetry in the Heschl's gyrus (Jancke et al. 2004). In addition, reduced or reversed asymmetry in the planum temporale has been observed in subjects with developmental dyslexia, a highly heritable disorder manifested by a specific impairment of reading ability (Hynd et al. 1990; Larsen et al. 1990). Linkage studies identify at least nine regions that are likely to

harbor candidate dyslexia susceptibility genes (Scerri and Schulte-Korne 2010). It remains to be determined whether these genes are required to establish structural bilateral asymmetry in the brain.

Functional asymmetries of the *C. elegans* nervous system

The *C. elegans* nervous system exhibits functional asymmetries in two pairs of left-right symmetrical neurons, the ASE and the AWC neurons (reviewed in Hobert et al. 2002).

Functional lateralization of the ASE neurons

The left and right ASE gustatory neurons (ASEL and ASER) are structurally symmetric in a number of features, including the location of their nuclei, axodendritic morphology, morphology of specialized sensory endings and synaptic partners (Ward et al. 1975; White et al. 1986). Although anatomically symmetric, the left and right ASE neurons display marked asymmetry in their functions and detect different sets of chemoattractants (Pierce-Shimomura et al. 2001; Ortiz et al. 2009). For example, ASEL primarily senses sodium and magnesium, whereas ASER primarily senses chloride and potassium (Pierce-Shimomura et al. 2001). This functional asymmetry is thought to be important to discriminate different salt cues: animals can chemotax toward a salt in a saturating level of another salt if the two salts are sensed by distinct ASE neurons, whereas they cannot do so if the two salts are sensed by a same ASE neuron (Pierce-Shimomura et al. 2001; Ortiz et al. 2009).

The ASE neurons display bilateral asymmetry in their patterns of gene expression. For example, the putative receptor-type transmembrane guanylyl cyclase genes *gcy-6, gcy-7* and *gcy-14* are expressed in ASEL but not in ASER, whereas the guanylyl cyclase genes *gcy-1, gcy-5* and *gcy-22* are expressed in ASER but not in ASEL (Yu et al. 1997; Ortiz et al. 2006). Mutants for some of these genes have been isolated and shown to be defective in chemotaxis to salts specific to an ASE neuron in which these genes are expressed: for example, mutants for *gcy-1,* which is normally expressed in ASER, are defective in chemotaxis to ASER-sensed potassium but not to ASEL-sensed sodium or magnesium, while mutants for *gcy-14*, which is normally expressed in ASEL, are defective in chemotaxis to ASEL-sensed sodium but not to ASER-sensed chloride, suggesting that asymmetric expression of these guanylyl cyclase genes is a molecular basis for the lateralized function of the ASE neurons.

Developmental mechanism that establishes the ASE bilateral asymmetry

The establishment of the ASE bilateral asymmetry occurs after the generation of the two post-mitotic ASE cells. The two ASE neurons are initially born with similar states, with both cells expressing ASEL- and ASER-specific genes, and this symmetry persists until an early larval stage (Johnston et al. 2005). Thus, the ASEL and ASER neurons are generated with a largely symmetrical, hybrid ASEL/ASER precursor fate, and during later development each ASE cell adopts a bilaterally asymmetric fate.

Genetic screens have identified genes required to establish the ASE bilateral asymmetry. The developmental mechanism that establishes the ASE bilateral asymmetry

involves a regulatory network composed of multiple transcription factors and a microRNA. At the core of this pathway are the C2H2 zinc-finger transcription factor DIE-1, the NKX-type homeobox protein COG-1 and the microRNA *lsy-6* (Chang et al. 2003; Johnston and Hobert 2003; Chang et al. 2004). These factors form a feedback loop in which *die-1* promotes expression of *lsy-6,* which inhibits translation of *cog-1,* which inhibits expression of *die-1*. It has been proposed that *die-1* is likely to be the output regulator of the loop and that the activity of DIE-1 determines whether each ASE cell adopts one of two mutually exclusive states, the ASEL or ASER fate (Johnston et al. 2005): in ASEL, *lsy-6* is active and downregulates *cog-1,* which results in activation of *die-1* function, whereas in ASER, *lsy-6* is inactive, and hence *cog-1* is active, which results in inactivation of *die-1* function. Although this feedback circuit is required for establishing the ASE bilateral asymmetry and explains how the two ASE neurons adopt distinct fates, a symmetry-breaking event that impinges upon the regulatory feedback loop to establish the bilateral asymmetry remains to be determined.

Factors acting downstream of this feedback loop have also been isolated. The Lim homeobox gene *lim-6* and the zinc-finger gene *fozi-1* are under the control of DIE-1 and are responsible for executing the ASEL cell fate (Pierce-Shimomura et al. 2001; Johnston et al. 2006). In addition, *ceh-36,* which encodes an *Otx/Otd* homeodomain transcription factor, was initially proposed to be required for the establishment of the ASE bilateral asymmetry (Chang et al. 2003). However, another study revealed that *ceh-36* mutant animals fail to express a bilaterally expressed ASE cell-fate reporter in both ASEL and ASER neurons, indicating that *ceh-36* is required for the specification of the general ASE cell fate rather than for the establishment of the bilateral asymmetry (Lanjuin et al. 2003).

Functional lateralization of the AWC neurons

Like the ASE neurons, the left and right AWC olfactory neurons are structurally similar but display bilateral asymmetry in their patterns of gene expression (Troemel et al. 1999). The G-protein-coupled receptor STR-2 is randomly expressed in either the left or the right AWC neuron, and never in both in individual animals. Approximately half of animals in a population express *str-2* exclusively in AWCL, whereas the other half express *str-2* in AWCR. The *str-2*-expressing AWC neuron is termed AWC^{ON}, while the non-*str-2*-expressing AWC neuron is called AWC^{OFF}. The AWC^{ON} and AWC^{OFF} neurons also display asymmetry in their functions. Cell killing experiments reveal that the AWC^{OFF} neuron is required for animals to chemotax toward a specific odor, 2,3-pentanedione, whereas the AWC^{ON} neuron is required for the response to another odor, butanone (Wes and Bargmann 2001). In addition, it has been observed that AWC^{OFF}, but not AWC^{ON}, is required for benzaldehyde chemotaxis in the presence of a high concentration of butanone, suggesting that asymmetric diversity in the left-right pair of the AWC neurons is important for odorant discrimination (Wes and Bargmann 2001).

Developmental mechanism that establishes the AWC bilateral asymmetry

The developmental mechanism that establishes the stochastic bilateral asymmetry of the AWC neurons involves a cell-cell interaction that likely occurs between the two AWC cells (Troemel et al. 1999). Cell killing experiments indicate that when a precursor cell of

one AWC cell is ablated during embryogenesis, the remaining AWC cell always adopts an AWC^{OFF} fate, suggesting that AWC^{OFF} is the default state. The two AWC neurons are located on opposite sides of the animals, but their axons contact each other (White et al. 1986). Mutations in axon guidance genes that disrupt these contacts cause a two-AWC^{OFF} phenotype, suggesting that the cell-cell communication between the AWC neurons occurs in the axons (Troemel et al. 1999). This cell-cell communication between the AWC neurons does not involve Notch signaling pathway, and it was observed that mutations in components of the *C. elegans* Notch signaling cascade did not cause defects in generating the AWC bilateral asymmetry (Troemel et al. 1999).

Genetic screens have identified several mutants that show neuronal symmetry (*Nsy*) defects, with either two AWC^{ON} or two AWC^{OFF}cells. Two *nsy* genes, *nsy-4* and *nsy-5,* were identified based on their loss-of-function phenotype of two AWC^{OFF} cells (Vanhoven et al. 2006; Chuang et al. 2007). These two genes appear to participate in the cell-cell communication that establishes the AWC asymmetry. *nsy-4* encodes a transmembrane protein similar to the claudin subfamily that likely modulates ion channel function or cell adhesion (Vanhoven et al. 2006), and *nsy-5* encodes an innexin protein that forms gap junction channels (Chuang et al. 2007). Consistent with the potential role of these genes in cell-cell communication, mosaic analyses identify both cell-autonomous and non cell-autonomous actions of these genes (Vanhoven et al. 2006; Chuang et al. 2007). Although it is not entirely clear how these genes function to establish the AWC asymmetry, genetic analysis suggests that they act in parallel pathways to mediate cell-cell interactions that involves the two AWC neurons and numerous other neurons that

connect with the AWC neurons through NSY-5-dependent gap junctions (Chuang et al. 2007).

Once the stochastic decision of the AWC^{ON} and AWC^{OFF} fates is determined through cell-cell interactions, a calcium signal appears to be triggered in a future AWC^{OFF} cell to execute the AWC^{OFF} fate. This calcium signaling initiates with calcium entry though voltage-gated calcium channels, which in turn activate the calcium/calmodulin-dependent protein kinase CaMKII, which then activates a downstream MAP kinase cascade to specify the AWC^{OFF} fate (Troemel et al. 1999; Sagasti et al. 2001; Tanaka-Hino et al. 2002; Chuang and Bargmann 2005). Thus, a relative difference in the strength of calcium signaling between the two AWC cells is thought to be established by cell-cell interaction, which in turn triggers asymmetric calcium signaling, leading to bilateral functional asymmetry of the AWC neurons.

Structural asymmetries of the *C. elegans* nervous system

In addition to functional asymmetry, the *C. elegans* nervous system also displays structural asymmetry. The anatomy of the *C. elegans* nervous system has been extensively characterized, and the adult hermaphrodite contains 302 neurons (Ward et al. 1975; Albertson and Thomson 1976; White et al. 1976; Hall 1977; White et al. 1986). The morphology, position, chemical and electric connectivity of all neurons are known. The complete description of the anatomy of the *C. elegans* nervous system reveal the precise cells that display anatomical bilateral asymmetry: of 193 neurons located in the head region of the hermaphrodite, 176 neurons are in bilaterally symmetrical pairs, and

17 are single left-right unpaired neurons. Of these 17 single unpaired neurons, ten neurons exhibit left-right symmetry in their patterns of axodendritic processes. The remaining seven neurons are single left-right unpaired neurons that also display bilateral asymmetry in their morphology. These asymmetric neurons present in the head region of the hermaphrodite are named AVL, I4, I6, MI, RID, RIH and RIS neurons.

The invariant cell lineage of *C. elegans*

The development of *C. elegans* has been extensively described at single-cell resolution. The direct observation of cell divisions, cell migrations and cell deaths in living animals led to the elucidation of the complete cell lineage of *C. elegans* (Sulston and Horvitz 1977; Kimble and Hirsh 1979; Sulston et al. 1983). These studies revealed that the somatic cell lineage of *C. elegans* is essentially invariant from animal to animal and identified the precise developmental origins of all somatic cells, including left-right paired and unpaired cells.

The complete cell lineage revealed that most left-right paired cells are generated from pairs of left-right analogous blastomeres that undergo left-right symmetric cell lineages (Sulston et al. 1983). For example, the left-right pairs of the ADL, OLL, ADF, AWB, ASE, ASJ and AUA neurons are generated from left-right symmetric cell lineages of two analogous blastomeres, ABalpppp and ABpraaap, that undergo identical cell lineages and give rise to these neurons on the left and right sides of animals, respectively (Figure 1). By contrast, most left-right unpaired cells arise from left-right asymmetric cell lineages. For example, of the seven asymmetric neurons present in the head region of the

hermaphrodite, six neurons arise from left-right asymmetric cell lineages in which symmetry of the cell lineage is disrupted by differential cell-fate determination on two sides (see below). The exception is the RID neuron, which arises from a precursor cell that lacks an apparent left-right analogous blastomere.

The ABaraap cell lineage gives rise to the single unpaired MI neuron

This thesis work aims to understand the mechanism by which left-right asymmetry is established in *C. elegans* cell lineages that give rise to asymmetric neurons, and in particular, the cell lineage that generates the MI neuron. The MI neuron is a pharyngeal motor neuron located in the anterior-dorsal region of the pharynx (Albertson and Thomson 1976). The MI neuron is unipolar and sends a single process circumferentially to the pharyngeal nerve ring. Neither the neurotransmitter used by the MI neuron nor the function of the MI neuron has been identified.

The MI neuron is generated from a left-right asymmetric cell lineage. The blastomere ABaraap divides and generates two daughter cells, ABaraapa and ABaraapp, which are a pair of left-right analogous blastomeres that undergo nearly identical cell lineages to give rise to six identical sets of left-right paired cells, including the M2, M3 and NSM pharyngeal neurons, the m1 and m2 pharyngeal muscles and the mc1 and mc2 pharyngeal marginal cells (Figure 2). The anteriormost descendants of these two left-right paired analogous blastomeres differ in their cell fates: the ABaraappaaa cell becomes the MI neuron on the right side of the cell lineage, and the ABaraapaaaa cell differentiates into the e3D pharyngeal epithelial cell on the left. The e3D epithelial cell is a member of three e3 pharyngeal epithelial cells that display three-fold radial symmetry: e3D, e3VL

and e3VR are located in the dorsal, ventral left and ventral right of the pharynx, respectively (Albertson and Thomson 1976). Thus, the left-right asymmetric ABaraap cell lineage gives rise on the right to the single unpaired MI neuron and on the left to the e3D epithelial cell, which is arranged with two other e3 cells to form a three-fold symmetric structure.

Concluding remarks

Anatomical and functional bilateral asymmetries of the brain are a common feature in many animals. Functional lateralization of the nervous system is thought to be important for behavior and cognitive functions and in at least some cases is generated by anatomical asymmetry. Abnormalities in brain asymmetry have been implicated in several neuropathologies. Despite the importance of neuroanatomical bilateral asymmetry, the developmental mechanisms that establish such asymmetry remain largely elusive.

Although mostly bilaterally asymmetric, the *C. elegans* nervous system displays both anatomical and functional asymmetry. This thesis work aims to understand the developmental mechanisms that establish anatomical asymmetry in the *C. elegans* nervous system and particularly concerns the development of the single asymmetric MI neuron, which is generated from the invariant left-right asymmetric ABaraap cell lineage. In Chapter Two, I describe the role of an evolutionarily conserved transcriptional cascade in establishing the bilateral asymmetry of the ABaraap cell lineage and show that this transcriptional cascade is asymmetrically activated on the right side of the cell lineage but not on the left, leading to the induction of a bilaterally asymmetric neurogenesis on the

right to give rise to the MI neuron. In Chapter Three, I report the isolation of a mutant histone gene that causes symmetry in this normally asymmetric cell lineage and show that nucleosome assembly machinery is required for the generation of the MI neuron and the bilateral asymmetry in this cell lineage, demonstrating a novel mechanism of establishing a neuroanatomical asymmetry by nucleosome assembly. In Chapter Four, I summarize additional observations that indicate the role of histone-modifying enzymes in establishing the asymmetry of the cell lineage and establish that chromatin-modifying factors are required to generate the bilateral asymmetry of the cell lineage.

Acknowledgments

I thank Adam Saffer and Kostas Boulias for comments about this chapter.

References

Afzelius BA. 1976. A human syndrome caused by immotile cilia. *Science* **193**: 317-319.

Aizawa H, Bianco IH, Hamaoka T, Miyashita T, Uemura O, Concha ML, Russell C, Wilson SW, Okamoto H. 2005. Laterotopic representation of left-right information onto the dorso-ventral axis of a zebrafish midbrain target nucleus. *Curr Biol* **15**: 238-243.

Aizawa H, Goto M, Sato T, Okamoto H. 2007. Temporally regulated asymmetric neurogenesis causes left-right difference in the zebrafish habenular structures. *Dev Cell* **12**: 87-98.

Albertson DG, Thomson JN. 1976. The pharynx of *Caenorhabditis elegans*. *Philos Trans R Soc Lond B Biol Sci* **275**: 299-325.

Barth KA, Miklosi A, Watkins J, Bianco IH, Wilson SW, Andrew RJ. 2005. *fsi* zebrafish show concordant reversal of laterality of viscera, neuroanatomy, and a subset of behavioral responses. *Curr Biol* **15**: 844-850.

Berker EA, Berker AH, Smith A. 1986. Translation of Broca's 1865 report. Localization of speech in the third left frontal convolution. *Arch Neurol* **43**: 1065-1072.

Bisazza A, Rogers LJ, Vallortigara G. 1998. The origins of cerebral asymmetry: a review of evidence of behavioural and brain lateralization in fishes, reptiles and amphibians. *Neurosci Biobehav Rev* **22**: 411-426.

Braitenberg V, Kemali M. 1970. Exceptions to bilateral symmetry in the epithalamus of lower vertebrates. *J Comp Neurol* **138**: 137-146.

Broca P. 1865. Sur la faculté du langage articulé. *Bull Soc Antropl* **6**: 337-393.

Chang S, Johnston RJ, Jr., Frokjaer-Jensen C, Lockery S, Hobert O. 2004. MicroRNAs act sequentially and asymmetrically to control chemosensory laterality in the nematode. *Nature* **430**: 785-789.

Chang S, Johnston RJ, Jr., Hobert O. 2003. A transcriptional regulatory cascade that controls left/right asymmetry in chemosensory neurons of *C. elegans*. *Genes Dev* **17**: 2123-2137.

Chuang CF, Bargmann CI. 2005. A Toll-interleukin 1 repeat protein at the synapse specifies asymmetric odorant receptor expression via ASK1 MAPKKK signaling. *Genes Dev* **19**: 270-281.

Chuang CF, Vanhoven MK, Fetter RD, Verselis VK, Bargmann CI. 2007. An innexin-dependent cell network establishes left-right neuronal asymmetry in *C. elegans*. *Cell* **129**: 787-799.

Collignon J, Varlet I, Robertson EJ. 1996. Relationship between asymmetric nodal expression and the direction of embryonic turning. *Nature* **381**: 155-158.

Concha ML, Burdine RD, Russell C, Schier AF, Wilson SW. 2000. A nodal signaling pathway regulates the laterality of neuroanatomical asymmetries in the zebrafish forebrain. *Neuron* **28**: 399-409.

Concha ML, Wilson SW. 2001. Asymmetry in the epithalamus of vertebrates. *J Anat* **199**: 63-84.

De Santi A, Sovrano VA, Bisazza A, Vallortigara G. 2001. Mosquitofish display differential left- and right-eye use during mirror-image scrutiny and predator-inspection responses. *Animal Behaviour* **61**: 305-310.

Engbretson GA, Reiner A, Brecha N. 1981. Habenular asymmetry and the central connections of the parietal eye of the lizard. *J Comp Neurol* **198**: 155-165.

Essner JJ, Amack JD, Nyholm MK, Harris EB, Yost HJ. 2005. Kupffer's vesicle is a ciliated organ of asymmetry in the zebrafish embryo that initiates left-right development of the brain, heart and gut. *Development* **132**: 1247-1260.

Frangou S, Sharma T, Sigmudsson T, Barta P, Pearlson G, Murray RM. 1997. The Maudsley Family Study. 4. Normal planum temporale asymmetry in familial schizophrenia. A volumetric MRI study. *Br J Psychiatry* **170**: 328-333.

Gamse JT, Kuan YS, Macurak M, Brosamle C, Thisse B, Thisse C, Halpern ME. 2005. Directional asymmetry of the zebrafish epithalamus guides dorsoventral innervation of the midbrain target. *Development* **132**: 4869-4881.

Gazzaniga MS. 2005. Forty-five years of split-brain research and still going strong. *Nat Rev Neurosci* **6**: 653-659.

Geschwind N, Levitsky W. 1968. Human brain: left-right asymmetries in temporal speech region. *Science* **161**: 186-187.

Hall DH. 1977. The posterior nervous system of the nematode *Caenorhabditis elegans*. California Institute of Technology, Pasadena.

Hamada H, Meno C, Watanabe D, Saijoh Y. 2002. Establishment of vertebrate left-right asymmetry. *Nat Rev Genet* **3**: 103-113.

Hews DK, Worthington RA. 2001. Fighting from the right side of the brain: left visual field preference during aggression in free-ranging male tree lizards (*Urosaurus ornatus*). *Brain Behav Evol* **58**: 356-361.

Hobert O, Johnston RJ, Jr., Chang S. 2002. Left-right asymmetry in the nervous system: the *Caenorhabditis elegans* model. *Nat Rev Neurosci* **3**: 629-640.

Hynd GW, Semrud-Clikeman M, Lorys AR, Novey ES, Eliopulos D. 1990. Brain morphology in developmental dyslexia and attention deficit disorder/hyperactivity. *Arch Neurol* **47**: 919-926.

Jancke L, Hanggi J, Steinmetz H. 2004. Morphological brain differences between adult stutterers and non-stutterers. *BMC Neurol* **4**: 23.

Johnston RJ, Hobert O. 2003. A microRNA controlling left/right neuronal asymmetry in *Caenorhabditis elegans*. *Nature* **426**: 845-849.

Johnston RJ, Jr., Chang S, Etchberger JF, Ortiz CO, Hobert O. 2005. MicroRNAs acting in a double-negative feedback loop to control a neuronal cell fate decision. *Proc Natl Acad Sci U S A* **102**: 12449-12454.

Johnston RJ, Jr., Copeland JW, Fasnacht M, Etchberger JF, Liu J, Honig B, Hobert O. 2006. An unusual Zn-finger/FH2 domain protein controls a left/right asymmetric neuronal fate decision in *C. elegans*. *Development* **133**: 3317-3328.

Kimble J, Hirsh D. 1979. The postembryonic cell lineages of the hermaphrodite and male gonads in *Caenorhabditis elegans*. *Dev Biol* **70**: 396-417.

Kitamura K, Miura H, Miyagawa-Tomita S, Yanazawa M, Katoh-Fukui Y, Suzuki R, Ohuchi H, Suehiro A, Motegi Y, Nakahara Y et al. 1999. Mouse Pitx2 deficiency leads to anomalies of the ventral body wall, heart, extra- and periocular mesoderm and right pulmonary isomerism. *Development* **126**: 5749-5758.

Kramer-Zucker AG, Olale F, Haycraft CJ, Yoder BK, Schier AF, Drummond IA. 2005. Cilia-driven fluid flow in the zebrafish pronephros, brain and Kupffer's vesicle is required for normal organogenesis. *Development* **132**: 1907-1921.

Kulynych JJ, Vladar K, Fantie BD, Jones DW, Weinberger DR. 1995. Normal asymmetry of the planum temporale in patients with schizophrenia. Three-dimensional cortical morphometry with MRI. *Br J Psychiatry* **166**: 742-749.

Lanjuin A, VanHoven MK, Bargmann CI, Thompson JK, Sengupta P. 2003. *Otx/otd* homeobox genes specify distinct sensory neuron identities in *C. elegans*. *Dev Cell* **5**: 621-633.

Larsen JP, Hoien T, Lundberg I, Odegaard H. 1990. MRI evaluation of the size and symmetry of the planum temporale in adolescents with developmental dyslexia. *Brain Lang* **39**: 289-301.

LeMay M. 1976. Morphological cerebral asymmetries of modern man, fossil man, and nonhuman primate. *Ann N Y Acad Sci* **280**: 349-366.

Levin M. 2005. Left-right asymmetry in embryonic development: a comprehensive review. *Mech Dev* **122**: 3-25.

Levin M, Johnson RL, Stern CD, Kuehn M, Tabin C. 1995. A molecular pathway determining left-right asymmetry in chick embryogenesis. *Cell* **82**: 803-814.

Li X, Branch CA, Ardekani BA, Bertisch H, Hicks C, DeLisi LE. 2007. fMRI study of language activation in schizophrenia, schizoaffective disorder and in individuals genetically at high risk. *Schizophr Res* **96**: 14-24.

Liang JO, Etheridge A, Hantsoo L, Rubinstein AL, Nowak SJ, Izpisua Belmonte JC, Halpern ME. 2000. Asymmetric nodal signaling in the zebrafish diencephalon positions the pineal organ. *Development* **127**: 5101-5112.

Lin CR, Kioussi C, O'Connell S, Briata P, Szeto D, Liu F, Izpisua-Belmonte JC, Rosenfeld MG. 1999. Pitx2 regulates lung asymmetry, cardiac positioning and pituitary and tooth morphogenesis. *Nature* **401**: 279-282.

Lippolis G, Bisazza A, Rogers LJ, Vallortigara G. 2002. Lateralization of predator avoidance responses in three species of toads. *Laterality* **7**: 163-183.

Lowe LA, Yamada S, Kuehn MR. 2001. Genetic dissection of nodal function in patterning the mouse embryo. *Development* **128**: 1831-1843.

Lu MF, Pressman C, Dyer R, Johnson RL, Martin JF. 1999. Function of Rieger syndrome gene in left-right asymmetry and craniofacial development. *Nature* **401**: 276-278.

Marszalek JR, Ruiz-Lozano P, Roberts E, Chien KR, Goldstein LS. 1999. Situs inversus and embryonic ciliary morphogenesis defects in mouse mutants lacking the KIF3A subunit of kinesin-II. *Proc Natl Acad Sci U S A* **96**: 5043-5048.

Meno C, Gritsman K, Ohishi S, Ohfuji Y, Heckscher E, Mochida K, Shimono A, Kondoh H, Talbot WS, Robertson EJ et al. 1999. Mouse Lefty2 and zebrafish antivin are feedback inhibitors of nodal signaling during vertebrate gastrulation. *Mol Cell* **4**: 287-298.

Meno C, Takeuchi J, Sakuma R, Koshiba-Takeuchi K, Ohishi S, Saijoh Y, Miyazaki J, ten Dijke P, Ogura T, Hamada H. 2001. Diffusion of nodal signaling activity in the absence of the feedback inhibitor Lefty2. *Dev Cell* **1**: 127-138.

Miklosi A, Andrew RJ. 1999. Right eye use associated with decision to bite in zebrafish. *Behav Brain Res* **105**: 199-205.

Miklosi A, Andrew RJ, Gasparini S. 2001. Role of right hemifield in visual control of approach to target in zebrafish. *Behav Brain Res* **122**: 57-65.

Milner B. 1962. *Interhemispheric relations and cerebral dominance*. Johns Hopkins Press, Baltimore.

Murcia NS, Richards WG, Yoder BK, Mucenski ML, Dunlap JR, Woychik RP. 2000. The Oak Ridge Polycystic Kidney (orpk) disease gene is required for left-right axis determination. *Development* **127**: 2347-2355.

Nonaka S, Shiratori H, Saijoh Y, Hamada H. 2002. Determination of left-right patterning of the mouse embryo by artificial nodal flow. *Nature* **418**: 96-99.

Nonaka S, Tanaka Y, Okada Y, Takeda S, Harada A, Kanai Y, Kido M, Hirokawa N. 1998. Randomization of left-right asymmetry due to loss of nodal cilia generating leftward flow of extraembryonic fluid in mice lacking KIF3B motor protein. *Cell* **95**: 829-837.

Okada Y, Nonaka S, Tanaka Y, Saijoh Y, Hamada H, Hirokawa N. 1999. Abnormal nodal flow precedes situs inversus in iv and inv mice. *Mol Cell* **4**: 459-468.

Okada Y, Takeda S, Tanaka Y, Belmonte JC, Hirokawa N. 2005. Mechanism of nodal flow: a conserved symmetry breaking event in left-right axis determination. *Cell* **121**: 633-644.

Ortiz CO, Etchberger JF, Posy SL, Frokjaer-Jensen C, Lockery S, Honig B, Hobert O. 2006. Searching for neuronal left/right asymmetry: genomewide analysis of nematode receptor-type guanylyl cyclases. *Genetics* **173**: 131-149.

Ortiz CO, Faumont S, Takayama J, Ahmed HK, Goldsmith AD, Pocock R, McCormick KE, Kunimoto H, Iino Y, Lockery S et al. 2009. Lateralized gustatory behavior of *C. elegans* is controlled by specific receptor-type guanylyl cyclases. *Curr Biol* **19**: 996-1004.

Penhune VB, Zatorre RJ, MacDonald JD, Evans AC. 1996. Interhemispheric anatomical differences in human primary auditory cortex: probabilistic mapping and volume measurement from magnetic resonance scans. *Cereb Cortex* **6**: 661-672.

Petty RG, Barta PE, Pearlson GD, McGilchrist IK, Lewis RW, Tien AY, Pulver A, Vaughn DD, Casanova MF, Powers RE. 1995. Reversal of asymmetry of the planum temporale in schizophrenia. *Am J Psychiatry* **152**: 715-721.

Piedra ME, Icardo JM, Albajar M, Rodriguez-Rey JC, Ros MA. 1998. Pitx2 participates in the late phase of the pathway controlling left-right asymmetry. *Cell* **94**: 319-324.

Pierce-Shimomura JT, Faumont S, Gaston MR, Pearson BJ, Lockery SR. 2001. The homeobox gene *lim-6* is required for distinct chemosensory representations in *C. elegans*. *Nature* **410**: 694-698.

Rankin CT, Bunton T, Lawler AM, Lee SJ. 2000. Regulation of left-right patterning in mice by growth/differentiation factor-1. *Nat Genet* **24**: 262-265.

Raya A, Izpisua Belmonte JC. 2006. Left-right asymmetry in the vertebrate embryo: from early information to higher-level integration. *Nat Rev Genet* **7**: 283-293.

Robins A, Lippolis G, Bisazza A, Vallortigara G, Rogers LJ. 1998. Lateralization of agonistic responses and hind-limb use in toads. *Animal Behaviour* **56**: 875-881.

Rossi A, Stratta P, Mattei P, Cupillari M, Bozzao A, Gallucci M, Casacchia M. 1992. Planum temporale in schizophrenia: a magnetic resonance study. *Schizophr Res* **7**: 19-22.

Ryan AK, Blumberg B, Rodriguez-Esteban C, Yonei-Tamura S, Tamura K, Tsukui T, de la Pena J, Sabbagh W, Greenwald J, Choe S et al. 1998. Pitx2 determines left-right asymmetry of internal organs in vertebrates. *Nature* **394**: 545-551.

Sagasti A, Hisamoto N, Hyodo J, Tanaka-Hino M, Matsumoto K, Bargmann CI. 2001. The CaMKII UNC-43 activates the MAPKKK NSY-1 to execute a lateral signaling decision required for asymmetric olfactory neuron fates. *Cell* **105**: 221-232.

Scerri TS, Schulte-Korne G. 2010. Genetics of developmental dyslexia. *Eur Child Adolesc Psychiatry* **19**: 179-197.

Shiratori H, Hamada H. 2006. The left-right axis in the mouse: from origin to morphology. *Development* **133**: 2095-2104.

St Amand TR, Ra J, Zhang Y, Hu Y, Baber SI, Qiu M, Chen Y. 1998. Cloning and expression pattern of chicken Pitx2: a new component in the SHH signaling pathway controlling embryonic heart looping. *Biochem Biophys Res Commun* **247**: 100-105.

Sulston JE, Horvitz HR. 1977. Post-embryonic cell lineages of the nematode, *Caenorhabditis elegans*. *Dev Biol* **56**: 110-156.

Sulston JE, Schierenberg E, White JG, Thomson JN. 1983. The embryonic cell lineage of the nematode *Caenorhabditis elegans*. *Dev Biol* **100**: 64-119.

Supp DM, Brueckner M, Kuehn MR, Witte DP, Lowe LA, McGrath J, Corrales J, Potter SS. 1999. Targeted deletion of the ATP binding domain of left-right dynein confirms its role in specifying development of left-right asymmetries. *Development* **126**: 5495-5504.

Supp DM, Witte DP, Potter SS, Brueckner M. 1997. Mutation of an axonemal dynein affects left-right asymmetry in inversus viscerum mice. *Nature* **389**: 963-966.

Sutherland RJ. 1982. The dorsal diencephalic conduction system: a review of the anatomy and functions of the habenular complex. *Neurosci Biobehav Rev* **6**: 1-13.

Tanaka-Hino M, Sagasti A, Hisamoto N, Kawasaki M, Nakano S, Ninomiya-Tsuji J, Bargmann CI, Matsumoto K. 2002. SEK-1 MAPKK mediates Ca2+ signaling to determine neuronal asymmetric development in *Caenorhabditis elegans*. *EMBO Rep* **3**: 56-62.

Troemel ER, Sagasti A, Bargmann CI. 1999. Lateral signaling mediated by axon contact and calcium entry regulates asymmetric odorant receptor expression in *C. elegans*. *Cell* **99**: 387-398.

Van Wagenen WP, Herren RY. 1940. Surgical division of commissural pathways in the corpus callosum: relation to spread of an epileptic attack. *Arch Neurol Psychiatry* **44**: 740-759.

Vanhoven MK, Bauer Huang SL, Albin SD, Bargmann CI. 2006. The claudin superfamily protein NSY-4 biases lateral signaling to generate left-right asymmetry in *C. elegans* olfactory neurons. *Neuron* **51**: 291-302.

Ward S, Thomson N, White JG, Brenner S. 1975. Electron microscopical reconstruction of the anterior sensory anatomy of the nematode *Caenorhabditis elegans*. *J Comp Neurol* **160**: 313-337.

Watson T. 1836. An account of some cases of transposition observed in the human body. *London Medical Gazette* **18**: 393-403.

Wes PD, Bargmann CI. 2001. *C. elegans* odour discrimination requires asymmetric diversity in olfactory neurons. *Nature* **410**: 698-701.

White JG, Southgate E, Thomson JN, Brenner S. 1976. The structure of the ventral nerve cord of *Caenorhabditis elegans*. *Philos Trans R Soc Lond B Biol Sci* **275**: 327-348.

-. 1986. The structure of the nervous system of the nematode *Caenorhabditis elegans*. *Philos Trans R Soc Lond B Biol Sci* **314**: 1-340.

Yoshioka H, Meno C, Koshiba K, Sugihara M, Itoh H, Ishimaru Y, Inoue T, Ohuchi H, Semina EV, Murray JC et al. 1998. Pitx2, a bicoid-type homeobox gene, is involved in a lefty-signaling pathway in determination of left-right asymmetry. *Cell* **94**: 299-305.

Yu S, Avery L, Baude E, Garbers DL. 1997. Guanylyl cyclase expression in specific sensory neurons: a new family of chemosensory receptors. *Proc Natl Acad Sci U S A* **94**: 3384-3387.

Figures

Figure 1. A Left-Right Symmetric Cell Lineage Generates Left-Right Paired Neurons. The ABalpppp and ABpraaap blastomeres undergo symmetric cell lineage and give rise to an identical set of left-right paired neurons. X indicates programmed cell death.

Figure 1.

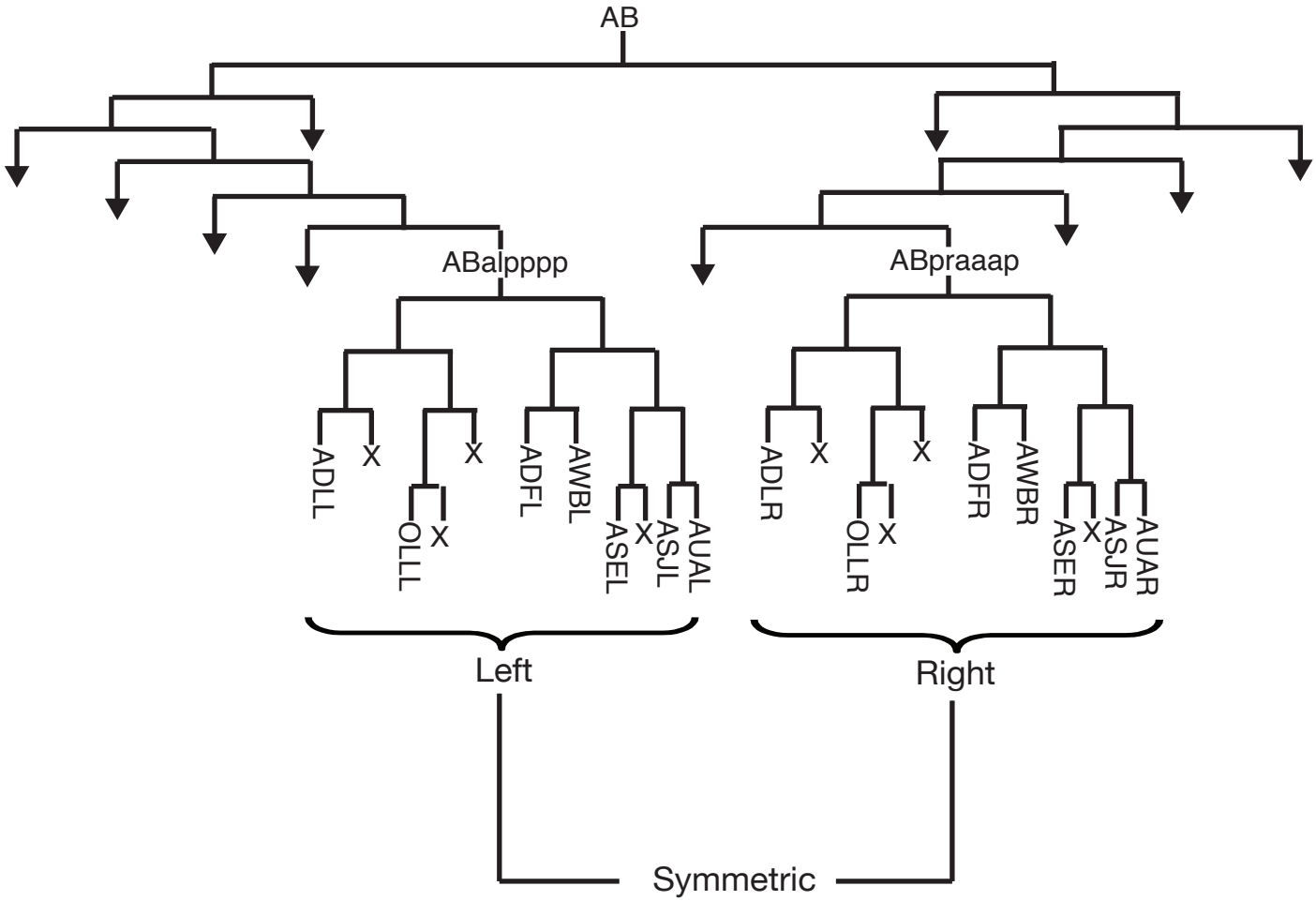
AB
ABalpppp
ABpraaap
ADLL
X
X
OLLL
X
ADFL
AWBL
ASEL
X
ASJL
AUAL
ADLR
X
X
OLLR
X
ADFR
AWBR
ASER
X
ASJR
AUAR
Left
Right
Symmetric

Figure 2. The Left-Right Asymmetric ABaraap Cell Lineage Generates the Single Unpaired MI neuron. The ABaraapa and ABaraapp blastomeres undergo asymmetric cell lineage and give rise to the single unpaired MI neuron on the right and the e3D epithelial cell on the left. X indicates programmed cell death.

Figure 2.

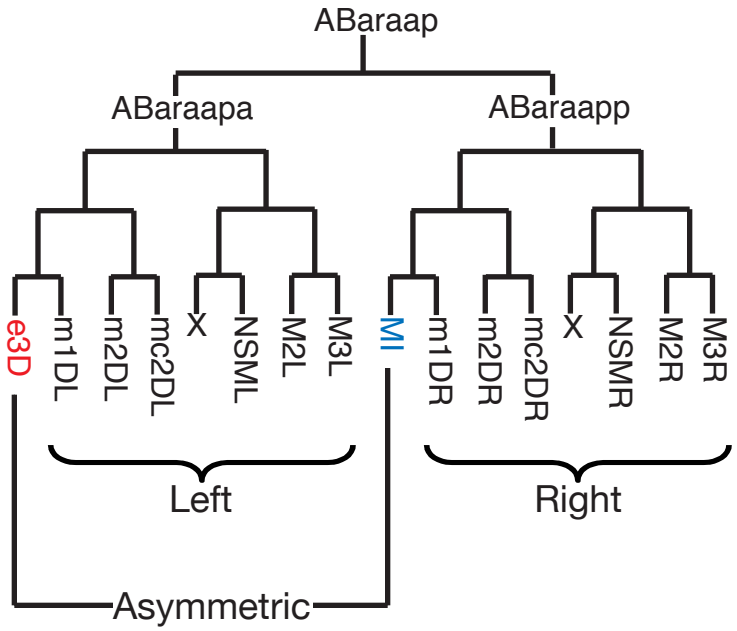
ABaraap
ABaraapa
ABaraapp
e3D
m1DL
m2DL
mc2DL
X
NSML
M2L
M3L
MI
m1DR
m2DR
mc2DR
X
NSMR
M2R
M3R
Left
Right
Asymmetric

Chapter II

Otx-dependent Expression of Proneural bHLH Genes Establishes a Neuronal Bilateral Asymmetry in *C. elegans*

Shunji Nakano, Ronald E. Ellis, and H. Robert Horvitz

Ronald E. Ellis isolated *ngn-1(n1921)* mutants and noted that the MI neuron is transformed into an e3D-like epithelial cell in *ngn-1(n1921)* mutants.

I performed the rest of the experiments.

Summary

Bilateral asymmetry in *Caenorhabditis elegans* arises in part from cell lineages that differ on the left and right sides of the animal. The unpaired MI neuron descends from the right side of an otherwise left-right symmetric cell lineage that generates the MI neuron on the right and the e3D epithelial cell on the left. We isolated mutations in three genes that caused left-right symmetry in this normally asymmetric cell lineage by transforming MI into an e3D-like cell. These genes encode the proneural bHLH proteins NGN-1 and HLH-2 and the *Otx* homeodomain protein CEH-36. We identified the precise precursor cells in which *ceh-36* and *ngn-1* act and showed that CEH-36 protein is asymmetrically expressed and is present in an MI progenitor cell on the right but not in its bilateral counterpart. This asymmetric CEH-36 expression promotes asymmetric *ngn-1* and *hlh-2* expression, which in turn induces asymmetric MI neurogenesis. Our results indicate that this left-right asymmetry is specified within the two sister cells that first separate the left and right branches of the cell lineage. We conclude that the components of an evolutionarily conserved *otx/bHLH* pathway act sequentially through multiple rounds of cell division on the right to relay an initial apparently cryptic asymmetry to the presumptive post-mitotic MI neuron, thereby creating an anatomical bilateral asymmetry in the *C. elegans* nervous system.

Introduction

Left-right asymmetry is a widespread feature of animal anatomy. Studies over the last decade have advanced our understanding of mechanisms that establish left-right asymmetry in visceral organs of vertebrate embryos (for reviews, see Levin 2005; Shiratori and Hamada 2006). In addition to visceral organs, the nervous systems of both vertebrates and invertebrates display anatomical asymmetry (Concha and Wilson 2001; Toga and Thompson 2003), and in some cases such neuroanatomical asymmetries have been shown to be important for nervous system function (Pascual et al. 2004; Barth et al. 2005). The identification of the molecular mechanisms by which neuroanatomical asymmetry is established is thus important to understand both neural development and neural function. To date, our knowledge of the molecular and cellular bases of specifying anatomical asymmetry within the nervous system is limited.

The nervous system of *Caenorhabditis elegans* displays bilateral asymmetry (for review, see Hobert et al. 2002). Because the complete cell lineage of *C. elegans* has been described and the somatic cell lineage is essentially invariant from animal to animal (Sulston and Horvitz 1977; Kimble and Hirsh 1979; Sulston et al. 1983), the developmental origins of all cells, including all left-right paired and unpaired cells, are known. Much of the left-right symmetry arises from pairs of left-right analogous blastomeres, which through bilaterally symmetric cell lineages give rise to sets of left-right paired cells. To create either left-right asymmetry or three-fold symmetry, the bilateral symmetry in cell lineages must be disrupted.

The *C. elegans* pharynx, the animal's feeding organ, contains single unpaired neurons as well as sets of cells arranged with three-fold symmetry (Albertson and

Thomson 1976). For example, the MI motor neuron is a single unpaired neuron located in the anterior-dorsal region of the pharynx. The cell body of the MI neuron sends a single unilateral process circumferentially to the pharyngeal nerve ring. Numerous epithelial cells in the pharynx display three-fold radial symmetry. For example, the three e3 epithelial cells are located on the ventral left (VL), ventral right (VR) and dorsal (D) regions of the pharynx. e3VL and e3VR are generated from a left-right symmetric cell lineage, whereas the e3D epithelial cell and the MI neuron are generated as lineally homologous descendants from a left-right asymmetric cell lineage. At the 50-cell stage of embryogenesis, the blastomere ABaraap divides and generates two multipotent daughter cells, ABaraapa and ABaraapp, which are a pair of left-right analogous blastomeres that give rise to six identical sets of left-right paired cells of diverse cell types, including the M2, M3 and NSM pharyngeal neurons, the m1 and m2 pharyngeal muscles and the mc2 pharyngeal marginal cells (Figure 1A). The anteriormost descendants of ABaraapa and ABaraapp differ in their cell fates: whereas ABaraapaaaa differentiates into the e3D epithelial cell, its lineally homologous cell ABaraappaaa becomes the MI neuron. When this left-right asymmetry is specified and how information concerning the asymmetry is transduced to generate MI on the right and e3D on the left are unknown.

In this study we report that *ngn-1,* a bHLH gene that is a member of the neurogenin gene subfamily, *hlh-2,* the *C. elegans* ortholog of the *Drosophila melanogaster* gene *Daughterless* and the mammalian gene *E2A,* and *ceh-36,* a *C. elegans* homolog of the mammalian homeodomain gene *Otx*, are required for breaking symmetry in this left-right asymmetric cell lineage. Loss-of-function mutations in these genes transform the presumptive MI neuron into an e3D-like epithelial cell, resulting in left-

right symmetry in this normally asymmetric cell lineage. We define a transcriptional cascade in which *ceh-36* promotes expression of *ngn-1* and *hlh-2* and show that induction of this transcriptional pathway is bilaterally asymmetric. We identify the precise precursor cells in which *ceh-36* and *ngn-1* act to establish the bilateral asymmetry. Our results suggest that the developmental program that establishes the bilateral asymmetry is triggered by the asymmetric expression of *ceh-36* between ABaraapa and ABaraapp, the pair of left-right sister cells that generate the left and right branches of the cell lineage, respectively.

Results

ngn-1 and *hlh-2* Mutants Lack the MI Neuron and Contain an Extra e3D-like Epithelial Cell

To identify genes required for establishing left-right asymmetry in the cell lineage that gives rise to the MI neuron on the right and the e3D epithelial cell on the left (Figure 1A), we performed genetic screens to look for mutations that affect this cell lineage. We particularly focused on identifying genes that when mutated result in a left-right symmetry in this normally asymmetric cell lineage. Such mutants might lack MI and contain an extra e3D-like cell, or alternatively lack e3D and contain an extra MI-like neuron. The MI neuron and the e3D epithelial cell can be identified using Nomarski optics based on their size, morphology, and the position of their nuclei within the pharynx (Figure 2A). We performed screens using Nomarski optics and recovered four mutations (*n1921, n5020, n5052* and *n5053)* that cause the apparent absence of MI and presence of an extra e3D-like cell (Figure 2B, C, see Experimental Procedures for details). As described below, *n1921, n5020* and *n5052* confer recessive phenotypes, fail to complement and are alleles of the gene *ngn-1*. *n5053* is an allele of the gene *hlh-2* (see below) and semidominantly causes the absence of MI and the presence of an extra e3D-like cell. Strains homozygous for the *n5053* mutation are not viable and die as embryos.

ngn-1 and *hlh-2* mutants lack a neuronal nucleus in the anterior-dorsal region of the pharynx where MI is normally located in wild-type animals. To confirm that the missing neuron in these mutants is the MI neuron, we tested if these mutant animals express a *gfp* cell-fate reporter that is normally expressed in the MI neuron in wild-type

animals. The reporter *sams-5::gfp* was expressed in the MI neuron of wild-type animals (Table 1A, Figure 2E, for identification of this reporter, see Experimental Procedures). We introduced the *sams-5::gfp* reporter into *ngn-1* and *hlh-2* mutants and found that *sams-5::gfp* was not expressed in these mutants (Table 1A, Figure 2F, G), indicating that MI is absent from the pharynx of these mutants.

ngn-1 and *hlh-2* mutants contain an extra nucleus that resembles the nucleus of the e3D epithelial cell (Figure 2B, C). To determine if this extra cell adopts the fate normally associated with e3D, we tested whether these extra cells express a *gfp* cell-fate marker that is expressed in the e3D epithelial cell of wild-type animals. The reporter *D2096.6::pes-10::gfp* was expressed in the e3 pharyngeal epithelial cells, including e3D, of wild-type animals (Figure 2I, Table 1B, for identification of this reporter, see Experimental Procedures). We introduced *D2096.6::pes-10::gfp* into *ngn-1* and *hlh-2* mutants and found that *D2096.6::pes-10::gfp* was also expressed in the extra cell with a nucleus morphologically similar to that of the e3D epithelial cell (Figure 2J, K, Table 1B), indicating that these mutants generate an extra e3D-like cell.

ngn-1 and *hlh-2* Mutations Generate Symmetry in a Normally Left-Right Asymmetric Cell Lineage

Using Nomarski optics, we found that the absence of MI and the presence of an extra e3D-like cell in *ngn-1* and *hlh-2* mutants were perfectly correlated: when MI was absent the extra e3D-like cell was always present, and when MI was present the extra e3D-like cell was always absent (n=600, data not shown). We did not observe any animals that

contained or lacked both MI and the extra e3D-like cell. This perfect correlation strongly suggested that these mutations transform MI into an e3D-like cell, thereby generating symmetry in a normally left-right asymmetric cell lineage (Figure 1B).

We tested the hypothesis that these mutations transform MI into an e3D-like cell using laser microsurgery experiments to determine whether the extra e3D-like cell in *ngn-1(n1921)* mutants is generated from the cell lineage that normally gives rise to MI. If ABaraappaaa, which normally becomes MI in wild-type animals, instead adopts an e3D-like cell fate in *ngn-1* mutants, then elimination of a precursor cell of ABaraappaaa from *ngn-1(n1921)* mutant embryos by laser ablation should result in the absence of the extra e3D-like cell (Figure 1C, D). We observed developing *ngn-1(n1921)* embryos and identified ABaraappa, the grandmother cell of the presumptive MI neuron. Elimination of ABaraappa by laser ablation prevented the generation of the extra e3D-like cell in *ngn-1(n1921)* animals (Table 1C). It is conceivable that this reduction in the number of the e3D-like cells could be attributed to the absence of e3D rather than of the extra e3D-like cell, if the intact ABaraappa cell were required to specify ABaraapaaaa to become the e3D cell. We ruled out this possibility by testing whether the MI grandmother cell, ABaraappa, is required for the fate specification of the e3D epithelial cell in wild-type animals. We observed developing wild-type embryos and performed laser ablation experiments to eliminate the MI grandmother cell and found that this operation did not change the number of the e3D cells compared to that in unoperated wild-type embryos (Figure 1C, Table 1C). We concluded that the extra e3D-like cell in *ngn-1(n1921)* mutants is generated from the cell lineage that normally gives rise to MI and that the MI

neuron is transformed into an e3D-like epithelial cell in *ngn-1* and *hlh-2* mutants, resulting in the loss of left-right asymmetry in the cell lineage (Figure 1B).

ngn-1 Encodes a bHLH Protein of the Neurogenin Subfamily

We mapped *n1921* to a 153 kb region of LG *IV* that includes the *ngn-1* locus. We generated a 15.1-kb *ngn-1* genomic DNA clone that contains 12.4 kb 5' upstream and 1.5 kb 3' downstream sequence of the predicted *ngn-1* coding region and found that this *ngn-1* genomic DNA clone rescued the MI transformation phenotype caused by *n1921* (Table 2A). We also performed an RNA interference (RNAi) experiment and found that RNAi using dsRNA corresponding to the predicted third exon of *ngn-1* phenocopied the *n1921* mutation (Table 3).

ngn-1 is predicted to encode a 184-amino-acid protein similar to members of the neurogenin bHLH subfamily (Figure 3). We determined the DNA sequence of *ngn-1* in our mutants and identified a mutation in each case (Figure 4A, see Figure 5 for details concerning the mutation found in *n5052*). In addition, we characterized an *ngn-1* deletion allele, *ngn-1(ok2200Δ),* which lacks the second and third exons of *ngn-1* and eliminates the entire coding sequence for the bHLH domain, thus likely defining a null allele of *ngn-1* (Figure 4A). *ngn-1(ok2200Δ)* mutants exhibited the MI transformation (Table 1A, B).

These findings establish that *ngn-1* is required for breaking symmetry in this cell lineage.

n5053 Is an Allele of *hlh-2*, the *C. elegans* Ortholog of *E2A/Daughterless*

We mapped *n5053* to a 2 map-unit interval of LG *I* between *dpy-5* and *unc-13*. This genomic region contains the gene *hlh-2,* the *C. elegans* ortholog of *E2A/Daughterless* (Krause et al. 1997). Because *E2A* in mammals and *Daughterless* in *Drosophila* encode bHLH proteins that form heterodimers with other bHLH proteins, including mammalian NeuroD1 (Poulin et al. 1997; Longo et al. 2008) and *Drosophila Atonal* (Jarman et al. 1993), respectively, both of which are closely related to the neurogenin subfamily, we examined whether *n5053* is an allele of *hlh-2*. We determined the DNA sequence of the *hlh-2* locus in *n5053* mutants and found a G-to-A transition mutation that alters the splice acceptor sequence preceding the second exon (Figure 4B). We generated an *hlh-2* genomic clone that contains 12.2 kb 5' upstream and 5.2 kb 3' downstream region of the *hlh-2* coding sequence and found that *n5053* mutants transformed with this *hlh-2* genomic clone were rescued for the MI transformation as well as the embryonic lethality (Table 2B, C). We also observed that RNAi treatment of *hlh-2* caused the MI transformation (Table 3). Furthermore, we isolated an *hlh-2* deletion allele, *hlh-2(n5287Δ),* that removes the entire coding sequence except for the first exon. This deletion eliminates the coding sequence corresponding to the entire bHLH domain, thus presumably defining a null allele of *hlh-2* (Figure 4B). In animals heterozygous for *hlh-2(n5287Δ)*, the MI neuron was transformed into an e3D-like cell (Table 1A, B), and animals homozygous for the *hlh-2(n5287Δ)* displayed embryonic lethality. These results indicate that loss of *hlh-2* function causes the MI transformation and suggest that *hlh-2* is a haplo-insufficient locus required for breaking bilateral symmetry in the cell lineage.

A physical interaction between NGN-1 and HLH-2 has been shown previously using yeast two-hybrid studies (Grove et al. 2009). We examined whether NGN-1 and HLH-2 directly interact using an *in vitro* pull-down assay with purified proteins and found that His-tagged NGN-1 proteins associated with HLH-2 proteins but not with a control protein, MBP (Figure 4C). These results suggest that NGN-1 and HLH-2 form a transcriptional heterodimer required for breaking symmetry in a left-right asymmetric cell lineage.

ngn-1 Acts Cell Autonomously to Establish a Left-Right Asymmetry

To identify when and where *ngn-1* functions to establish left-right asymmetry in the cell lineage, we performed a mosaic analysis of *ngn-1*. Specifically, we generated *ngn-1(n1921)* mutant animals carrying an extrachromosomal array containing the *ngn-1* rescuing construct marked with the cell-autonomous *gfp* markers *sur-5::gfp* (Yochem et al. 1998) and *unc-119::gfp* (Maduro and Pilgrim 1995). Extrachromosomal arrays in *C. elegans* are mitotically unstable, resulting in the generation of clones of cells that lose the arrays. We examined *ngn-1(n1921)* animals carrying the array using Nomarski optics equipped with epifluorescence and examined ABaraappaaa, which normally becomes MI in wild-type animals to determine (1) the fate of ABaraappaaa, i.e., an MI neuronal fate or an e3D-like epithelial fate, judged by the size and the morphology of its nucleus and (2) the presence or the absence of the array in the ABaraappaaa cell, judged by GFP fluorescence. Based on these two criteria, each animal was classified into one of four categories: Class I animals, ABaraappaaa differentiated into an MI neuron that retained

the array; Class II animals, ABaraappaaa differentiated into an MI neuron that lacked the array; Class III animals, ABaraappaaa was transformed into an e3D-like cell that retained the array; and Class IV animals, ABaraappaaa was transformed into an e3D-like cell that lacked the array (Figure 4D). If *ngn-1* acts cell autonomously to establish the left-right asymmetry in the cell lineage, then ABaraappaaa transformed into an e3D-like cell should not retain the array, resulting in the absence of the Class III animals. Of 300 animals examined, 36 animals contained ABaraappaaa transformed into an e3D-like cell. All of these 36 animals were classified as Class IV, in which ABaraappaaa adopted an e3D-like cell fate and did not retain the array; no animals were categorized as Class III (Figure 4D). The remaining 264 animals contained an ABaraappaaa that differentiated into an MI neuron. Of these animals, 251 animals were classified as Class I, in which ABaraappaaa differentiated into an MI neuron that retained the array, which is consistent with the cell-autonomous action of *ngn-1*. The remaining 13 animals were categorized as Class II, in which ABaraappaaa differentiated as normal into an MI neuron despite the absence of the array. These 13 Class II animals presumably at least in part reflect the incomplete penetrance of the *ngn-1(n1921)* mutation (Table 1A, B). In short, our data support a strong association between the specification of the MI neuron fate and the presence of the array in ABaraappaaa ($p < 0.001$) and indicate that *ngn-1* acts cell-autonomously to break bilateral symmetry in the cell lineage.

We further examined the 36 animals of Class IV, in which ABaraappaaa was transformed into an e3D-like cell that had lost the array. We determined the cell division at which the array had been mitotically lost by scoring the presence or absence of the array in cells that shared a precursor cell with ABaraappaaa at some point of their lineage

history. From this analysis, we identified 10 animals that had an extra e3D-like cell and had lost the array at the cell division of ABaraapp (Figure 4E). This observation indicates that the presence of a functional *ngn-1* gene in ABaraapp is insufficient to generate an MI neuron and thus that to generate MI a functional *ngn-1* gene is necessary at or later than the stage of ABaraappa, the MI grandmother cell. By contrast, we identified no animals that had lost the array at the next cell division, that of the MI grandmother cell, ABaraappa (Figure 4E). This result suggests that in all animals in which the array was present in the MI grandmother cell, ABaraappaaa differentiated as normal into an MI neuron whether the array was (Class I animals) or was not (Class II animals) transmitted to the presumptive MI neuron. Thus, the presence of the array in the MI grandmother cell was sufficient to rescue the MI transformation phenotype of *ngn-1(n1921)* mutants. Together, these findings indicate that the presence of the *ngn-1* wild-type gene in the MI grandmother cell is both necessary and sufficient to generate an MI neuron and establish left-right asymmetry in the cell lineage.

Expression of *ngn-1* and *hlh-2* Is Left-Right Asymmetric

To identify when and where *ngn-1* is expressed during embryogenesis, we generated a translational *ngn-1::gfp* fusion gene by an in-frame insertion of a *gfp* coding sequence into the 3' end of the *ngn-1* coding sequence flanked by the 12.4 kb 5' upstream and 1.5 kb 3' downstream genomic sequence. We integrated this *ngn-1::gfp* transgene into the *C. elegans* genome and found that the *ngn-1::gfp* transgene rescued the MI transformation defect of *ngn-1(n1921)* mutants (Table 2A), indicating that this *ngn-1::gfp* is functional.

We used this *ngn-1::gfp* to examine expression of *ngn-1* during embryonic development. Because mosaic analysis of *ngn-1* suggested the cell-autonomous action of *ngn-1,* we asked whether *ngn-1* is expressed in the cell lineage that gives rise to the MI neuron. We observed developing embryos carrying *ngn-1::gfp* and found that NGN-1::GFP protein became detectable in the nucleus of the MI mother cell (Figure 6A-C). By contrast, NGN-1::GFP was not detectable in the e3D mother cell (Figure 6A-C), indicating that expression of *ngn-1* is left-right asymmetric within this asymmetric cell lineage.

We also analyzed *hlh-2* expression during embryogenesis. Immunostaining experiments using an HLH-2 antibody had demonstrated previously that HLH-2 is present in all cells up to the 100-200-cell stage of embryonic development (Krause et al. 1997). To test specifically whether *hlh-2* is expressed in the MI mother cell, we generated a translational *hlh-2::gfp* fusion gene by an in-frame insertion of a *gfp* coding sequence to the 3' end of the *hlh-2* coding sequence flanked by the 18.7 kb 5' upstream and 10.6 kb 3' downstream genomic sequence. We integrated this *hlh-2::gfp* transgene into the *C. elegans* genome and found that *hlh-2::gfp* rescued the MI transformation as well as the embryonic lethality of *hlh-2(n5053)* mutants (Table 2B, C), indicating that *hlh-2::gfp* is functional. We observed developing embryos carrying *hlh-2::gfp* and found that, like NGN-1::GFP, HLH-2::GFP was also localized asymmetrically: HLH-2::GFP was detectable in the MI mother cell but not in the e3D mother cell (Figure 6G-I). These results indicate that both *ngn-1* and *hlh-2* are expressed asymmetrically and suggest that this left-right asymmetric expression of *ngn-1* and *hlh-2* establishes bilateral asymmetry in the cell lineage.

ceh-36, an *Otx/Otd* Homeodomain Gene, Is Required for Establishing the e3D-MI Bilateral Asymmetry

To identify factors that regulate the left-right asymmetric expression of *ngn-1* and *hlh-2,* we performed additional genetic screens to look for mutations that cause left-right symmetry in this normally asymmetric cell lineage. We mutagenized wild-type animals carrying the e3D cell-fate reporter, *D2096.6::pes-10::gfp,* and screened for mutants in which an extra e3D-like cell was present or e3D was absent (see Chapter IV). Among the isolates we recovered were three allelic mutations (*n5333, n5339* and *n5340*) that caused the presence of an extra e3D-like cell (Table 1B, Figure 2L). We introduced the MI cell-fate reporter *sams-5::gfp* into these mutants and observed that these mutants failed to generate the MI neuron (Table 1A, Figure 2H), indicating that, like *ngn-1* and *hlh-2* mutations, these mutations transform MI into an e3D-like cell, thereby generating symmetry in the normally asymmetric cell lineage (Figure 1B).

We mapped *n5333* to a 100 kb region of LG *X* that includes the gene *ceh-36*. We generated a 5.7 kb *ceh-36* genomic DNA clone that contains 2.5 kb 5' upstream and 1.1 kb 3' downstream sequence of the *ceh-36* coding region and found that this *ceh-36* genomic DNA clone rescued the MI transformation phenotype caused by *n5333* (Table 4). *ceh-36* encodes a 257 amino acid protein similar to members of the *Otx/Otd* homeodomain subfamily (Chang et al. 2003; Lanjuin et al. 2003; Koga and Ohshima 2004). We determined the DNA sequence of *ceh-36* in our mutants and identified a mutation in each case (Figure 7A). In addition, we characterized a *ceh-36* deletion allele, *ceh-36(ok795Δ),* which lacks the entire coding sequence of *ceh-36* except for the first

exon, thus likely defining a null allele of *ceh-36* (Figure 7A). We observed that animals homozygous for the *ceh-36(ok795Δ)* deletion displayed larval lethality and exhibited the MI transformation (Table 1A, B). These findings establish that *ceh-36* is required for breaking symmetry in this cell lineage.

Establishment of the MI-e3D Asymmetry Does Not Require Genes that Specify Non-anatomical Neuronal Bilateral Asymmetries

Some aspects of left-right asymmetry in the *C. elegans* nervous system are not apparent anatomically: left-right pairs of the ASE gustatory neurons and the AWC olfactory neurons are each morphologically similar but distinct both functionally (Pierce-Shimomura et al. 2001; Wes and Bargmann 2001) and in their patterns of gene expression (Yu et al. 1997; Troemel et al. 1999; Ortiz et al. 2006).

We tested if genes that specify the left-right asymmetry of the ASE neurons and the AWC neurons are required to establish bilateral asymmetry in the cell lineage that gives rise to the MI neuron. We observed that in *cog-1, lim-6, lin-49* and *lsy-6* mutants, in which the asymmetry of the ASE neurons is lost (Chang et al. 2003; Johnston and Hobert 2003), and in *inx-19, nsy-4* and *unc-43* mutants, in which the asymmetry of the AWC neurons is lost (Troemel et al. 1999; Vanhoven et al. 2006; Chuang et al. 2007), both the MI neuron and the e3D epithelial cell were correctly specified (Table 5A, B). We also asked if mutations in genes encoding components of Notch signaling pathway, including *lin-12* and *glp-1* (Yochem et al. 1988; Austin and Kimble 1989), and Wnt signaling pathway, including *pop-1* (Lin et al. 1995), affect the MI-e3D bilateral asymmetry. We observed that in *lin-12, glp-1* and *pop-1* mutants, both MI and e3D were normally present

(Table 5C). These results indicate that *ceh-36, ngn-1* and *hlh-2* represent novel components that establishes a bilateral asymmetry in the *C. elegans* nervous system.

ngn-1 Is Required for the General Cell-Fate Specification of the AWC Neurons

ceh-36 has been previously shown to be required for the general cell-fate specification of the AWC and ASE neurons (Lanjuin et al. 2003). We asked whether *ngn-1* is also required for the general cell-fate specification of the AWC and ASE neurons. We introduced a general cell-fate reporter for the ASE neurons, *flp-6::gfp* (Kim and Li 2004), into *ngn-1(ok2200Δ)* mutants and found that the expression of this reporter in *ngn-1(ok2200Δ)* mutants was indistinguishable from that in wild-type animals (Table 6). We also introduced a general cell-fate reporter for the AWC neurons, *odr-1::dsRed* (Vanhoven et al. 2006), into *ngn-1(ok2200Δ)* mutants and observed that expression of *odr-1::dsRed* was often missing in *ngn-1(ok2200Δ)* mutants (Table 7), indicating that, like *ceh-36, ngn-1* is required for the general cell-fate specification of the AWC neurons.

ceh-36 Acts Cell Autonomously to Establish a Left-Right Asymmetry

To identify when and where *ceh-36* functions to generate the MI neuron, we performed a mosaic analysis of *ceh-36* similar to our *ngn-1* mosaic analysis. We generated *ceh-36 (n5333)* mutant animals carrying an extrachromosomal array containing the *ceh-36* rescuing construct marked with the cell-autonomous *gfp* markers *sur-5::gfp* (Yochem et al. 1998) and *unc-119::gfp* (Maduro and Pilgrim 1995) and determined in each animal (1)

the fate of ABaraappaaa, i.e., an MI neuronal fate or an e3D-like fate and (2) the presence or the absence of the array in the ABaraappaaa cell. Based on these criteria, we classified each animal into one of four categories, as we did in our *ngn-1* mosaic analysis (Figure 7B). Of 350 animals examined, 28 animals contained ABaraappaaa transformed into an e3D-like epithelial cell. All of these 28 animals were classified as Class IV; no animals were categorized as Class III. The remaining 322 animals contained an ABaraappaaa that differentiated into an MI neuron. Of these animals, 288 animals were classified as Class I, and the remaining 34 animals were categorized as Class II (Figure 7B). In short, our data support a strong association between the specification of the MI neuron fate and the presence of the array in ABaraappaaa ($p < 0.001$) and indicate that *ceh-36* acts cell-autonomously to break bilateral symmetry in the cell lineage.

We further examined the 28 animals of Class IV, in which ABaraappaaa was transformed into an e3D-like cell that had lost the array and determined the cell division at which the array had been mitotically lost. We identified eight animals that had an extra e3D-like cell and had lost the array at the cell division of ABaraap (Figure 7C). By contrast, we identified no animals that had lost the array at the next cell division, that of the MI great grandmother cell, ABaraapp (Figure 7C). Together, these findings indicate that the presence of the *ceh-36* wild-type gene in the MI great grandmother cell is both necessary and sufficient to rescue the MI transformation defect of *ceh-36(n5333)*.

Left-Right Asymmetric Expression of *ngn-1* and *hlh-2* Is Abolished in *ceh-36* Mutants

Our mosaic analyses suggest that the site of *ceh-36* action is one cell division earlier than that of *ngn-1* action: our *ceh-36* mosaic analysis indicates that the presence of the *ceh-36* wild-type gene in the MI great grandmother cell (ABaraapp) is both necessary and sufficient to generate the MI neuron, while our *ngn-1* mosaic analysis indicates that the presence of the *ngn-1* wild-type gene in the MI grandmother cell (ABaraappa) is both necessary and sufficient to generate the MI neuron (Figure 7D). Because these observations suggest that *ceh-36* acts upstream of or in parallel to *ngn-1*, we examined expression of *ngn-1* in *ceh-36(n5333)* mutant embryos. We introduced the *ngn-1::gfp* transgene into *ceh-36(n5333)* mutants, observed developing *ceh-36(n5333)* mutant embryos carrying *ngn-1::gfp* and found that NGN-1::GFP was not detectable in the nucleus of the MI mother cell (Figure 6D-F). We also asked whether expression of *hlh-2* in the MI mother cell requires *ceh-36*. We introduced the *hlh-2::gfp* transgene into *ceh-36(n5333)* mutants, observed developing *ceh-36(n5333)* mutant embryos carrying *hlh-2::gfp* and found that, like NGN-1::GFP, HLH-2::GFP was not localized to the nucleus of the MI mother cell (Figure 6J-L). These observations indicate that establishment of left-right asymmetric expression of *ngn-1* and *hlh-2* requires *ceh-36* and that *ceh-36* acts upstream of *ngn-1* and *hlh-2* to establish left-right asymmetry in the cell lineage.

Expression of *ceh-36* Is Left-Right Asymmetric

To identify when and where *ceh-36* is expressed during embryogenesis, we generated a translational *ceh-36::gfp* fusion gene by an in-frame insertion of a *gfp* coding sequence

into the 3' end of the *ceh-36* coding sequence flanked by the 2.5 kb 5' upstream and 1.1 kb 3' downstream genomic sequence. We integrated this *ceh-36::gfp* transgene into the *C. elegans* genome and found that the *ceh-36::gfp* transgene rescued the MI transformation defect of *ceh-36(n5333)* mutants (Table 4), indicating that this *ceh-36::gfp* is functional. We asked whether *ceh-36* is expressed in the cell lineage that gives rise to the MI neuron. We observed developing wild-type embryos carrying the *ceh-36::gfp* transgene and found that CEH-36::GFP was localized to the nucleus of the MI grandmother cell but not to that of the e3D grandmother cell (Figure 8A-C). CEH-36::GFP in the MI grandmother cell became detectable 25 minutes after this cell was generated. We also found that CEH-36::GFP was present in the nucleus of the MI mother cell but not in that of the e3D mother cell (Figure 8D-F). These results indicate that expression of *ceh-36* is left-right asymmetric and suggest that this left-right asymmetric expression of *ceh-36* triggers expression of *ngn-1* and *hlh-2* on the right side of the cell lineage but not on the left, leading to a bilaterally asymmetric neurogenesis that gives rise to the MI neuron.

Discussion

Bilateral asymmetry is a conserved and fundamental feature of nervous systems. Despite its importance, the molecular and cellular mechanisms that establish neuroanatomical asymmetry have been largely elusive. Although *Otx* homeodomain proteins and proneural bHLH transcription factors have been shown to play pivotal roles in neurogenesis, they have not previously been shown to establish bilateral asymmetry. In this study, we establish that two proneural bHLH genes, *ngn-1* and *hlh-2,* and the *Otx* homeodomain gene *ceh-36* are required for the generation of the single unpaired MI motor neuron by breaking left-right symmetry in an otherwise symmetric cell lineage. Our results indicate that expression of *ceh-36* is left-right asymmetric in this cell lineage and that CEH-36 proteins are present in the MI grandmother cell but not in the e3D grandmother cell. *ceh-36* is required for the left-right asymmetric expression of *ngn-1* and *hlh-2*. We propose that the asymmetric localization of CEH-36 proteins promotes left-right asymmetric expression of *ngn-1* and *hlh-2* in the MI grandmother cell but not in the e3D grandmother cell. The *ngn-1* and *hlh-2* products generated in the MI grandmother cell are then transmitted to the MI mother cell, leading to the formation of a heterodimer between NGN-1 and HLH-2 in the MI mother cell but not in the e3D mother cell. This asymmetric localization of NGN-1 and HLH-2 then induces an asymmetric neurogenic program, giving rise to the MI neuron on the right side of the cell lineage and the e3D epithelial cell on the left (Figure 8G). Thus, the left-right asymmetric activation of the *ceh-36, ngn-1* and *hlh-2* transcriptional cascade induces a bilaterally asymmetric neurogenic program that establishes left-right asymmetry in the cell lineage.

Our *ceh-36* mosaic analysis indicates that the presence of the *ceh-36* wild-type gene in the MI great grandmother cell (ABaraapp) is necessary and sufficient to generate an MI neuron. This observation suggests that transcription of *ceh-36* initiates in this cell (Figure 8G). Our expression analysis of *ceh-36* supports this notion: we observed a CEH-36::GFP functional protein localized to the nucleus of the MI grandmother cell 25 minutes after its generation. Because fluorophore formation of the variant of GFP we used requires at least 30 minutes (Heim et al. 1995), and because the MI great grandmother cell divides about 30 minutes after its generation to give rise to the MI grandmother cell, it is highly likely that transcription of *ceh-36* indeed initiates in the MI great grandmother cell. By contrast, our expression analysis of *ceh-36* indicates that CEH-36::GFP was not detectable in the e3D grandmother cell. This observation suggests that *ceh-36* is not transcribed in the e3D great grandmother cell, ABaraapa. We suggest that the developmental program establishing the bilateral asymmetry in this cell lineage is triggered by an asymmetric transcription of *ceh-36* in which *ceh-36* is transcribed in the MI great grandmother cell, ABaraapp, but not in the e3D great grandmother cell, ABaraapa (Figure 8G). The great grandmother cells of MI and e3D are the earliest precursor cells that separate the left and right sides of the cell lineage. Our results thus reveal that the determination of the left-right asymmetry of this cell lineage occurs at least three cell generations prior to the generation of MI and e3D and suggest that the commitment to produce this bilaterally asymmetric cell lineage occurs within ABaraapa and ABaraapp, the two blastomeres that generate the left and right branches of the cell lineage.

Our results indicate that mutations in genes required to establish the bilateral asymmetries of the AWC and ASE neurons do not affect the MI-e3D asymmetry and thus suggest that the *ceh-36*/*ngn-1*/*hlh-2* transcriptional cascade is a novel pathway that establishes a bilateral asymmetry in the *C. elegans* nervous system. The AWC bilateral asymmetry is established after the generation of the two post-mitotic AWC neurons through an interaction between these cells (e.g., Chuang et al. 2007). Likewise, the ASE bilateral asymmetry is established by a regulatory pathway that acts within the two post-mitotic ASE neurons (Johnston et al. 2005). By contrast, our results indicate that *ceh-36* and *ngn-1* act within dividing cells that are progenitors to MI and e3D to establish the MI-e3D bilateral asymmetry. Thus, our studies reveal a novel mechanism for how the asymmetric activation of a genetic pathway that functions through three rounds of cell division leads to an anatomical bilateral asymmetry manifested by post-mitotic differentiated cells.

Our finding that loss-of-function mutations in *ngn-1* and *ceh-36* caused transformation of the MI neuron into a non-neuronal e3D epithelial-like fate demonstrates that the role of neurogenin and *otx* genes in promoting neurogenesis is evolutionarily conserved from *C. elegans* to mammals (Fode et al. 1998; Ma et al. 1998; Omodei et al. 2008). Do these genes in vertebrates also act to establish bilateral asymmetry in the nervous system? The epithalamus of the diencephalon displays anatomical asymmetries in many vertebrate species (Concha and Wilson 2001). For example, in zebrafish the habenular nuclei in the dorsal diencephalon display anatomical left-right asymmetry (Concha et al. 2000). It has been shown that the establishment of this left-right difference in the habenular structure requires asymmetry in the timing of

neurogenesis (Aizawa et al. 2007) and that the habenula express the zebrafish *ngn1* gene (Mueller and Wullimann 2003). In addition, the zebrafish *ngn3* gene is asymmetrically expressed in the anterior-ventral diencephalon, with stronger expression on the left side than on the right (Wang et al. 2001). Furthermore, in mammals, *otx2* is required for the generation of the mesencephalic dopaminergic neurons, in which it promotes expression of *ngn2* in the mesencephalic dopaminergic progenitors (Omodei et al. 2008). It has been shown that *ngn2* is also required for the generation of the mesencephalic dopaminergic neurons, including those located in the retro-rubral area (Andersson et al. 2006), and that the retro-rubral area displays bilateral asymmetry in the number of the dopaminergic neurons (Zaborszky and Vadasz 2001). Given our results, these observations raise the intriguing possibility that an evolutionarily conserved transcriptional cascade composed of an *otx* homeodomain gene and a neurogenin bHLH gene is involved in establishment of nervous system bilateral asymmetry in many animals, including mammals.

Experimental Procedures

C. elegans Strains

C. elegans strains were cultured at 20 °C as described previously (Brenner 1974). N2 (Bristol) was the wild-type strain. The following extrachromosomal arrays, integrants and mutations were used and have been described (Riddle et al. 1997), except those from this study or otherwise indicated:

LG*I*: *dpy-5(e61), hlh-2(n5053, n5287)* (this study), *unc-13(e51), unc-55(e1170), inx-19(ky634*) (Chuang et al. 2007), *pop-1(q645)* (Siegfried and Kimble 2002).

LG*II*: *nIs362[D2096.6::pes-10::gfp, lin-15AB(+)]* (this study), *cog-1(ot28)* (Chang et al. 2003).

LG*III*: *nIs394[ngn-1::gfp, lin-15AB(+)]* (this study), *ynIs67[flp-6::gfp]* (Kim and Li 2004), *lin-12(n137sd, n941)*, *glp-1(e2141)*.

LG*IV*: *lin-1(e1275), ngn-1(n1921, n5020, n5052, ok2200)* (this study, *ok2200* was provided by the *C. elegans* Gene Knockout Consortium), *unc-17(e245), nIs407[hlh-2::gfp, lin-15AB(+)]* (this study), *unc-43(n498sd, n1186), nsy-4(ky616)* (Vanhoven et al. 2006), *lin-49(sa470)* (Chamberlin et al. 1999).

LG*V*: *nIs396[sams-5::gfp, lin-15AB(+)]* (this study).

LG*X*: *ceh-36(n5333, n5339, n5340, ok795Δ)* (this study, *ok795Δ* was provided by the *C. elegans* Gene Knockout Consortium), *kyIs258[odr-1::dsRed]* (Vanhoven et al. 2006), *lin-15AB(n765)*, *nIs363[D2096.6::pes-10::gfp, lin-15AB(+)]* (this study), *nIs445[ceh-36::gfp, lin-15AB(+)]* (this study), *lim-6(nr2073)* (Chang et al. 2003).

Extrachromosomal arrays: *nEx1538[ngn-1(+), lin-15AB(+), sur-5::gfp], nEx1564[ngn-1(frameshift), lin-15AB(+), sur-5::gfp], nEx1613[hlh-2(+), sur-5::gfp],*

nEx1622[hlh-2(frameshift), sur-5::gfp], nEx1638[ngn-1(+), sur-5::gfp, unc-119::gfp], nEx1703[ceh-36(+), sur-5::gfp, unc-119::gfp, lin-15AB(+)], nEx1704[ceh-36(frameshift), sur-5::gfp, unc-119::gfp, lin-15AB(+)] (all this study).

Isolation of *ngn-1(n1921, n5020 and n5052)* and *hlh-2(n5053)*

The wild-type N2 strain was mutagenized with ethyl methanesulfonate (EMS), and F_2 progeny were observed using Nomarski optics (Brenner 1974). *ngn-1(n5020* and *n5052)* and *hlh-2(n5053)*/+ were isolated from screens looking for animals in which the MI neuron was missing and an extra e3D-like epithelial cell was present. *ngn-1(n1921)* was recovered from screens looking for animals in which one or more extra neuronal cells were present in the anterior pharynx. The extra neuronal cells in the anterior pharynx of *ngn-1(n1921)* mutants result from a dislocation of the M2 neurons, which are normally located in the posterior pharynx (Ellis 1989).

Isolation of *ceh-36(n5333, n5339* and *n5340)*

Wild-type animals carrying the *D2096.6::pes-10::gfp* reporter were mutagenized with EMS, and F_3 progeny were observed using a fluorescence-equipped dissecting microscope. *ceh-36(n5333, n5339 and n5340)* were isolated as animals that contained an extra cell expressing the *D2096.6::pes-10::gfp* reporter.

Isolation of *hlh-2(n5287Δ)*

Genomic DNA pools from EMS-mutagenized animals were screened by PCR for deletion alleles of *hlh-2*, essentially as described (Jansen et al. 1997; Liu et al. 1999). *hlh-2(n5287Δ)* was isolated from a frozen stock and backcrossed to the wild type four times. The *hlh-2(n5287Δ)* allele removes sequence between nucleotide 18388 of cosmid M05B5 and nucleotide 2042 of cosmid C01H6 and inserts the 15 bp sequence GAGCAATGGCGGCAG at that site.

Identification of MI and e3D Cell Fate Reporters

As previously reported, the reporter *sams-5::gfp* is expressed in a single pharyngeal neuron of wild-type animals (The Genome BC *C. elegans* Gene Expression Consortium). We identified this cell as the MI neuron based on the morphology and position of its nucleus (Albertson and Thomson 1976). The *D2096.6::gfp* was previously shown to be expressed in pharyngeal epithelial cells, pharyngeal muscle cells, and pharyngeal marginal cells (Gaudet and Mango 2002). We generated a variant of the *D2096.6::gfp* reporter, *D2096.6::pes-10::gfp,* that retains expression in the e3 pharyngeal epithelial cells, including e3D, but lacks expression in the pharyngeal muscle cells or pharyngeal marginal cells.

Mapping of *n1921*

We isolated F_2 Lin non-Unc and Unc non-Lin progeny from the strain *lin-1(e1275) n1921 unc-17(e245)* after crossing with the wild-type polymorphic strain CB4856 and determined the presence or absence of *n1921* using Nomarski optics and by identifying crossover sites, essentially as described (Wicks et al. 2001). We mapped *n1921* to a 153-

kb interval between nucleotides 121452 of cosmid Y69A2AR and 8514 of cosmid Y54G2A.

Mapping of *n5333*

We isolated F_2 Dpy non-Unc and Unc non-Dpy progeny from the strain *nIs361; dpy-6(e14) n5333 unc-3(e151)* after crossing with the wild-type polymorphic strain CB4856 carrying *nIs361* and determined the presence or absence of *n5333* using a fluorescence-equipped dissecting microscope and by identifying crossover sites, essentially as described (Wicks et al. 2001). We mapped *n5333* to a 100-kb interval between nucleotides 4694 of cosmid R03E1 and 4554 of cosmid E02H4.

RNA Interference

We performed RNAi of *ngn-1* or *hlh-2* by growing *eri-1(mg366)* or wild-type animals, respectively, on HT115(DE3) *E. coli* harboring the *ngn-1* RNAi construct (pSN241) or the *hlh-2* RNAi construct (pSN243), respectively. The presence or absence of the MI neuron in the progeny of the animals grown on these bacteria was determined using Nomarski optics.

Cell Ablation

The wild-type or *ngn-1(n1921)* mutant embryos carrying the *D2096.6::pes-10::gfp* reporter were directly observed from the 28-cell stage until the generation of ABaraappa. Laser microsurgery of ABaraappa was performed as described previously (Avery and

Horvitz 1987). The operated embryos were recovered and grown at 20 °C. After hatching, the number of e3D-like epithelial cells was determined using the *D2096.6::pes-10::gfp* reporter.

Mosaic Analyses

We observed animals of genotype *ngn-1(n1921); nEx1638[ngn-1(+), sur-5::gfp, unc-119::gfp]* and of genotype *ceh-36(n5333) lin-15AB(n765); nEx1703[ceh-36(+), sur-5::gfp, unc-119::gfp, lin-15AB(+)]* using Nomarski optics equipped with epifluorescence. Fisher's tests were used for statistical analyses of the association between the fate specification of the MI neuron and the presence of the array in ABaraappaaa. To determine the cell division at which the array was lost in the Class IV animals, we determined the presence or absence of the array as judged by GFP fluorescence in the following cells: e1D, e1VL, e1VR, e2VR, e3D, e3VR, I2R, I5, M2L, M2R, M3L, M3R, mc2DL, mc2DR, MCR, NSML and NSMR. Based on the cell lineages that give rise to these cells (Sulston et al. 1983), we determined the cell division at which the array was lost.

Expression Analyses of *ngn-1::gfp*, *hlh-2::gfp* and *ceh-36::gfp*

Gravid hermaphrodites carrying the *ngn-1::gfp, hlh-2::gfp* and *ceh-36::gfp* reporters were dissected to obtain early-stage embryos. The cell divisions of these embryos were directly observed using Nomarski optics and epifluorescence.

Germline Transformation Experiments

Germline transformation experiments were performed as described (Mello et al. 1991). To generate animals carrying the *sams-5::gfp* reporter, we injected pSN363 into *lin-15AB(n765)* mutants at 50 ng/µl together with 20 ng/µl of EK L15, a *lin-15* rescuing plasmid (Clark et al. 1994). To generate animals carrying the *D2096.6::pes-10::gfp* reporter, we injected pSN330 into *lin-15AB(n765)* mutants at 80 ng/µl together with 25 ng/µl of EK L15. For transformation rescue of *ngn-1(n1921),* we injected pSN265*[ngn-1(+)]* or pSN286*[ngn-1(frameshift)]* into *ngn-1(n1921); lin-15AB(n765)* mutants at 5 ng/µl together with 25 ng/µl of EK L15 and pTG96*[sur-5::gfp]* (Yochem et al. 1998). For transformation rescue of *hlh-2(n5053),* we injected pSN292*[hlh-2(+)]* or pSN300*[hlh-2(frameshift)]* into the wild-type at 1 ng/µl together with 25 ng/µl of pTG96. The resulting animals carrying the extrachromosomal arrays were mated to transfer the arrays into an *hlh-2(n5053)*/+ background. To generate mosaic animals for *ngn-1*, we injected pSN265*[ngn-1(+)]* into *ngn-1(n1921)* mutants at 5 ng/µl together with 40 ng/µl of pTG96*[sur-5::gfp]* and 40 ng/µl of pSN276*[unc-119::gfp]*. For *ngn-1::gfp* and *hlh-2::gfp* expression analyses, we injected pSN349*[ngn-1::gfp]* or pSN372*[hlh-2::gfp]* into *lin-15AB(n765)* animals at 5 ng/µl or 1 ng/µl, respectively, together with 25 ng/µl of EK L15. For transformation rescue of *ceh-36(n5333)* and mosaic analysis of *ceh-36,* we injected pSN388*[ceh-36(+)]* or pSN394*[ceh-36(frameshift)]* into *ceh-36(n5333)* mutants at 5 ng/µl together with 40 ng/µl of pTG96*[sur-5::gfp]* and 40 ng/µl of pSN276*[unc-119::gfp]*. For *ceh-36::gfp* expression analysis, we injected pSN402*[ceh-36::gfp]* into *lin-15AB(n765)* animals at 20 ng/µl together with 25 ng/µl of EK L15.

Physical Interaction between His-NGN-1 and HLH-2

We purified His-NGN-1 proteins from an *E. coli* BL21(DE3) strain carrying pSN261 using an Ni-NTA (Qiagen) column and HLH-2 proteins from an *E. coli* ER2566 strain carrying pSN252 using the IMPACT™ system (New England BioLabs). Purified His-NGN-1 (1 μM) was mixed with HLH-2 protein or MBP (Maltose Binding Protein) (1μM) in the presence of Ni-NTA agarose, and the protein mixtures were washed three times. We eluted the proteins bound to the Ni-NTA with 200 mM imidazole solution and analyzed the amount of the HLH-2 or MBP proteins in the eluates by western blot analysis using anti-HLH-2 antibody (kindly provided by Michael Krause) or anti-MBP antibody (New England BioLabs).

Molecular biology

To create the *sams-5::gfp* reporter (pSN363), we amplified 447 bp of the *sams-5* genomic sequence by PCR using the wild-type genomic DNA and the primers 5'-GAGCATGCGTGGCACTCTCTATCCAGACA-3' and 5'-CTCTAGAAACTTGTTCTTGGACATTGTAGCA-3'. The resulting PCR product was digested by SphI and XbaI and cloned into the vector pPD122.56 digested by the same restriction enzymes. To create the *D2096.6::pes-10::gfp* reporter (pSN330), we amplified 1.7 kb of the *D2096.6* genomic sequence by PCR using the wild-type genomic DNA and the primers 5'-GCCAAGCTTGTGTTGGATACGGTGGAACA-3' and 5'-CTGCTAGCGGCTCGCGCAAGAGCACACTGT-3'. The resulting PCR product was digested by HindIII and NheI and cloned into the pPD122.53 digested by the same

restriction enzymes to generate pSN328. We further modified pSN328 to increase the GFP fluorescence signal. Expression of *D2096.6::gfp* was shown to be dependent on the transcription factor PHA-4, and introduction of an "UP" mutation (Gaudet and Mango 2002) into a PHA-4 binding site of the *D2096.6* promoter region was shown to increase the affinity of PHA-4 to the *D2096.6* promoter, resulting in an increase of the GFP fluorescence signal of the *D2096.6::gfp* reporter (Gaudet and Mango 2002). To generate the *D2096.6::pes-10::gfp* reporter (pSN330), we performed site-directed mutagenesis using pSN328 and the primers 5'-TCCAGTGTCCAGCCATCTGTTTGCGTCGTTTCAAATGCTCGA-3' and 5'-TCGAGCATTTGAAACGACGCAAACAGATGGCTGGACACTGGA-3' to introduce an UP mutation into the *D2096.6* promoter region of pSN328.

To generate an expression construct for His-NGN-1 (pSN261), we amplified a full-length *ngn-1* cDNA sequence by PCR using yk411e12 and the primers 5'-GCTGGTCATATGTACCATCATTCACCATTCT-3' and 5'-GCGGATCCTCAATGATGTGGGAAGCTTGG-3'. The resulting PCR product was digested by NdeI and BamHI and cloned into the vector pPROEX (Life Technologies) digested by the same restriction enzymes. To generate an expression construct for HLH-2 (pSN252), we amplified a full-length *hlh-2* cDNA sequence by PCR using yk492c11 and the primers 5'-GCACCATGGCGGATCCAAATAGCCA-3' and 5'-GGTGGTTGCTCTTCCGCAAAACCGTGGATGTCCAAACT-3'. The resulting PCR product was digested by NcoI and SapI and cloned into the vector pTYB3 (New England BioLabs) digested by the same restriction enzymes. To generate the *unc-119::gfp* reporter (pSN276), we amplified 2.3 kb of *unc-119* genomic sequence by PCR using the wild-

type genomic DNA and the primers 5'-GCGCATGCTCCAATCGGAAACGCGAACA-3' and 5'-GCTCTAGATTCATATATGCTGTTGTAGCTGA-3'. The resulting PCR product was digested by SphI and XbaI and cloned into the vector pPD122.56 digested by the same restriction enzymes. To generate the *ngn-1* genomic clone (pSN265) capable of rescuing the MI transformation defect caused by *n1921,* we transformed the yeast FY2 strain with the vector pRS426 (Christianson et al. 1992) digested by BamHI and XhoI and the six PCR products amplified using the wild-type genomic DNA and the following six pairs of the primers: 5'-GTAACGCCAGGGTTTTCCCAGTCACGACGCGCGAAAAGACAGCTGAAACGGT-3' and 5'-GTTTGCGCACTTCTGGGGCTACAGT-3', 5'-ACCCTTAGCACCCAGTTTTTAGGCTTC-3' and 5'-GGCGTGGCATAGATCCATTGGTAGA-3', 5'-GCTCGAAATGAGCTCTGAATTTCGGCGA-3' and 5'-GTCGATGCACCATGTCTGTTATTGCT-3', 5'-CCAAACACAGTGGAGATAGGCGCTAACA-3' and 5'-GGGCACCACTGTGGAAAATGACTGACT3', 5'-CCACCATATCTCCAGACTGGTGTTCCGGT-3' and 5'-GCCAAGTGAGAGCAAATTTGACTAGACGA-3', 5'-CACCATTCCAATCACCATGCTTCCCA-3' and 5'-GCGGATAACAATTTCACACAGGAAACAGCCTTGGATTGGATCAACATTTGGT-3'. Plasmid DNA was isolated from transformed yeast and amplified in TOP10 *E. coli* strain (Invitrogen). To generate the *ngn-1* genomic clone carrying a frameshift mutation (pSN286), we transformed the yeast FY2 strain as we did to generate pSN265 (see

above), except that one of the PCR products corresponding to the *ngn-1* coding sequence was generated by a two-step site-directed mutagenesis. In the first PCR amplification, two PCR products were obtained using the wild-type genomic DNA and the two sets of the primers: 5'-CCACCATATCTCCAGACTGGTGTTCCGGT-3' and 5'-TCCATATCATTTTCTCGTTCACATATCTAAATCTTGCTCGCCA-3', 5'-GCCAAGTGAGAGCAAATTTGACTAGACGA-3' and 5'-TGGCGAGCAAGATTTAGATATGTGAACGAGAAAATGATATGGA-3'. The resulting two PCR products were used for the template of the second PCR amplification using the primers 5'-CCACCATATCTCCAGACTGGTGTTCCGGT-3' and 5'-GCCAAGTGAGAGCAAATTTGACTAGACGA-3'. Plasmid DNA was isolated from transformants and transferred to and prepared from TOP10 *E. coli*. To generate a derivative of pRS426 with a reduced copy number in *E. coli* (pSN291), we amplified the *rop* gene using pBR322 and primers 5'-GGCACTAGTGGAACACCTACATCTGTATTAACGA-3' and 5'-CTATGAGCTCCGCTTACAGACAAGCTGTGACCGT-3'. The resulting PCR product was digested by SpeI and SacI and cloned into the vector pRS426 digested by the same restriction enzymes. To generate the *hlh-2* genomic clone (pSN292) capable of rescuing the lethality and transformation of the MI neuron into an e3D-like epithelial cell of *n5053,* we transformed the yeast FY2 strain with pSN291 digested with BamHI and XhoI and the six PCR products amplified using wild-type genomic DNA and the six pairs of the following primers: 5'-GTAACGCCAGGGTTTTCCCAGTCACGACGGCAACGGAGAGCCGATGTTACGGT-3' and 5'-CTTCCGACCGCACATCTGGTATTGGT-3', 5'-

GGATCTTGCACAATTGAGCTGGGT-3' and 5'-GCCGAATTTGCCGAATTTGCCGT-3', 5'-GTTGCCGTGCTTAACAAACTCGGA-3' and 5'-GTTGGCTATTTGGATCCGCCATTGA-3', 5'-CTTCAAATGGGGTTGTCTTGACGA-3' and 5'-GTTGAGAAATCACAGGACCTCCA-3', 5'-CGAGTTCGTGACATCAATTCGGCA-3' and 5'-GAGGCAGCCAGCTGGAATCAAATCT-3', 5'-CAGACAATCCTGTGGTTGTGTTGA-3' and 5'-CGTTAATACAGATGTAGGTGTTCCACTAGTGAGGTCCTTGACCAAAAGTGATCA-3'. Plasmid DNA was isolated from transformed yeast and amplified in TOP10 *E. coli*. To generate the *hlh-2* genomic clone carrying a frameshift mutation (pSN300), we transformed the yeast FY2 strain as we did to generate pSN292 (see above), except that one of the PCR products corresponding to the *hlh-2* coding sequence was generated by a two-step site-directed mutagenesis. In the first PCR amplification, two PCR products were obtained using the wild-type genomic DNA and the two sets of the primers: 5'-CTTCAAATGGGGTTGTCTTGACGA-3' and 5'-ATCCGTTGTTTGCACTCGGAGGATACGG-3', 5'-GTTGAGAAATCACAGGACCTCCA-3' and 5'-CCGTATCCTCCGAGTGCAAACAACGGAT-3'. The resulting two PCR products were used for the template of the second PCR amplification using the primers 5'-CTTCAAATGGGGTTGTCTTGACGA-3' and 5'-GTTGAGAAATCACAGGACCTCCA-3'. Plasmid DNA was isolated from transformed yeast and amplified in the TOP10 *E. coli*. To generate a translational *ngn-1::gfp* transgene (pSN349), we inserted a *gfp* coding sequence into the 3' end of the *ngn-1*

genomic sequence. We amplified the *gfp* coding sequence by PCR using pPD95.75 and primers 5'-TCAGAGCCCAAGCTTCCCACATCATAGCTTGCATGCCTGCAGGTCGA-3' and 5'-ACTTTGAACAAAAAATTGTGCTATTTGTATAGTTCATCCAT-3'. The resulting PCR product was used to transform the yeast FY2 strain together with pRS426 digested by BamHI and XhoI and the six PCR products using the wild-type genomic DNA and the six pairs of the following primers: 5'-GTAACGCCAGGGTTTTCCCAGTCACGACGCGCGAAAAGACAGCTGAAACGGT-3' and 5'-GTTTGCGCACTTCTGGGGCTACAGT-3', 5'-ACCCTTAGCACCCAGTTTTTAGGCTTC-3' and 5'-GGCGTGGCATAGATCCATTGGTAGA-3', 5'-GCTCGAAATGAGCTCTGAATTTCGGCGA-3' and 5'-GTCGATGCACCATGTCTGTTATTGCT-3', 5'-CCAAACACAGTGGAGATAGGCGCTAACA-3' and 5'-GGGCACCACTGTGGAAAATGACTGACT-3', 5'-CCACCATATCTCCAGACTGGTGTTCCGGT-3' and 5'-AGTCGACCTGCAGGCATGCAAGCTATGATGTGGGAAGCTTGGGCTCT-3', 5'-GCATGGATGAACTATACAAATAGCACAATTTTTTGTTCAAAGT-3' and 5'-GCGGATAACAATTTCACACAGGAAACAGCCTTGGATTGGATCAACATTTGGT-3'. Plasmid DNA was isolated from transformed yeast and amplified in TOP10 *E. coli*. To generate a translational *hlh-2::gfp* transgene (pSN372), a *gfp* coding sequence was inserted into the 3' end of the *hlh-2* genomic sequence. The *E. coli* SW102 strain (Warming et al. 2005) harboring the fosmid WRM0610DG01 (Source BioScience) was

transformed with a PCR product amplified using pGalK and primers: 5'-AAGATGCTTGATGACAATGCACCATCCGCGCAGTTTGGACATCCACGGTTTCCTGTTGACAATTAATCATCGGCA-3' and 5'-GATTGGGAATGATAGTTTGAAATGCTTAAAAAGTCAATTTTTAAATTTATCAGCACTGTCCTGCTCCTT-3'. Transformants capable of growing on plates containing galactose as a whole carbon source were subsequently transformed with a PCR product amplified using pPD95.75 and primers: 5'-AAGATGCTTGATGACAATGCACCATCCGCGCAGTTTGGACATCCACGGTTTAGCTTGCATGCCTGCAGGTCGA-3' and 5'-AGATTGGGAATGATAGTTTGAAATGCTTAAAAAGTCAATTTTTAAATTTATTTGTATAGTTCATCCATGCCA-3'. Transformants capable of growing on plates containing 2-deoxy-galactose and glycerol were selected. Plasmid DNA was prepared from the transformants and was verified to contain a recombined fosmid in which the *gfp* coding sequence was inserted into the 3' end of the *hlh-2* genomic sequence. To generate an *ngn-1* RNAi construct (pSN241), we amplified the third exon of the *ngn-1* gene by PCR using the wild-type genomic DNA and the primers 5'-GCTCTAGACGAGACGGGTTCCTGTGGCCT-3' and 5'-GCTCGAGTCAATGATGTGGGAAGCT-3'. The resulting PCR product was digested by XbaI and XhoI and cloned into the vector pPD129.36 digested by the same restriction enzymes. To generate an *hlh-2* RNAi construct (pSN243), we amplified the third exon of the *hlh-2* gene by PCR using the wild-type genomic DNA and the primers 5'-GCTCTAGAATGGTCTTGGTGGAGATACCA-3' and 5'-CGCAAGCTTTCTCGAGCATTATTCTGTGA-3'. The resulting PCR product was

digested by XbaI and HindIII and cloned into the vector pPD129.36 digested by the same restriction enzymes. To generate the *ceh-36* genomic clone (pSN388) capable of rescuing the MI transformation of *ceh-36(n5333)* mutants, we amplified 5.7 kbp of the *ceh-36* genomic sequence by PCR using the wild-type genomic DNA and the primers 5'-CCTAGGATTATGGTATTCGCAGACAGT-3' and 5'-GTGGTAGGGAACATTAATCCAGTGAGT-3'. The resulting PCR product was cloned into the pGEM-T easy vector (Promega). To generate a *ceh-36* genomic clone carrying a frameshift mutation (pSN394), we performed site-directed mutagenesis using pSN388 (see above) and the primers 5'-AGCGGTCGTCGAGCAGGTCGGCGGTGAACGTACCTCGTTCAACAGAGGA-3' and 5'-TCCTCTGTTGAACGAGGTACGTTCACCGCCGACCTGCTCGACGACCGCT-3'. To generate a *ceh-36* genomic clone carrying XmaI and NheI restriction enzyme sites (pSN398), we performed site-directed mutagenesis using pSN388 (see above) and the primers 5'-AAATATTACTGCCTACTCTCCACTTCCCGGGATGCGCTAGCTAAGTTTTGAATATTCCCTTTTG-3' and 5'-CAAAAGGGAATATTCAAAACTTAGCTAGCGCATCCCGGGAAGTGGAGAGTAGGCAGTAATATTT-3'. To generate a translational *ceh-36::gfp* transgene (pSN402), we amplified a *gfp* coding sequence using pPD95.79 and the primers 5'-GGATCCCCGGGATTGGCCAAAGGA-3' and 5'-CCGCTAGCGAAGTCAGAGGCACGGGCGCGAGA-3'. The resulting PCR product

was digested with XmaI and NheI and cloned into pSN398 (see above) digested by the same restriction enzymes.

Acknowledgments

We thank Yuji Kohara for *ngn-1* and *hlh-2* cDNA; Michael Krause for the HLH-2 antibody; Andy Fire for expression vectors; the *Caenorhabditis* Genetics Center, which is funded by the NIH National Center for Research Resources (NCRR), for strains; Na An, Beth Castor, Elissa Murphy, Rita Droste, Tove Ljungars and Nikhil Bhatla for technical assistance; and Brendan Galvin and Daniel Denning for critical reading of the manuscript. S.N. was supported in part by an MIT Praecis Presidential Fellowship and a McGovern Institute Schoemaker Graduate Fellowship. H.R.H is an Investigator of the Howard Hughes Medical Institute and the David H. Koch Professor of Biology at MIT.

References

Aizawa H, Goto M, Sato T, Okamoto H. 2007. Temporally regulated asymmetric neurogenesis causes left-right difference in the zebrafish habenular structures. *Dev Cell* **12**: 87-98.

Albertson DG, Thomson JN. 1976. The pharynx of *Caenorhabditis elegans*. *Philos Trans R Soc Lond B Biol Sci* **275**: 299-325.

Andersson E, Jensen JB, Parmar M, Guillemot F, Bjorklund A. 2006. Development of the mesencephalic dopaminergic neuron system is compromised in the absence of neurogenin 2. *Development* **133**: 507-516.

Austin J, Kimble J. 1989. Transcript analysis of *glp-1* and *lin-12*, homologous genes required for cell interactions during development of *C. elegans*. *Cell* **58**: 565-571.

Avery L, Horvitz HR. 1987. A cell that dies during wild-type *C. elegans* development can function as a neuron in a *ced-3* mutant. *Cell* **51**: 1071-1078.

Barth KA, Miklosi A, Watkins J, Bianco IH, Wilson SW, Andrew RJ. 2005. *fsi* zebrafish show concordant reversal of laterality of viscera, neuroanatomy, and a subset of behavioral responses. *Curr Biol* **15**: 844-850.

Brenner S. 1974. The genetics of *Caenorhabditis elegans*. *Genetics* **77**: 71-94.

Chamberlin HM, Brown KB, Sternberg PW, Thomas JH. 1999. Characterization of seven genes affecting *Caenorhabditis elegans* hindgut development. *Genetics* **153**: 731-742.

Chang S, Johnston RJ, Jr., Hobert O. 2003. A transcriptional regulatory cascade that controls left/right asymmetry in chemosensory neurons of *C. elegans*. *Genes Dev* **17**: 2123-2137.

Christianson TW, Sikorski RS, Dante M, Shero JH, Hieter P. 1992. Multifunctional yeast high-copy-number shuttle vectors. *Gene* **110**: 119-122.

Chuang CF, Vanhoven MK, Fetter RD, Verselis VK, Bargmann CI. 2007. An innexin-dependent cell network establishes left-right neuronal asymmetry in *C. elegans*. *Cell* **129**: 787-799.

Clark SG, Lu X, Horvitz HR. 1994. The *Caenorhabditis elegans* locus *lin-15*, a negative regulator of a tyrosine kinase signaling pathway, encodes two different proteins. *Genetics* **137**: 987-997.

Concha ML, Burdine RD, Russell C, Schier AF, Wilson SW. 2000. A nodal signaling pathway regulates the laterality of neuroanatomical asymmetries in the zebrafish forebrain. *Neuron* **28**: 399-409.

Concha ML, Wilson SW. 2001. Asymmetry in the epithalamus of vertebrates. *J Anat* **199**: 63-84.

Ellis RE, Massachusetts Institute of Technology. Dept. of Biology. 1989. A genetic analysis of the control and execution of programmed cell death in the nematode *Caenorhabditis elegans*. p. 229 leaves.

Fode C, Gradwohl G, Morin X, Dierich A, LeMeur M, Goridis C, Guillemot F. 1998. The bHLH protein NEUROGENIN 2 is a determination factor for epibranchial placode-derived sensory neurons. *Neuron* **20**: 483-494.

Gaudet J, Mango SE. 2002. Regulation of organogenesis by the *Caenorhabditis elegans* FoxA protein PHA-4. *Science* **295**: 821-825.

Grove CA, De Masi F, Barrasa MI, Newburger DE, Alkema MJ, Bulyk ML, Walhout AJ. 2009. A multiparameter network reveals extensive divergence between *C. elegans* bHLH transcription factors. *Cell* **138**: 314-327.

Heim R, Cubitt AB, Tsien RY. 1995. Improved green fluorescence. *Nature* **373**: 663-664.

Hobert O, Johnston RJ, Jr., Chang S. 2002. Left-right asymmetry in the nervous system: the *Caenorhabditis elegans* model. *Nat Rev Neurosci* **3**: 629-640.

Jansen G, Hazendonk E, Thijssen KL, Plasterk RH. 1997. Reverse genetics by chemical mutagenesis in *Caenorhabditis elegans*. *Nat Genet* **17**: 119-121.

Jarman AP, Grau Y, Jan LY, Jan YN. 1993. *atonal* is a proneural gene that directs chordotonal organ formation in the *Drosophila* peripheral nervous system. *Cell* **73**: 1307-1321.

Johnston RJ, Hobert O. 2003. A microRNA controlling left/right neuronal asymmetry in *Caenorhabditis elegans*. *Nature* **426**: 845-849.

Johnston RJ, Jr., Chang S, Etchberger JF, Ortiz CO, Hobert O. 2005. MicroRNAs acting in a double-negative feedback loop to control a neuronal cell fate decision. *Proc Natl Acad Sci U S A* **102**: 12449-12454.

Kim K, Li C. 2004. Expression and regulation of an FMRFamide-related neuropeptide gene family in *Caenorhabditis elegans*. *J Comp Neurol* **475**: 540-550.

Kimble J, Hirsh D. 1979. The postembryonic cell lineages of the hermaphrodite and male gonads in *Caenorhabditis elegans*. *Dev Biol* **70**: 396-417.

Koga M, Ohshima Y. 2004. The *C. elegans ceh-36* gene encodes a putative homemodomain transcription factor involved in chemosensory functions of ASE and AWC neurons. *J Mol Biol* **336**: 579-587.

Krause M, Park M, Zhang JM, Yuan J, Harfe B, Xu SQ, Greenwald I, Cole M, Paterson B, Fire A. 1997. A *C. elegans E/Daughterless* bHLH protein marks neuronal but not striated muscle development. *Development* **124**: 2179-2189.

Lanjuin A, VanHoven MK, Bargmann CI, Thompson JK, Sengupta P. 2003. *Otx/otd* homeobox genes specify distinct sensory neuron identities in *C. elegans*. *Dev Cell* **5**: 621-633.

Levin M. 2005. Left-right asymmetry in embryonic development: a comprehensive review. *Mech Dev* **122**: 3-25.

Lin R, Thompson S, Priess JR. 1995. *pop-1* encodes an HMG box protein required for the specification of a mesoderm precursor in early *C. elegans* embryos. *Cell* **83**: 599-609.

Liu LX, Spoerke JM, Mulligan EL, Chen J, Reardon B, Westlund B, Sun L, Abel K, Armstrong B, Hardiman G et al. 1999. High-throughput isolation of *Caenorhabditis elegans* deletion mutants. *Genome Res* **9**: 859-867.

Longo A, Guanga GP, Rose RB. 2008. Crystal structure of E47-NeuroD1/beta2 bHLH domain-DNA complex: heterodimer selectivity and DNA recognition. *Biochemistry* **47**: 218-229.

Ma Q, Chen Z, del Barco Barrantes I, de la Pompa JL, Anderson DJ. 1998. *neurogenin1* is essential for the determination of neuronal precursors for proximal cranial sensory ganglia. *Neuron* **20**: 469-482.

Maduro M, Pilgrim D. 1995. Identification and cloning of *unc-119*, a gene expressed in the *Caenorhabditis elegans* nervous system. *Genetics* **141**: 977-988.

Mello CC, Kramer JM, Stinchcomb D, Ambros V. 1991. Efficient gene transfer in *C. elegans*: extrachromosomal maintenance and integration of transforming sequences. *Embo J* **10**: 3959-3970.

Mueller T, Wullimann MF. 2003. Anatomy of neurogenesis in the early zebrafish brain. *Brain Res Dev Brain Res* **140**: 137-155.

Omodei D, Acampora D, Mancuso P, Prakash N, Di Giovannantonio LG, Wurst W, Simeone A. 2008. Anterior-posterior graded response to Otx2 controls proliferation and differentiation of dopaminergic progenitors in the ventral mesencephalon. *Development* **135**: 3459-3470.

Ortiz CO, Etchberger JF, Posy SL, Frokjaer-Jensen C, Lockery S, Honig B, Hobert O. 2006. Searching for neuronal left/right asymmetry: genomewide analysis of nematode receptor-type guanylyl cyclases. *Genetics* **173**: 131-149.

Pascual A, Huang KL, Neveu J, Preat T. 2004. Neuroanatomy: brain asymmetry and long-term memory. *Nature* **427**: 605-606.

Pierce-Shimomura JT, Faumont S, Gaston MR, Pearson BJ, Lockery SR. 2001. The homeobox gene *lim-6* is required for distinct chemosensory representations in *C. elegans*. *Nature* **410**: 694-698.

Poulin G, Turgeon B, Drouin J. 1997. NeuroD1/beta2 contributes to cell-specific transcription of the proopiomelanocortin gene. *Mol Cell Biol* **17**: 6673-6682.

Riddle DL, Blumenthal T, Meyer BJ, Priess J. 1997. *C. elegans II*. Cold Spring Harbor Laboratory Press, Plainview, N.Y.

Shiratori H, Hamada H. 2006. The left-right axis in the mouse: from origin to morphology. *Development* **133**: 2095-2104.

Siegfried KR, Kimble J. 2002. POP-1 controls axis formation during early gonadogenesis in *C. elegans*. *Development* **129**: 443-453.

Sulston JE, Horvitz HR. 1977. Post-embryonic cell lineages of the nematode, *Caenorhabditis elegans*. *Dev Biol* **56**: 110-156.

Sulston JE, Schierenberg E, White JG, Thomson JN. 1983. The embryonic cell lineage of the nematode *Caenorhabditis elegans*. *Dev Biol* **100**: 64-119.

Toga AW, Thompson PM. 2003. Mapping brain asymmetry. *Nat Rev Neurosci* **4**: 37-48.

Troemel ER, Sagasti A, Bargmann CI. 1999. Lateral signaling mediated by axon contact and calcium entry regulates asymmetric odorant receptor expression in *C. elegans*. *Cell* **99**: 387-398.

Vanhoven MK, Bauer Huang SL, Albin SD, Bargmann CI. 2006. The claudin superfamily protein NSY-4 biases lateral signaling to generate left-right asymmetry in *C. elegans* olfactory neurons. *Neuron* **51**: 291-302.

Wang X, Chu LT, He J, Emelyanov A, Korzh V, Gong Z. 2001. A novel zebrafish bHLH gene, *neurogenin3*, is expressed in the hypothalamus. *Gene* **275**: 47-55.

Warming S, Costantino N, Court DL, Jenkins NA, Copeland NG. 2005. Simple and highly efficient BAC recombineering using galK selection. *Nucleic Acids Res* **33**: e36.

Wes PD, Bargmann CI. 2001. *C. elegans* odour discrimination requires asymmetric diversity in olfactory neurons. *Nature* **410**: 698-701.

Wicks SR, Yeh RT, Gish WR, Waterston RH, Plasterk RH. 2001. Rapid gene mapping in *Caenorhabditis elegans* using a high density polymorphism map. *Nat Genet* **28**: 160-164.

Yochem J, Gu T, Han M. 1998. A new marker for mosaic analysis in *Caenorhabditis elegans* indicates a fusion between hyp6 and hyp7, two major components of the hypodermis. *Genetics* **149**: 1323-1334.

Yochem J, Weston K, Greenwald I. 1988. The *Caenorhabditis elegans lin-12* gene encodes a transmembrane protein with overall similarity to *Drosophila* Notch. *Nature* **335**: 547-550.

Yu S, Avery L, Baude E, Garbers DL. 1997. Guanylyl cyclase expression in specific sensory neurons: a new family of chemosensory receptors. *Proc Natl Acad Sci U S A* **94**: 3384-3387.

Zaborszky L, Vadasz C. 2001. The midbrain dopaminergic system: anatomy and genetic variation in dopamine neuron number of inbred mouse strains. *Behav Genet* **31**: 47-59.

Table 1.

ngn-1, *hlh-2* and *ceh-36* mutations cause symmetry in a normally asymmetric cell lineage

(A) *ngn-1*, *hlh-2* and *ceh-36* mutants fail to generate the MI neuron

Genotype	% animals missing MI [c]	*n*
wild-type	0	50
ngn-1(n1921)	98	100
ngn-1(n5020)	97	100
ngn-1(n5052)	62	100
ngn-1(ok2200Δ)	99	100
hlh-2(n5053)/ + [a]	30	100
hlh-2(n5287Δ)/ + [a]	32	100
ceh-36(n5333)	94	100
ceh-36(n5339)	42 [d]	100
ceh-36(n5340)	91 [d]	100
ceh-36(ok795Δ)[b]	93	82

(B) *ngn-1*, *hlh-2* and *ceh-36* mutants generate an extra e3D-like epithelial cell

Genotype	% animals with one or two e3D-like cells [e]		*n*
	one e3D-like cell	two e3D-like cells	
wild-type	100	0	50
ngn-1(n1921)	5	95	100
ngn-1(n5020)	9	91	100

ngn-1(n5052)	42	58	100
ngn-1(ok2200Δ)	2	98	100
hlh-2(n5053)/ + [a]	87	13	100
hlh-2(n5287Δ)/ + [a]	85	15	100
ceh-36(n5333)	3	97	100
ceh-36(n5339)	51	49	100
ceh-36(n5340)	5	95	100
ceh-36(ok795Δ)[b]	4	96	98

(C) Ablation of the MI grandmother prevents the generation of the extra e3D-like epithelial cell

		% animals with one or two e3D-like cells [e]		
Genotype	Cell ablated	one e3D-like cell	two e3D-like cells	*n*
wild-type	None	100	0	50
ngn-1(n1921)	None	4	96	50
wild-type	ABaraappa	100	0	3
ngn-1(n1921)	ABaraappa	100	0	5

[a] To score *hlh-2(n5053)/+* and *hlh-2(n5287Δ)/ +* animals, we allowed hermaphrodites of genotype *dpy-5(e61) + unc-13(e51)/ + hlh-2 +* to self-fertilize and examined their non-Dpy non-Unc progeny.

[b] To score *ceh-36(ok795Δ)* animals, we allowed hermaphrodite of genotype *ceh-36(ok795Δ)/+* to self-fertilize and examined progeny that arrested development at the first larval stage.

[c] The absence of the MI neuron was determined using an MI cell-fate marker, *sams-5::gfp*. All strains were homozygous for the *sams-5::gfp* reporter *nIs396*. The populations of animals of

each genotype examined in (A) were different from those examined in (B).

[d] The absence of the MI neuron in these animals was determined using Nomarski microscopy.

[e] The number of the e3D-like epithelial cells was determined using an e3D cell-fate marker, *D2096.6::pes-10::gfp*. All strains except for *ceh-36(ok795Δ)* were homozygous for the *D2096.6::pes-10::gfp* reporter *nIs363*. The number of the e3D-like epithelial cells in *ceh-36(ok795Δ)* mutants was determined using the *D2096.6::pes-10::gfp* reporter *nIs362*.

Table 2. Rescue experiments by *ngn-1* and *hlh-2* transgenes

(A) Rescue of *ngn-1(n1921)* by *ngn-1* transgenes

Genotype	% animals missing MI [a]	*n*
wild-type	0	50
ngn-1(n1921)	96	50
ngn-1(n1921); nEx[ngn-1(+)]	8	50
ngn-1(n1921); nEx[ngn-1(frameshift)]	94	50
ngn-1(n1921); nIs[ngn-1::gfp]	4	50

(B) Rescue of *hlh-2(n5053)* by *hlh-2* transgenes

Genotype	% animals missing MI [a]	*n*
wild-type	0	50
hlh-2(n5053)/ + [b]	32	50
hlh-2(n5053)/+; nEx[hlh-2(+)] [b]	0	50
hlh-2(n5053)/+; nEx[hlh-2(frameshift)] [b]	26	50
hlh-2(n5053)/+; nIs[hlh-2::gfp] [b]	0	50

(C) Rescue of embryonic lethality in *hlh-2(n5053)* mutants by the *hlh-2* transgenes

Transgene present in the parent of *dpy-5(e61) hlh-2(n5053) unc-13(e51)/ +++*	% Dpy Unc progeny [c]	*n*
no transgene	0	647
nEx[hlh-2(+)]	12	348
nEx[hlh-2(frameshift)]	0	313

nIs[hlh-2::gfp]	18	296

[a] The presence or absence of the MI neuron was determined using Nomarski microscopy.

[b] We allowed hermaphrodites of genotype *dpy-5(e61)* + + *unc-55(e1170)* / + *hlh-2(n5053) unc-13(e51)* + with or without each transgene to self-fertilize and examined their Non-Dpy non-Unc progeny.

[c] We allowed hermaphrodites of genotype *dpy-5(e61) hlh-2(n5053) unc-13(e51)*/ +++ with or without each transgene to self-fertilize and determined the fraction of Dpy Unc progeny.

Table 3. RNA interference of *ngn-1* and *hlh-2* cause symmetry in a normally asymmetric cell lineage

Genotype [a]	% animals missing MI [b]	*n*
vector(RNAi)	0	50
hlh-2(RNAi)	62	100
eri-1(mg366); vector(RNAi)	0	50
eri-1(mg366); ngn-1(RNAi)	92	100

[a] The wild-type or *eri-1(mg366)* strain was grown on bacteria expressing the double-stranded RNA, and the presence or absence of the MI neuron in their progeny was scored using Nomarski microscopy.

[b] The presence or absence of the MI neuron was determined using Nomarski microscopy.

Table 4. Rescue experiments demonstrating that *ceh-36* is required to break left-right symmetry in the cell lineage

Genotype	% animals missing MI [a]	*n*
wild-type	0	50
ceh-36(n5333)	96	50
ceh-36(n5333); nEx[ceh-36(+)]	4	50
ceh-36(n5333); nEx[ceh-36(frameshift)]	96	50
ceh-36(n5333); nIs[ceh-36::gfp]	4	50

[a] The presence or absence of the MI neuron was determined using Nomarski microscopy.

Table 5. Candidate-gene approaches did not identify genes required to establish the bilateral asymmetry in the ABaraap cell lineage

(A) Mutations affecting the ASE bilateral asymmetry do not affect the MI-e3D asymmetry

Genotype	% MI or e3D absent [a]	*n*
wild-type	0	50
cog-1(ot28)	0	50
lim-6(nr2073)	0	50
lin-49(sa470)	0	50
lsy-6(ot71)	0	50

(B) Mutations affecting the AWC bilateral asymmetry do not affect the MI-e3D asymmetry

Genotype	% MI or e3D absent [a]	*n*
wild-type	0	50
inx-19(ky634)	0	50
nsy-4(ky616)	0	50
unc-43(n498 n1186)	0	50
unc-43(n498sd)	0	50

(C) Mutations in *lin-12*, *glp-1* and *pop-1* do not affect the MI-e3D bilateral asymmetry

Genotype	% MI or e3D absent [a]	*n*
wild-type	0	50

lin-12(n137sd)	0	50
lin-12(n941)[b]	0	30
pop-1(q645)[b]	0	30
glp-1(e2141)	0	30

[a] The presence or absence of MI and e3D was determined using Nomarski microscopy.

[b] To score these animals, we allowed hermaphrodites of genotype *pop-1/hT2[qIs48]* and *lin-12/hT2[qIs48]* to self-fertilize and examined their *myo-2::gfp*-negative progeny.

Table 6. *ngn-1* is not required for the general cell-fate specification of the ASE neurons

Genotype [a]	% animals with zero, one or two ASEs expressing *flp-6::gfp*			*n*
	zero ASE	one ASE	two ASEs	
wild-type	0	0	100	30
ngn-1(ok2200Δ)	0	0	100	30

[a] All strains were homozygous for the *flp-6::gfp* reporter *ynIs67*.

Table 7. *ngn-1* is required for the general cell-fate specification of the AWC neurons

Genotype [a]	% animals with zero, one or two AWCs expressing *odr-1::dsRed*			*n*
	zero AWC	one AWC	two AWCs	
wild-type	0	0	100	50
ngn-1(ok2200Δ)	5	44	46	50
ngn-1(ok2200Δ); nEx[ngn-1(+)]	0	2	98	50

[a] All strains were homozygous for the *odr-1::dsRed* reporter *kyIs258*.

Figures

Figure 1. The MI Neuron Is Generated from a Left-right Asymmetric Cell Lineage. (A) In the wild type, left-right asymmetry in the ABaraap cell lineage is seen in the different cell fates of the MI neuron and the e3D epithelial cell. (B) In *ngn-1, hlh-2* and *ceh-36* mutants, left-right asymmetry in the cell lineage is lost as a result of the cell-fate transformation of the presumptive MI neuron into an e3D-like cell. (C, D) The predicted ABaraap cell lineages of (C) the wild type and (D) *n1921* mutants after laser ablation of the grandmother cell of the MI neuron, ABaraappa. X in red indicates the cell killing of ABaraappa by laser microsurgery.

Figure 1.

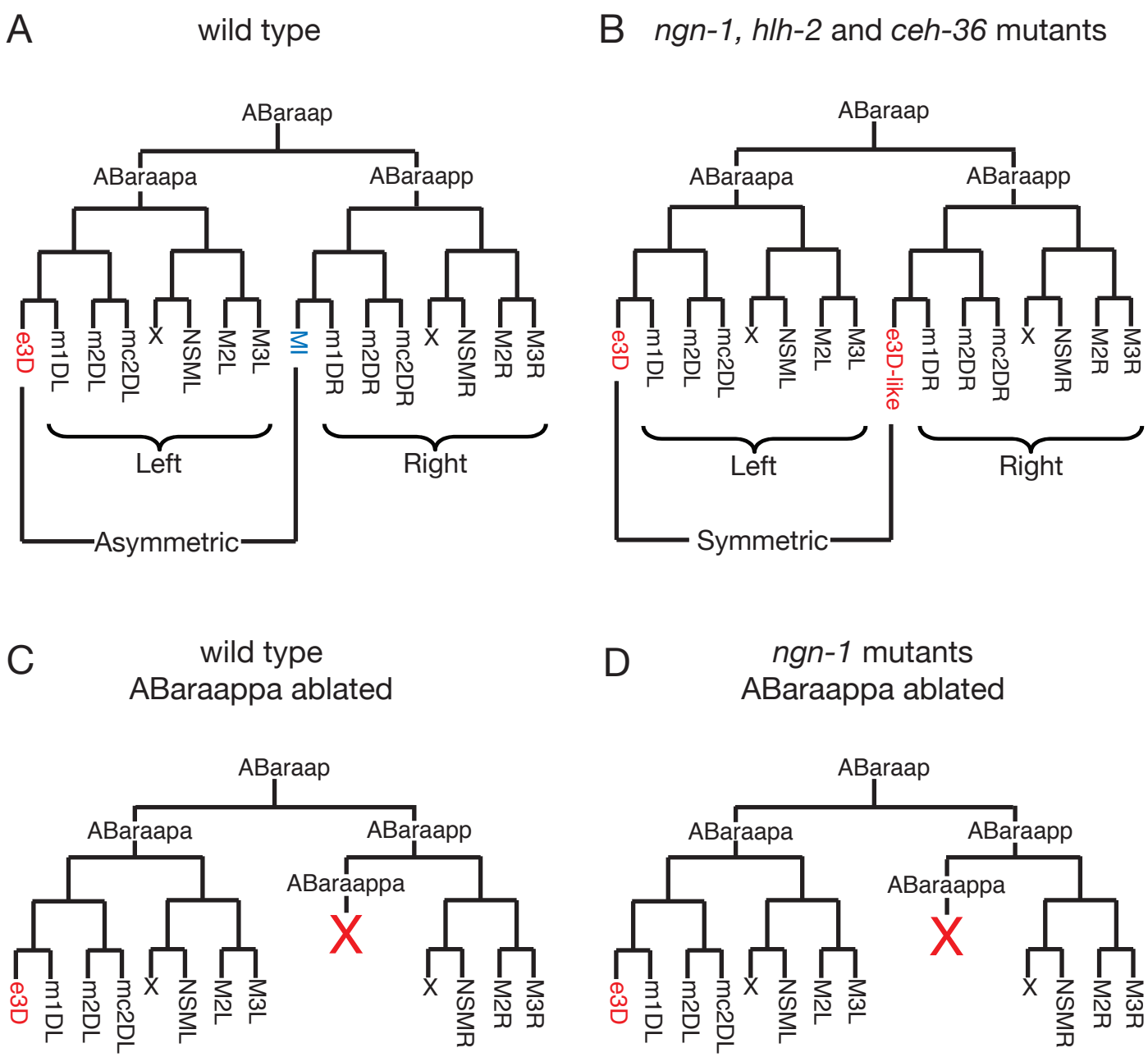
A
wild type
ABaraap
ABaraapa
ABaraapp
e3D
m1DL
m2DL
mc2DL
X
NSML
M2L
M3L
MI
m1DR
m2DR
mc2DR
X
NSMR
M2R
M3R
Left
Right
Asymmetric
B
ngn-1, hlh-2 and ceh-36 mutants
ABaraap
ABaraapa
ABaraapp
e3D
m1DL
m2DL
mc2DL
X
NSML
M2L
M3L
e3D-like
m1DR
m2DR
mc2DR
X
NSMR
M2R
M3R
Left
Right
Symmetric
C
wild type
ABaraappa ablated
ABaraap
ABaraapa
ABaraapp
ABaraappa
X
e3D
m1DL
m2DL
mc2DL
X
NSML
M2L
M3L
X
NSMR
M2R
M3R
D
ngn-1 mutants
ABaraappa ablated
ABaraap
ABaraapa
ABaraapp
ABaraappa
X
e3D
m1DL
m2DL
mc2DL
X
NSML
M2L
M3L
X
NSMR
M2R
M3R

Figure 2. *ngn-1(n1921), hlh-2(n5053)* and *ceh-36(n5333)* Cause Transformation of the MI Neuron into an e3D-like Epithelial Cell. (A) Nomarski image of a region of the anterior wild-type pharynx. The wild-type pharynx contains the MI neuron (arrow) and the e3D epithelial cell (arrowhead). The nucleus of the MI neuron is small and granular, while that of the e3D epithelial cell is larger, oval in shape, and has a distinct nucleolus. (B-D) Nomarski image of a region of anterior (B) *ngn-1(n1921),* (C) *hlh-2(n5053)* and (D) *ceh-36(n5333)* pharynges. The pharynx in these mutants lacks the MI neuron (dotted arrow) and contains two e3D-like epithelial cells (arrowheads). (E) *sams-5::gfp* reporter expression in the wild type. The *sams-5::gfp* reporter is expressed in the MI neuron (arrow). (F-H) *sams-5::gfp* reporter expression in (F) *ngn-1(n1921)*, (G) *hlh-2(n5053)* and (H) *ceh-36(n5333)* mutants. The *sams-5::gfp* reporter failed to be expressed in the pharynx of these mutants. (I) *D2096.6::pes-10::gfp* reporter expression in the wild type. The *D2096.6::pes-10::gfp* reporter was expressed in the e3D epithelial cell (arrowhead). (J-L) *D2096.6::pes-10::gfp* reporter expression in (J) *ngn-1(n1921)*, (K) *hlh-2(n5053)* and (L) *ceh-36(n5333)* mutants. The *D2096.6::pes-10::gfp* reporter was expressed in the e3D epithelial cell and the extra e3D-like epithelial cell (arrowheads). Scale bar, 5 μm.

Figure 2.

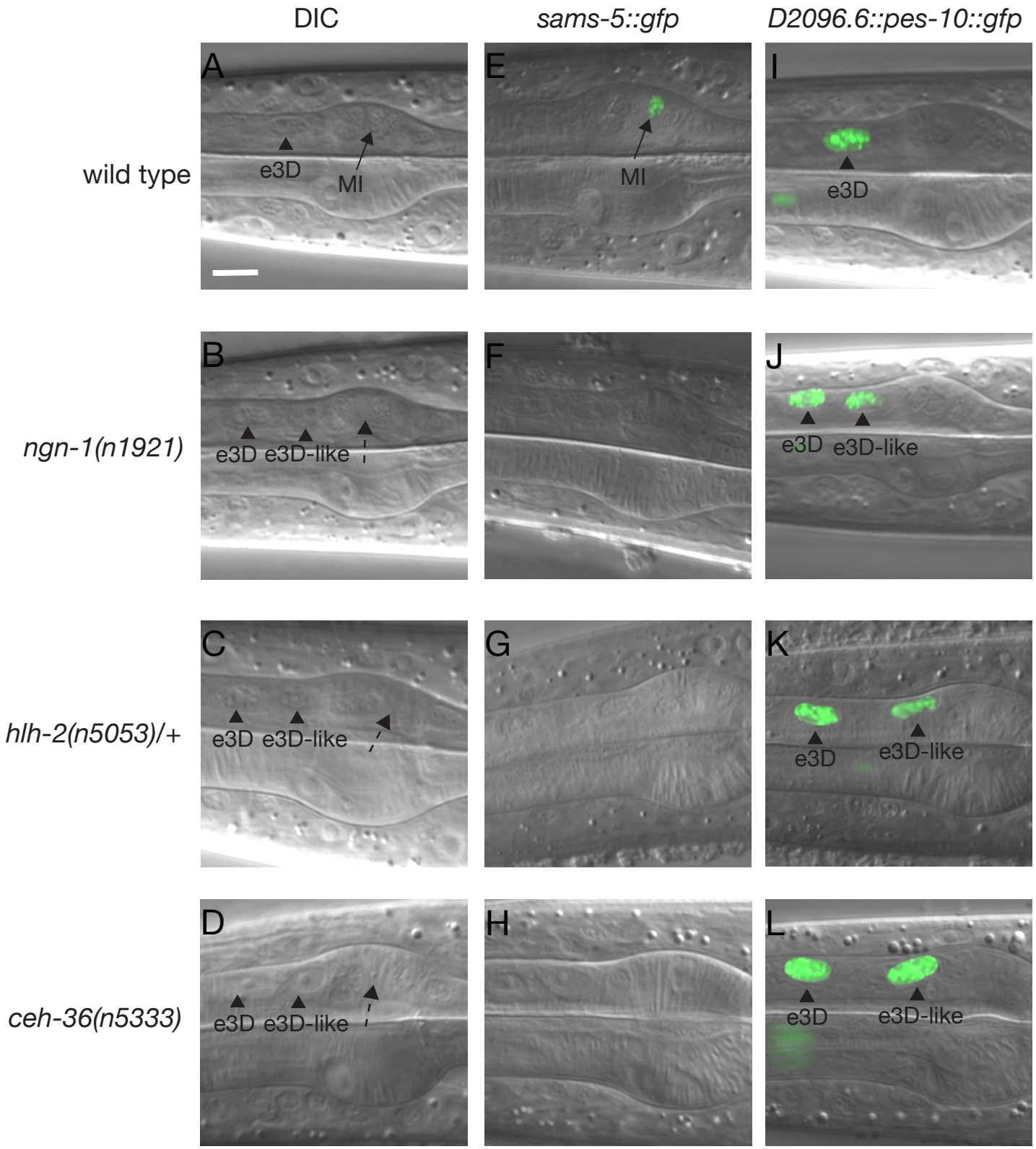
DIC
sams-5::gfp
D2096.6::pes-10::gfp
wild type
ngn-1(n1921)
hlh-2(n5053)/+
ceh-36(n5333)
A
B
C
D
E
F
G
H
I
J
K
L
e3D
MI
e3D-like

Figure 3. NGN-1 is a bHLH Protein of the Neurogenin Subfamily. Alignment of the bHLH domain of the predicted NGN-1 protein (accession no. NP_500236) with its *Xenopus tropicalis* homolog *neurog 1* (accession no. NP_001116895), *Danio rerio* homolog Neurog 1 (accession no. NP_571116), and *Mus musculus* homolog NEUROG 3 (accession no. NP_033849). Black and gray boxes indicate residues identical and similar among the four proteins, respectively.

Figure 3.

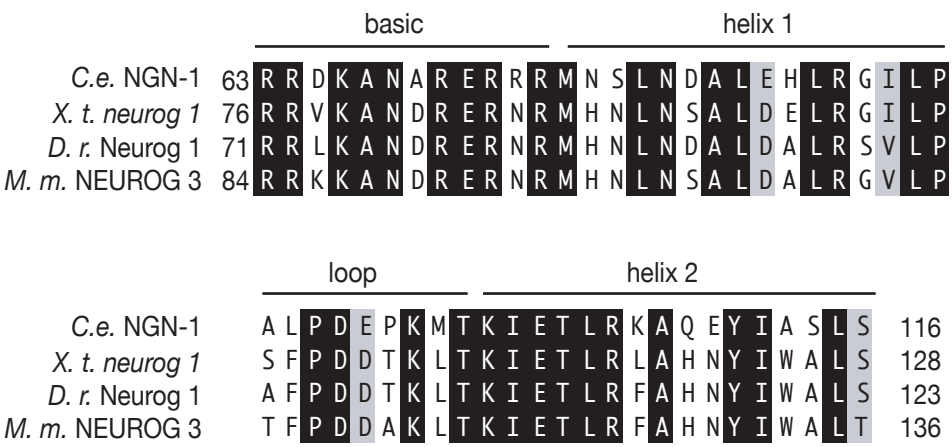
basic
helix 1
C.e. NGN-1 63 R R D K A N A R E R R R M N S L N D A L E H L R G I L P
X. t. neurog 1 76 R R V K A N D R E R N R M H N L N S A L D E L R G I L P
D. r. Neurog 1 71 R R L K A N D R E R N R M H N L N D A L D A L R S V L P
M. m. NEUROG 3 84 R R K K A N D R E R N R M H N L N S A L D A L R G V L P
loop
helix 2
C.e. NGN-1 A L P D E P K M T K I E T L R K A Q E Y I A S L S 116
X. t. neurog 1 S F P D D T K L T K I E T L R L A H N Y I W A L S 128
D. r. Neurog 1 A F P D D T K L T K I E T L R F A H N Y I W A L S 123
M. m. NEUROG 3 T F P D D A K L T K I E T L R F A H N Y I W A L T 136

Figure 4. NGN-1 Binds to HLH-2 and Acts Cell-Autonomously. (A) Gene structure of *ngn-1* and mutations associated with each mutant are shown. The black boxes indicate exons, and white boxes untranslated regions. (B) Gene structure of *hlh-2* and mutations associated with *hlh-2* mutants are shown. The black boxes indicate exons, and white boxes untranslated regions. (C) *In vitro* pull-down experiments between hexa-histidine-tagged NGN-1 (His-NGN-1) and HLH-2. Proteins included in each reaction are indicated. The amounts of HLH-2 protein (left panel) and MBP protein (right panel) in the initial reaction mixture (10% input) and in the bound fraction (Pull down) after extensive washing was determined by western blot analyses. The numbers indicate the positions of molecular weight markers. (D) Mosaic analysis of *ngn-1*. Mosaic animals were grouped into four classes based on cell fates and the presence of the extrachromosomal array in ABaraappaaa (see text). The number of mosaic animals in each class is indicated. (E) Determination of the site of the extrachromosomal array loss in each of the 36 Class IV animals with an e3D-like ABaraappaaa cell lacking the array. A portion of the cell lineage showing the origin of ABaraappaaa is shown. The numbers represent the fraction of Class IV animals in which the extrachromosomal array was lost at the corresponding cell division.

Figure 4.

A

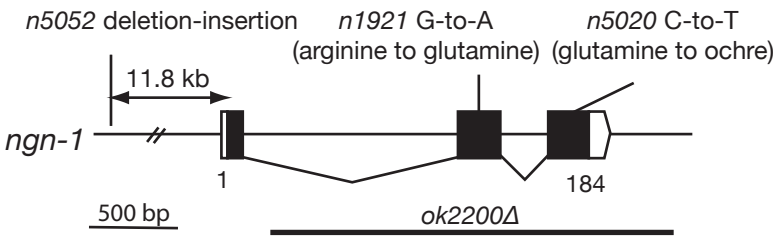

B

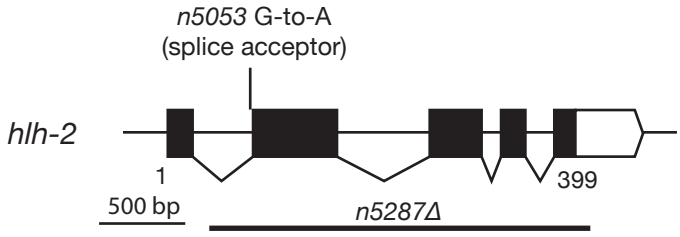

C

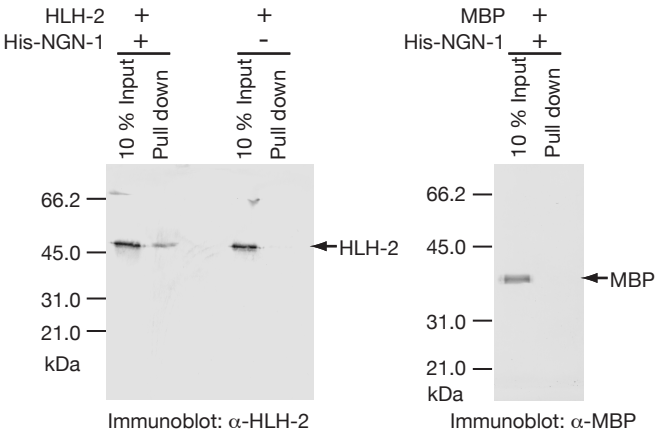

D

GFP expression in ABaraappaaa	ABaraappaaa fate: MI neuronal	ABaraappaaa fate: e3D-like epithelial
positive	251 (Class I)	0 (Class III)
negative	13 (Class II)	36 (Class IV)

E

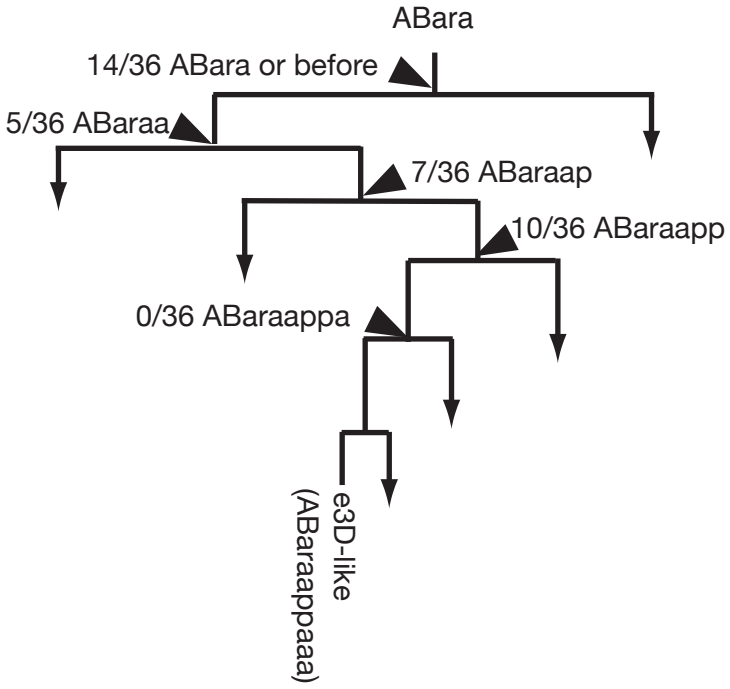

Figure 5. The deletion-insertion Mutation Associated with *ngn-1(n5052).* The gene structures of *ngn-1* and *mdf-2* are shown. The black boxes indicate exons, the white boxes untranslated regions. The DNA sequences of the wild-type and *ngn-1(n5052)* strains are aligned. Uppercase letters correspond to the DNA sequence present in both strains (indicated by the asterisks) and lowercase letters to the DNA sequence associated with the deletion-insertion mutation.

Figure 5.

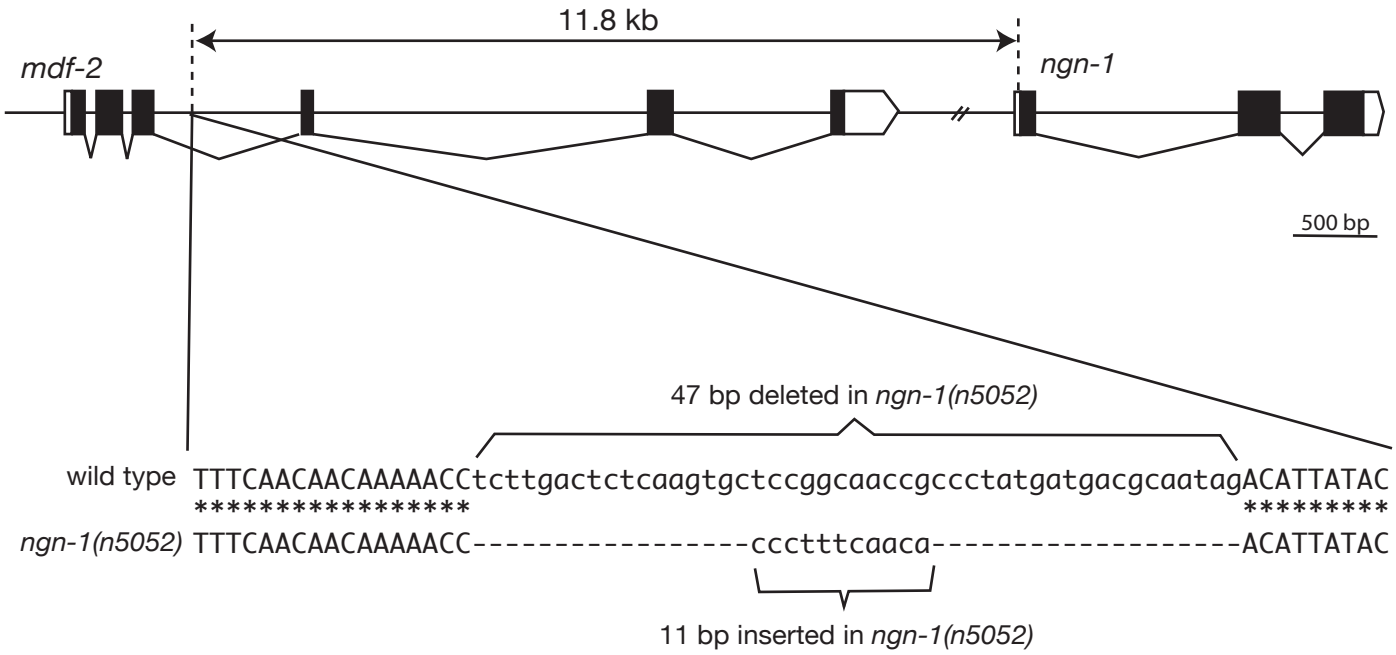
11.8 kb
mdf-2
ngn-1
500 bp
47 bp deleted in ngn-1(n5052)
wild type TTTCAACAACAAAAACCtcttgactctcaagtgctccggcaaccgccctatgatgacgcaatagACATTATAC
****
****
ngn-1(n5052) TTTCAACAACAAAAACC----------ccctttcaaca----------ACATTATAC
11 bp inserted in ngn-1(n5052)

Figure 6. Expression of *ngn-1* and *hlh-2* Is Left-right Asymmetric. (A) Nomarski image of a wild-type embryo carrying *ngn-1::gfp*. (B) Fluorescence image of the same embryo. (C) Merged image of (A) and (B). (D) Nomarski image of a *ceh-36(n5333)* mutant embryo carrying *ngn-1::gfp*. (E) Fluorescence image of the same embryo. (F) Merged image of (D) and (E). (G) Nomarski image of a wild-type embryo carrying *hlh-2::gfp*. (H) Fluorescence image of the same embryo. (I) Merged image of (G) and (H). (J) Nomarski image of a *ceh-36(n5333)* embryo carrying *hlh-2::gfp*. (K) Fluorescence image of the same embryo. (L) Merged image of (J) and (K). The arrows indicate the MI mother cell, ABaraappaa, and the arrowheads the e3D mother cell, ABaraapaaa. Anterior is to the left, ventral to the top. Scale bar, 5 μm.

Figure 6.

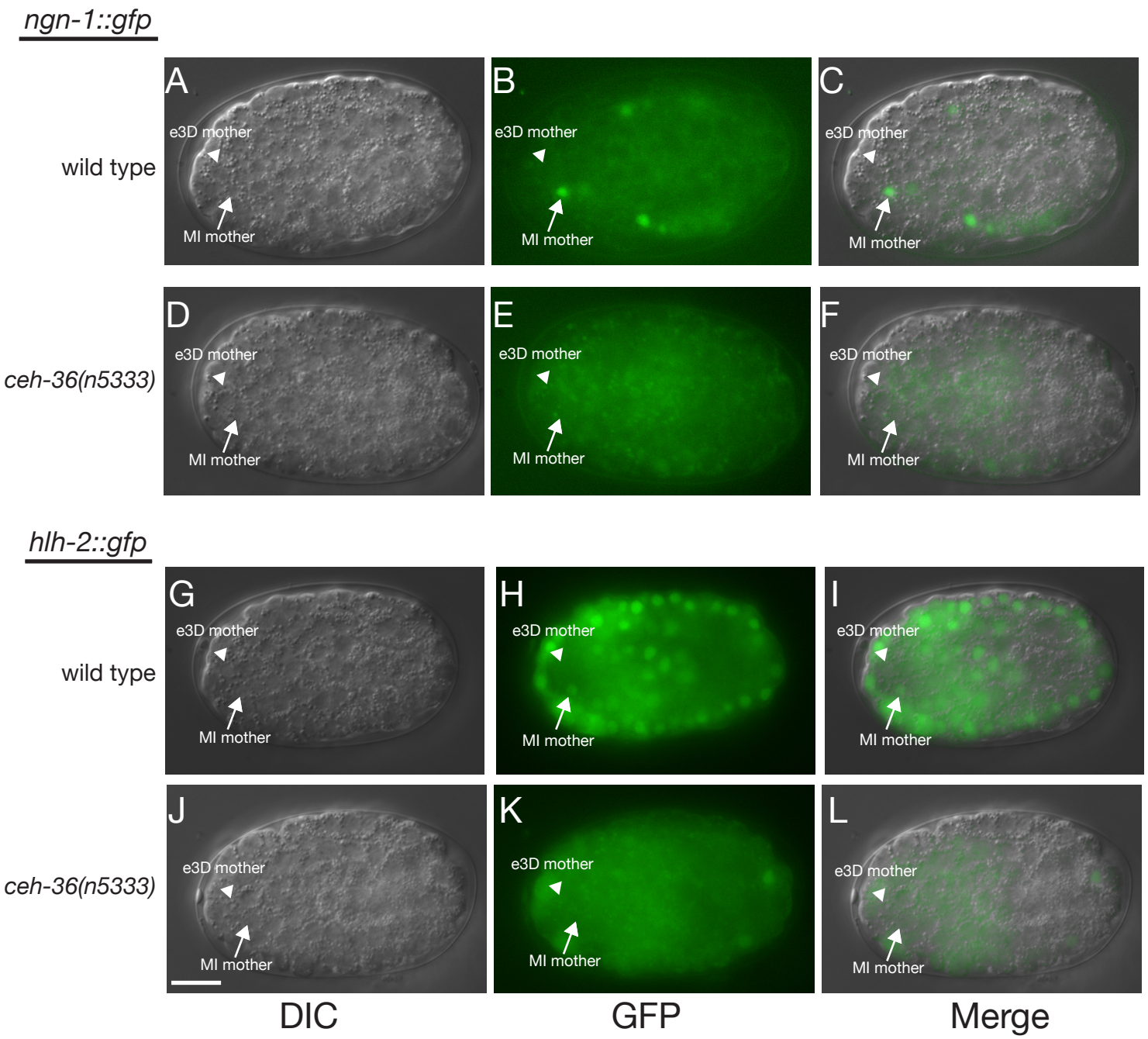
ngn-1::gfp
wild type
ceh-36(n5333)
hlh-2::gfp
wild type
ceh-36(n5333)
A
B
C
D
E
F
G
H
I
J
K
L
e3D mother
MI mother
DIC
GFP
Merge

Figure 7. *ceh-36* Acts Cell-Autonomously to Establish a Bilateral Asymmetry. (A) Gene structure of *ceh-36* and mutations associated with each mutant are shown. The black boxes indicate exons, and white boxes untranslated regions. (B) Mosaic analysis of *ceh-36*. Mosaic animals were grouped into four classes based on cell fates and the presence of the extrachromosomal array in ABaraappaaa (see text). The number of mosaic animals in each class is indicated. (C) Determination of the site of the extrachromosomal array loss in each of the 28 Class IV animals with an e3D-like ABaraappaaa cell lacking the array. A portion of the cell lineage showing the origin of ABaraappaaa is shown. The numbers represent the fraction of the Class IV animals in which the extrachromosomal array was lost at the corresponding cell division. (D) Cell lineage diagram indicates the sites of actions of *ceh-36* and *ngn-1*. The wild-type *ceh-36* gene in the MI great grandmother cell (ABaraapp) is necessary and sufficient to rescue the MI transformation of *ceh-36(n5333)* mutants. The wild-type *ngn-1* gene in the MI grandmother cell (ABaraappa) is necessary and sufficient to rescue the MI transformation of *ngn-1(n1921)* mutants.

Figure 7.

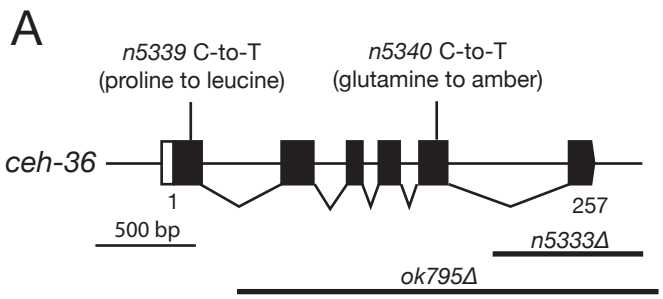

B

GFP expression in ABaraappaaa	ABaraappaaa fate: MI neuronal	ABaraappaaa fate: e3D-like epithelial
positive	288 (Class I)	0 (Class III)
negative	34 (Class II)	28 (Class IV)

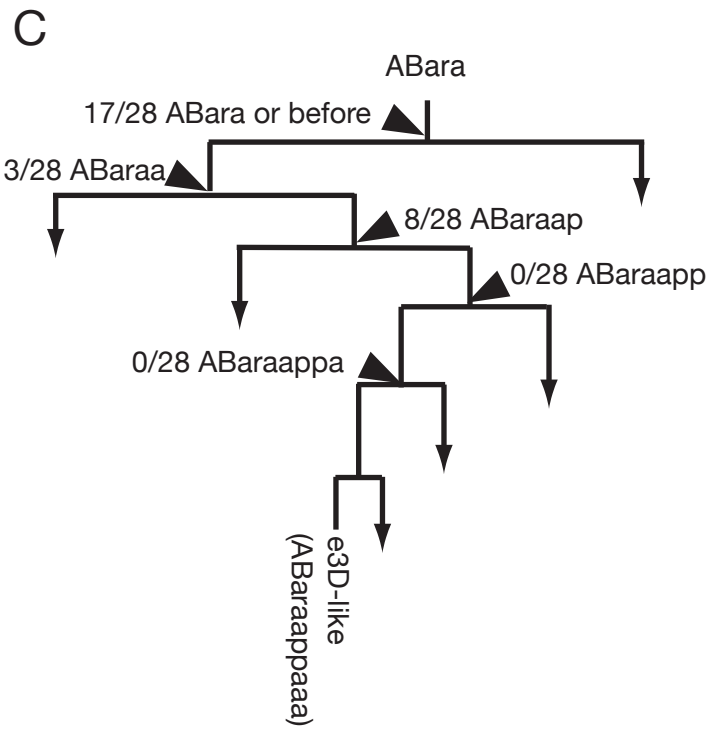

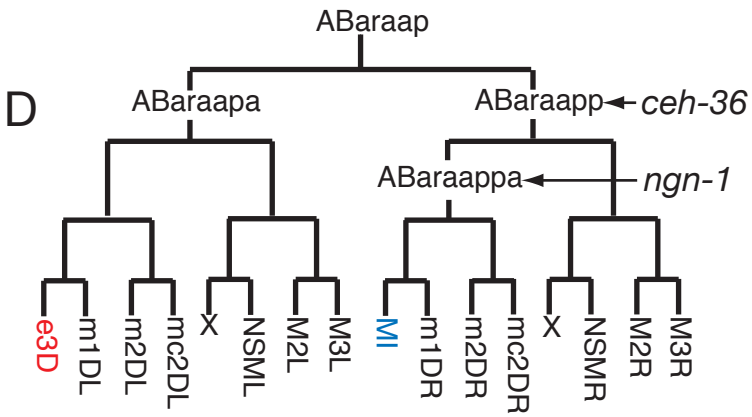

Figure 8. Expression of *ceh-36* Is Left-Right Asymmetric. (A-C) Expression of *ceh-36* at the stage of the MI grandmother cell. (A) Nomarski image of an embryo carrying *ceh-36::gfp*. (B) Fluorescence image of the same embryo. (C) Merged image of (A) and (B). The arrows indicate the MI grandmother cell, ABaraappa, and the arrowheads the e3D grandmother cell, ABaraapaa. (D-E) Expression of *ceh-36* at the stage of the MI mother cell. (D) Nomarski image of an embryo carrying *ceh-36::gfp*. (E) Fluorescence image of the same embryo. (F) Merged image of (D) and (E). The arrows indicate the MI mother cell, ABaraappaa, and the arrowheads the e3D mother cell, ABaraapaaa. Anterior is to the left, ventral to the top. Scale bar, 5 μm. (F) A model for the establishment of the left-right asymmetric cell lineage. The ellipses represent proteins. The solid and dotted arrows in red indicate the presence and absence of transcriptional induction, respectively. "Target" represents a locus induced by a heterodimer of NGN-1 and HLH-2.

Figure 8.

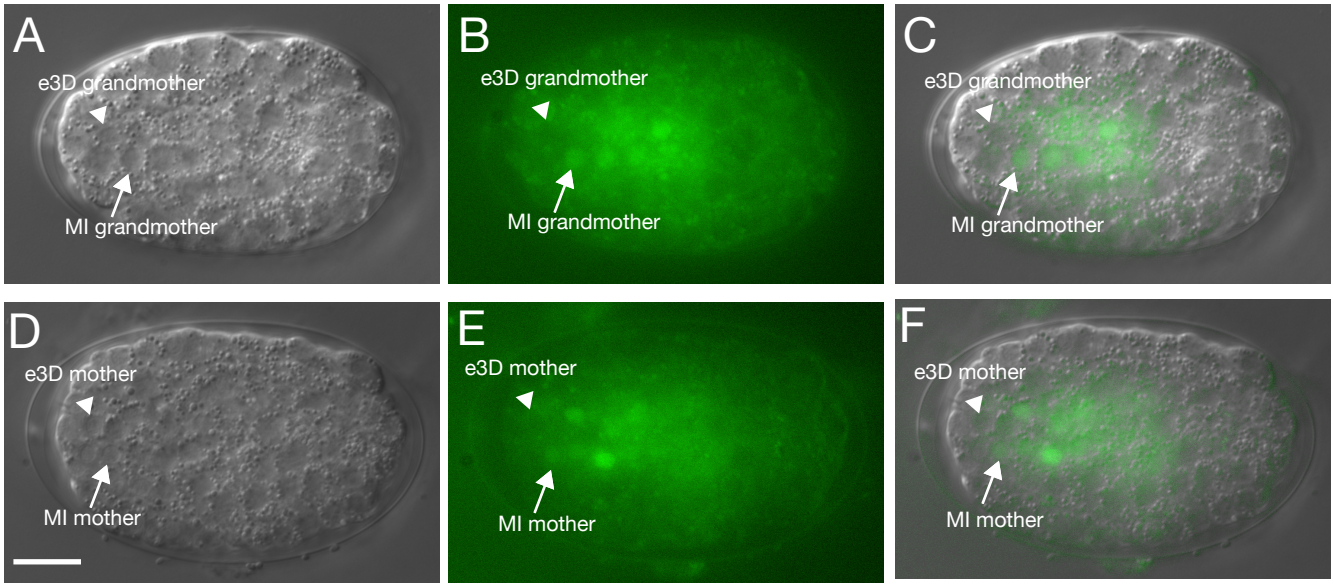
A
e3D grandmother
MI grandmother
B
e3D grandmother
MI grandmother
C
e3D grandmother
MI grandmother
D
e3D mother
MI mother
E
e3D mother
MI mother
F
e3D mother
MI mother

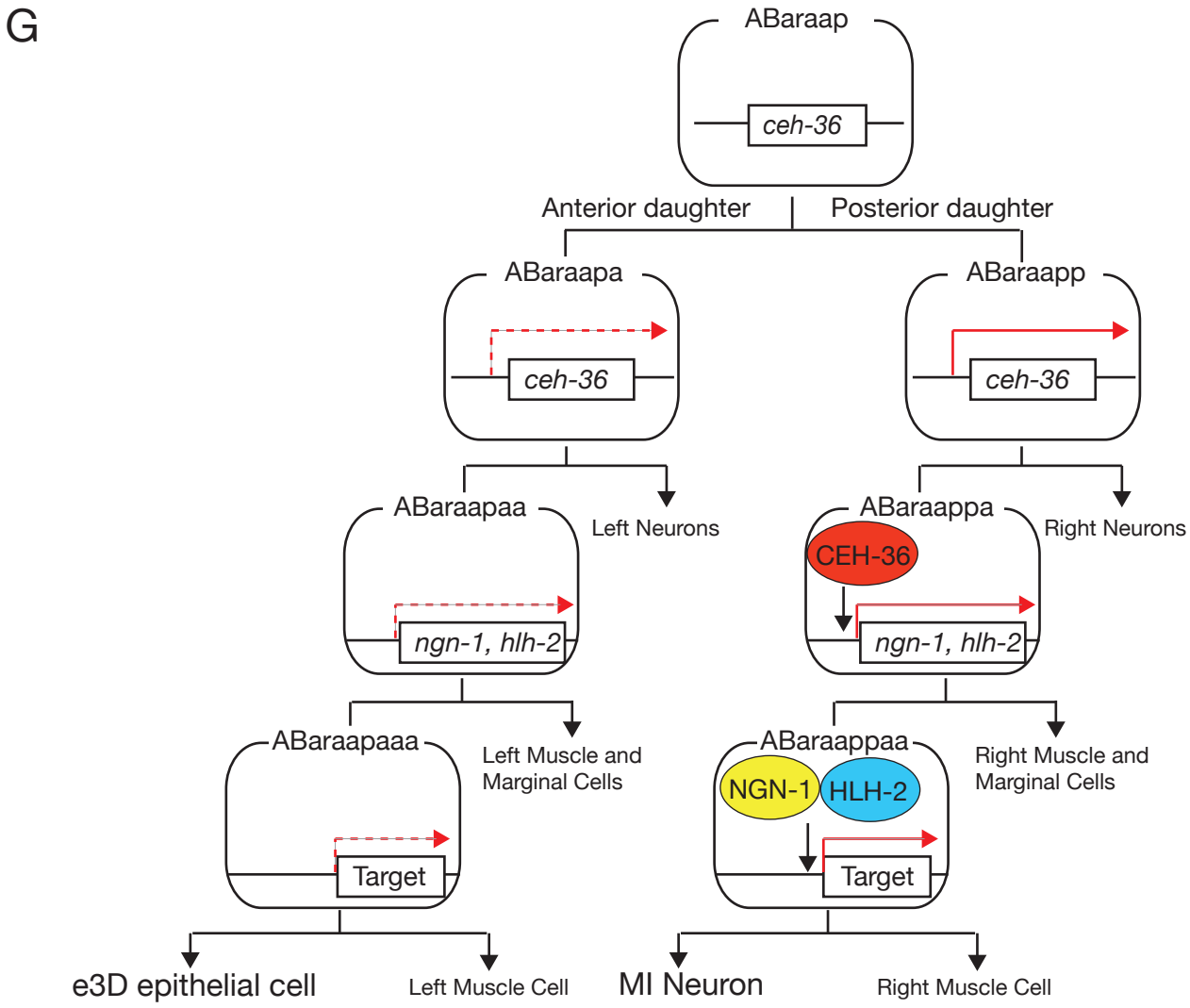
G
ABaraap
ceh-36
Anterior daughter
Posterior daughter
ABaraapa
ceh-36
ABaraapp
ceh-36
ABaraapaa
Left Neurons
ABaraappa
Right Neurons
CEH-36
ngn-1, hlh-2
ngn-1, hlh-2
ABaraapaaa
Left Muscle and Marginal Cells
ABaraappaa
NGN-1
HLH-2
Right Muscle and Marginal Cells
Target
Target
e3D epithelial cell
Left Muscle Cell
MI Neuron
Right Muscle Cell

Chapter III

Histone H3 mutations and loss of the CAF-1 complex eliminate a *C. elegans* neuronal bilateral asymmetry

Shunji Nakano and H. Robert Horvitz

Abstract

Replication-dependent histone H3 proteins are deposited onto replicating DNA by chromatin assembly factor 1 (CAF-1) [1-4]. Genetic analysis of histone functions in multicellular organisms has been challenging because of the high copy number of histone genes. Here we report the first isolation of a mutant allele of a histone H3 gene in a multi-cellular organism recovered from genetic screens. This mutation is an allele of a *C. elegans* replication-dependent histone H3 gene, *his-9,* and causes the loss of a single left-right unpaired MI neuron. The MI neuron normally is generated from the right side of an otherwise left-right symmetric cell lineage that on the left generates the e3D epithelial cell [5]. We show that the absence of the MI neuron in *his-9* mutants results from left-right symmetry in this normally asymmetric cell lineage, with the MI neuron transformed into an e3D-like epithelial cell. This mutant allele of *his-9* causes an altered-function activity that is predicted to impair the interaction of the mutant HIS-9 proteins with another histone H3 molecule and inhibit the formation of a histone H3-H4 tetramer. We further show that the *C. elegans* CAF-1 complex is required to establish the bilateral asymmetry in this cell lineage and propose that CAF-1-mediated nucleosome formation is compromised in animals carrying a *his-9* gain-of-function mutation. Our results indicate a novel mechanism of establishment of a neuroanatomical bilateral asymmetry by CAF-1-mediated nucleosome assembly and implicate a new therapeutic strategy for treatment of diseases that result from abnormal chromatin regulation, including cancers.

Results and Discussion

Anatomical and functional bilateral asymmetries of the brain are widespread features of humans and other animals and are thought to be important for behavior and cognitive functions [6]. Molecular mechanisms that establish brain bilateral asymmetry remain largely elusive. Although mostly bilaterally symmetric, the *C. elegans* nervous system displays a variety of bilateral asymmetries [7]. For example, the MI motor neuron is a single left-right unpaired neuron located in the pharynx [8]. The MI neuron is generated from an invariant left-right asymmetric cell lineage [5] in which the blastomere ABaraap divides and generates two daughter cells, ABaraapa and ABaraapp, that give rise to identical sets of left-right paired cells, except for two cells, the left-right unpaired MI neuron on the right side of the cell lineage and the e3D pharyngeal epithelial cell on the left (Fig. 1a).

To elucidate the mechanism that establishes the left-right asymmetry in this cell lineage, we performed genetic screens using an e3D cell-fate reporter, *D2096.6::pes-10::gfp* (see Chapter II), and looked for mutants in which an extra e3D-like cell was present or e3D was absent (see Chapter IV). Among the isolates we recovered was the mutation, *n5357,* which caused the presence of an extra e3D-like cell (Fig. 1b). We introduced an MI cell-fate reporter, *sams-5::gfp* (see Chapter II), into *n5357* mutants and observed that MI was missing in *n5357* animals (Fig. 1b), indicating that MI is transformed into an e3D-like cell, resulting in left-right symmetry in this normally asymmetric cell lineage (Fig. 1a). *n5357* causes a cold-sensitive and semi-dominant phenotype (Fig. 1c). To ask whether *n5357* is a gain- or loss-of-function mutation, we performed a gene-dosage study. We found that the presence of a free duplication

chromosome covering the *n5357* region neither enhanced or suppressed the MI transformation caused by *n5357* (Fig. 1d, and see Methods for details), indicating that *n5357* is a gain-of-function mutation and is likely an altered-function mutation.

We mapped *n5357* to a 55 kb interval of chromosome *II* (Fig. 2a). This region contains a cluster of 13 predicted histone genes. We performed DNA sequence analysis of *n5357* and identified a mutation in the gene *his-9*, which encodes a histone H3 protein [9]. The amino acid sequence of HIS-9 protein displays higher identity to those of the human replication-dependent histones H3.1 and H3.2 than to that of the replication-independent histone H3.3 (Fig. 3). The *C. elegans* genome contains 13 other replication-dependent histone H3 genes that encode proteins with amino acid sequences identical to that of HIS-9 protein. *n5357* animals carry a transition mutation that is predicted to alter the glutamine 125 codon to an ochre stop codon (Fig. 2a). To test whether this DNA lesion is responsible for MI transformation in *n5357* animals, we generated genomic clones carrying the wild-type *his-9(+)* or a mutant *his-9(Q125ochre)* gene and three wild-type histone genes (*his-10, his-11* and *his-12*) located 5' upstream of *his-9* (Fig. 2b). Because our gene dosage study indicated that *n5357* is an altered-function mutation, we tested whether introduction of the *his-9(Q125ochre)* clone into wild-type animals causes MI transformation. We observed that wild-type animals transformed with the *his-9(Q125ochre)* clone displayed MI transformation (Fig. 2b). By contrast, wild-type animals carrying the wild-type *his-9(+)* clone did not show MI transformation (Fig. 2b), indicating that the transition mutation we identified in *n5357* animals is responsible for MI transformation. To test whether this mutation alters the activity of the HIS-9 protein rather than that of HIS-10, HIS-11 or HIS-12 protein, we introduced a frameshift

mutation into the *his-9* locus of the *his-9(Q125ochre)* clone and found that this genomic clone, *his-9(f.s.Q125ochre),* did not cause MI transformation (Fig. 2b). We conclude that *n5357* is an allele of *his-9* that causes symmetry in this normally left-right asymmetric cell lineage.

Previous crystal-structure analysis of the nucleosome core particle identified the histone H3 amino acid residues that mediate the interactions between two histone H3s and between histones H3 and H4 [10] (Fig. 4a). The *his-9(Q125ochre)* mutation is predicted to eliminate two residues, leucine 126 and isoleucine 130, that are engaged in the H3-H3 interaction. To elucidate the cause of *his-9* gain-of-function activity, we introduced into wild-type animals *his-9* genomic clones in which the *his-9* coding sequences were truncated at the glutamine 125 codon (*ΔQ125-A135),* the arginine 116 codon *(ΔR116-A135),* the aspartic acid 106 codon *(ΔD106-A135)* and the leucine 92 codon *(ΔL92-A135)* (Fig. 4b). We observed that the *his-9(ΔQ125-A135), his-9(ΔR116-A135)* and *his-9(ΔD106-A135)* clones, all of which eliminate HIS-9 residues important for the H3-H3 interaction, caused MI transformation (Fig. 4b). By contrast, the *his-9(ΔL92-A135)* clone, which is predicted to lack residues involved in both the H3-H3 and H3-H4 interactions, did not cause MI transformation (Fig. 4b). These results suggest that a mutant HIS-9 protein that is unable to interact with another H3 protein but retains its interaction with an H4 protein results in an altered-function activity.

An interaction between two histone H3 proteins is important for the formation of the histone H3-H4 heterotetramer, and this interaction is mediated in part by a hydrogen bond between histidine 113 of one histone H3 protein and aspartic acid 123 of another histone H3 molecule [10]. To test whether the lack of histone H3-H3 interaction sites results

in an altered-function activity of *his-9*, we generated mutant *his-9* genomic clones in which the histidine 113 codon or the aspartic acid 123 codon was altered to an aspartic acid codon (H113D) or a histidine codon (D123H), respectively (Fig. 4b). We introduced each mutant *his-9* clone into wild-type animals and observed that both *his-9(H113D)* and *his-9(D123H)* clones caused MI transformation (Fig. 4b). By contrast, the wild-type *his-9(+)* clone did not cause MI transformation (Fig. 4b). These results strongly suggest that mutant HIS-9 proteins unable to form a histone H3-H4 heterotetramer through interaction with another histone H3 protein display an altered-function activity and cause left-right symmetry in this normally asymmetric cell lineage.

We previously showed that the establishment of the bilateral asymmetry in this cell lineage requires asymmetric expression of a transcriptional cascade in which the *Otx* homeodomain protein CEH-36 is expressed in the MI grandmother cell but not in the e3D grandmother cell, and that CEH-36 promotes asymmetric expression of two proneural bHLH proteins, NGN-1 and HLH-2, in the MI mother cell but not in the e3D mother cell (see Chapter II). We therefore examined the expression of CEH-36, NGN-1 and HLH-2 in animals carrying the *his-9(H113D)* transgene. We found that expression of these proteins remained left-right asymmetric (data not shown), indicating that the altered-function *his-9* activity affects a process downstream of or in parallel to the left-right asymmetric expression of CEH-36, NGN-1 and HLH-2.

Biochemical studies have revealed that human CAF-1 mediates the incorporation of histones H3-H4 into nucleosomes [2]. CAF-1 preferentially binds to a histone H3-H4 heterodimer that contains the replication-dependent histone H3.1 rather than the replication-independent histone H3.3 [3]. CAF-1 is composed of three subunits, p150, p60

and p48 [11,12]. The *C. elegans* genome encodes proteins homologous to these factors, including the p150 homolog T06D10.2 [13], the p60 homolog Y71G12B.1 [13] and the p48 homologs LIN-53 [14] and RBA-1 [15]. We observed that inactivation of *T06D10.2, Y71G12b.1* and *rba-1* but not of *lin-53* by RNA interference (RNAi) caused the MI transformation phenotype (Figs. 5a, b; data for *lin-53* not shown); in addition, RNAi treatment of all of these genes caused incompletely penetrant embryonic lethality (data not shown). Furthermore, we isolated a deletion allele of *rba-1, rba-1(n5418Δ),* that eliminates the entire coding sequence of *rba-1* (Fig. 5c), thus presumably defining a null allele of *rba-1*. We examined *rba-1(n5418Δ)* mutants and another deletion mutants, *rba-1(tm3122Δ)* (Fig. 5c; *tm3122Δ* was provided by S. Mitani, personal communication), and observed that both deletion mutants displayed maternal-effect embryonic lethality: *rba-1(n5418Δ)* and *rba-1(tm3122Δ)* deletion homozygous animals derived from their respective heterozygous mothers did not show MI transformation (Fig. 5d). These observations suggested that the MI transformation defect in the *rba-1* mutants might be maternally rescued. To test whether *rba-1* is required to specify the MI neuronal fate, we asked whether the zygotic loss of *rba-1* activity enhances the MI transformation defect in a sensitized background. We observed that both *rba-1(n5418Δ)* and *rba-1(tm3122Δ)* mutations enhanced the MI transformation defect of *his-9(n5357)* mutants (Fig. 5d). These results indicate that the *C. elegans* CAF-1 complex is required to establish the bilateral asymmetry in this cell lineage.

Although biochemical studies have been performed to elucidate the mechanism of CAF-1-mediated nucleosome formation [3,16-18], the role of CAF-1 in the development of multicellular organisms remains largely unknown. Our results indicate that in *C. elegans*

the CAF-1 complex is required to establish the bilateral asymmetry in a specific cell lineage and thus suggest a novel mechanism of establishment of a neuronal bilateral asymmetry by CAF-1-dependent nucleosome formation. We propose that CAF-1-mediated nucleosome formation is compromised in animals carrying a *his-9* gain-of-function mutation that disrupts the formation of the histone H3-H4 heterotetramer. Specifically, we hypothesize that a mutant HIS-9 protein forms a heterodimer with a histone H4 protein and that this mutant HIS-9-H4 heterodimer binds to CAF-1. CAF-1 bound by a mutant HIS-9-H4 heterodimer cannot complete the deposition of a histone H3-H4 heterotetramer because of the lack of an interaction between the mutant HIS-9 protein and another histone H3 molecule (Fig. 6).

Abnormality in chromatin regulation is thought to cause numerous human diseases, including cancers [19]. In some cases, aberrant patterns of histone H3 methylation are thought to cause inappropriately high expression of an oncogene(s) [20-22] and abnormally low expression of a tumour-suppressor gene(s) [23-25]. Given our observation that expression of mutant histone H3 proteins recapitulated the loss-of-function phenotype of CAF-1 and a previous report that depletion of p60 induced cell death in proliferating but not in quiescent human cells [26], introduction of these mutant histone H3 proteins into cells with abnormal chromatin regulation might be of therapeutic benefits for the treatment of such diseases.

Methods

C. elegans strains

C. elegans strains were cultured as previously described [27]. N2 (Bristol) was the wild-type strain. All strains were cultured at 20 °C unless otherwise indicated. The following extrachromosomal arrays, integrants, duplication chromosomes and mutations were used and have been described [28], except those from this study or otherwise indicated:

LG*I*: *rba-1(n5418Δ, tm3122Δ)* (this study; *tm3122Δ* was provided by Shohei Mitani), *nIs450[his-9(H114D), unc-76(+), unc-25::mStrawberry]* (this study).

LG*II*: *rrf-3(pk1426)* [29], *rol-1(e91), his-9(n5357)* (this study) *unc-52(e444), nIs447[his-9(+), unc-76(+), tph-1::mStrawberry]* (this study).

LG*III*: *nIs394[ngn-1::gfp, lin-15AB(+)]* (Chapter II).

LG*IV*: *nIs407[hlh-2::gfp, lin-15AB(+)]* (Chapter II), *nIs451[his-9(H114D), unc-76(+), unc-25::mStrawberry]* (this study).

LG*V*: *nIs396[sams-5::gfp, lin-15AB(+)]* (Chapter II).

LG*X*: *nIs445[ceh-36::gfp, lin-15AB(+)]* (Chapter II), *nIs363[D2096.6::pes-10::gfp, lin-15AB(+)]* (Chapter II).

Free duplications and extrachromosomal arrays: *mnDp34(II;f)* [30], *nEx1708[his-9(+), unc-76(+), tph-1::mStrawberry], nEx1709[his-9(Q125ochre), unc-76(+), tph-1::mStrawberry], nEx1711[his-9(H113D), unc-76(+), unc-25::mStrawberry], nEx1712[his-9(D123H), unc-76(+), sre-1::mStrawberry], nEx1713[his-9(f.s. Q125ochre), unc-76(+), tph-1::mStrawberry], nEx1723[his-9(ΔR116-A135), unc-76(+),*

tph-1::mStrawberry], nEx1724[his-9(ΔD106-A135), unc-76(+), tph-1::mStrawberry], nEx1725[his-9(ΔL92-A135), unc-76(+), tph-1::mStrawberry] (this study).

Isolation of *n5357*

We mutagenized wild-type animals carrying the *D2096.6::pes-10::gfp* reporter with ethyl methanesulfonate (EMS), and F_3 progeny were observed using a fluorescence-equipped dissecting microscope. *his-9(n5357)* was isolated as an animal that contained an extra cell expressing the *D2096.6::pes-10::gfp* reporter.

Gene-dosage study of *n5357*

We allowed hermaphrodites of genotype *rol-1(e91) n5357 unc-52(e444); nIs363; mnDp34* to self-fertilize at 15 °C and determined the MI transformation defect of their Rol Unc and non-Rol non-Unc progeny at 15 °C. We noted that the MI transformation defect in these Rol Unc (*rol-1 n5357 unc-52/rol-1 n5357 unc-52)* animals was less severe than that of animals of genotype *n5357/n5357*. We found that this difference in the penetrance of the MI transformation defects was caused by the presence of a mutation(s) that partially suppresses MI transformation and is derived from strains carrying *unc-52(e444)*. We did not further study this suppressor activity.

Mapping of *n5357*

We crossed *rol-1(e91) n5357 unc-52(e444)* animals with the wild-type polymorphic strain CB4856 and isolated F_2 Rol non-Unc progeny, determined the presence or absence

of *n5357* and identified crossover sites, essentially as described [31]. We mapped *n5357* to a 55 kb interval between nucleotides 13781415 and 13837046 of LG*II*.

RNAi experiments

We performed RNAi of *rba-1* by growing wild-type animals on *E. coli* HT115(DE3) harboring the *rba-1* RNAi construct (Open Biosystems) and RNAi of *T06D10.2* and *Y71G12B.1* by growing RNAi-sensitive *rrf-3(pk1426)* animals on *E. coli* HT115(DE3) harboring the *T06D10.2* (pSN411) and *Y71G12B.1* (pSN392) RNAi construct, respectively. The MI transformation defect in the progeny of these animals was determined using the *D2096.6::pes-10::gfp* reporter.

Isolation of *rba-1(n5418Δ)*

Genomic DNA pools from EMS-mutagenized animals were screened by PCR for deletion alleles of *rba-1*, essentially as described [32]. *rba-1(n5418Δ)* was isolated and backcrossed to the wild-type N2 strain four times. The *rba-1(n5418Δ)* allele removes sequence between nucleotides 35977 and 37677 of cosmid K07A1.

Molecular biology

To create the genomic *his-9(+)* clone, we amplified 3.8 kb of the *his-9* genomic sequence by PCR using the wild-type genomic DNA and the primers 5'-CCAACAAGTGCCAAATTCACTGCTATTGCA-3' and 5'-GTGATAATATCCCATGTAAATCAACGT-3'. The resulting PCR product was cloned into the pGEM-T easy vector (Promega). To create mutant *his-9* clones, we performed

site-directed mutagenesis using the wild-type *his-9* genomic clone as a template. We generated a frameshift construct by inserting a single thymine base after the threonine 3 codon of *his-9*. The codon changes we used were as follows: CAT-to-GAC(H113D) and GAC-to-CAT(D123H). To create the *mStrawberry* expression vectors pSN198 and pSN199, we cloned the *mStrawberry* coding sequence [33] into the AgeI and EcoRI sites of the vector pPD95.75 and pPD122.56, respectively. To create *unc-25::mStrawberry,* we amplified 1.8 kb of the *unc-25* genomic sequence by PCR using the wild-type genomic DNA and the primers 5'-CGAATTTTTGCATGCAAAAAACACCCACTTTTTGATC-3' and 5'-CGGGATCCTCGAGCACAGCATCACTTTCGTCAGCAGC-3'. The resulting PCR product was digested with BamHI and SphI and cloned into the vector pSN198 digested with the same restriction enzymes. To create *sre-1::mStrawberry,* we amplified 4.0 kb of the *sre-1* genomic sequence by PCR using the wild-type genomic DNA and the primers 5'-GCAAGCTTCATGAATATGTACCTATCACGA-3' and 5'-CAGGCATGCAACGGCGAGTATTGTAAATTCA-3'. The resulting PCR product was digested with HindIII and SphI and cloned into the vector pSN198 digested with the same restriction enzymes. To create *tph-1::mStrawberry,* we amplified 1.7 kb of the *tph-1* genomic sequence by PCR using the wild-type genomic DNA and the primers 5'-GCGCATGCTTCTCGCGAATTGCGGCCGACA-3' and 5'-GCGGATCCGAGCTGAAAGTACAGAAATTACTGA-3'. The resulting PCR product was digested with BamHI and SphI and cloned into the vector pSN199 digested with the same restriction enzymes. To generate the RNAi construct of *T06D10.2* (pSN411), we amplified the *T06D10.2* genomic sequence by PCR using the wild-type genomic DNA and the primers 5'- GTCTAGATGGATGAATCTCATGTTACCGA-3' and 5'-

CCTCGAGTTAGTAGAACTTGACTGCAATCA-3'. The resulting PCR product was digested with XbaI and XhoI and cloned into the vector pPD129.36 digested with the same restriction enzymes. To generate the RNAi construct of *Y71G12B.1* (pSN392), we amplified the *Y71G12B.1* genomic sequence by PCR using the wild-type genomic DNA and the primers 5'-GTCTAGAAAACGTCTATTCGTCGCCAGCA-3' and 5'-GCTCGAGTAGGTTCCATATAAATCCGACGA-3'. The resulting PCR product was digested with XbaI and XhoI and cloned into the vector pPD129.36 digested with the same restriction enzymes.

Germline transformation experiments

Germline transformation experiments were performed as described [34]. To generate animals carrying the *his-9* genomic constructs, we injected each *his-9* genomic clone into *unc-76(e911)* mutants at 1 ng/µl together with 20 ng/µl of p76-16B, an *unc-76* rescuing plasmid [35], and 40 ng/ul of *tph-1::mStrawberry, sre-1::mStrawberry* or *unc-25::mStrawberry*.

Acknowledgements

We thank A. Fire for expression vectors; S. Mitani and the *Caenorhabditis* Genetics Center, which is funded by the NIH National Center for Research Resources (NCRR), for strains; N. An, R. Droste and T. Ljungars for technical assistance; and D. Denning and M. Nakano for comments on the manuscript. H.R.H is an Investigator of the Howard Hughes Medical Institute and the David H. Koch Professor of Biology at MIT.

References

1 Shibahara, K. & Stillman, B. Replication-dependent marking of DNA by PCNA facilitates CAF-1-coupled inheritance of chromatin. *Cell* **96**, 575-585 (1999).

2 Smith, S. & Stillman, B. Purification and characterization of CAF-I, a human cell factor required for chromatin assembly during DNA replication in vitro. *Cell* **58**, 15-25 (1989).

3 Tagami, H., Ray-Gallet, D., Almouzni, G. & Nakatani, Y. Histone H3.1 and H3.3 complexes mediate nucleosome assembly pathways dependent or independent of DNA synthesis. *Cell* **116**, 51-61 (2004).

4 Hoek, M. & Stillman, B. Chromatin assembly factor 1 is essential and couples chromatin assembly to DNA replication *in vivo*. *Proc Natl Acad Sci U S A* **100**, 12183-12188 (2003).

5 Sulston, J. E., Schierenberg, E., White, J. G. & Thomson, J. N. The embryonic cell lineage of the nematode *Caenorhabditis elegans*. *Dev Biol* **100**, 64-119 (1983).

6 Toga, A. W. & Thompson, P. M. Mapping brain asymmetry. *Nat Rev Neurosci* **4**, 37-48 (2003).

7 Hobert, O., Johnston, R. J., Jr. & Chang, S. Left-right asymmetry in the nervous system: the *Caenorhabditis elegans* model. *Nat Rev Neurosci* **3**, 629-640 (2002).

8 Albertson, D. G. & Thomson, J. N. The pharynx of *Caenorhabditis elegans*. *Philos Trans R Soc Lond B Biol Sci* **275**, 299-325 (1976).

9 Pettitt, J., Crombie, C., Schumperli, D. & Muller, B. The *Caenorhabditis elegans* histone hairpin-binding protein is required for core histone gene expression and is

essential for embryonic and postembryonic cell division. *J Cell Sci* **115**, 857-866 (2002).

10 Luger, K., Mader, A. W., Richmond, R. K., Sargent, D. F. & Richmond, T. J. Crystal structure of the nucleosome core particle at 2.8 A resolution. *Nature* **389**, 251-260 (1997).

11 Kaufman, P. D., Kobayashi, R., Kessler, N. & Stillman, B. The p150 and p60 subunits of chromatin assembly factor I: a molecular link between newly synthesized histones and DNA replication. *Cell* **81**, 1105-1114 (1995).

12 Verreault, A., Kaufman, P. D., Kobayashi, R. & Stillman, B. Nucleosome assembly by a complex of CAF-1 and acetylated histones H3/H4. *Cell* **87**, 95-104 (1996).

13 *WormBase*, <http://ws204.wormbase.org/ > (2009).

14 Lu, X. & Horvitz, H. R. *lin-35* and *lin-53*, two genes that antagonize a *C. elegans* Ras pathway, encode proteins similar to Rb and its binding protein RbAp48. *Cell* **95**, 981-991 (1998).

15 Solari, F. & Ahringer, J. NURD-complex genes antagonise Ras-induced vulval development in *Caenorhabditis elegans*. *Curr Biol* **10**, 223-226 (2000).

16 Margueron, R. & Reinberg, D. Chromatin structure and the inheritance of epigenetic information. *Nat Rev Genet* **11**, 285-296 (2010).

17 Xu, M. *et al*. Partitioning of histone H3-H4 tetramers during DNA replication-dependent chromatin assembly. *Science* **328**, 94-98 (2010).

18 Polo, S. E., Roche, D. & Almouzni, G. New histone incorporation marks sites of UV repair in human cells. *Cell* **127**, 481-493 (2006).

19 Lund, A. H. & van Lohuizen, M. Epigenetics and cancer. *Genes Dev* **18**, 2315-2335 (2004).

20 Guenther, M. G. *et al*. Aberrant chromatin at genes encoding stem cell regulators in human mixed-lineage leukemia. *Genes Dev* **22**, 3403-3408 (2008).

21 Krivtsov, A. V. *et al*. H3K79 methylation profiles define murine and human MLL-AF4 leukemias. *Cancer Cell* **14**, 355-368 (2008).

22 Okada, Y. *et al*. hDOT1L links histone methylation to leukemogenesis. *Cell* **121**, 167-178 (2005).

23 Beke, L., Nuytten, M., Van Eynde, A., Beullens, M. & Bollen, M. The gene encoding the prostatic tumor suppressor PSP94 is a target for repression by the Polycomb group protein EZH2. *Oncogene* **26**, 4590-4595 (2007).

24 Cao, Q. *et al*. Repression of E-cadherin by the polycomb group protein EZH2 in cancer. *Oncogene* **27**, 7274-7284 (2008).

25 Herranz, N. *et al*. Polycomb complex 2 is required for E-cadherin repression by the Snail1 transcription factor. *Mol Cell Biol* **28**, 4772-4781 (2008).

26 Nabatiyan, A. & Krude, T. Silencing of chromatin assembly factor 1 in human cells leads to cell death and loss of chromatin assembly during DNA synthesis. *Mol Cell Biol* **24**, 2853-2862 (2004).

27 Brenner, S. The genetics of *Caenorhabditis elegans*. *Genetics* **77**, 71-94 (1974).

28 Riddle, D. L., Blumenthal, T., Meyer, B. J. & Priess, J. *C. elegans II*. (Cold Spring Harbor Laboratory Press, 1997).

29 Simmer, F. *et al*. Loss of the putative RNA-directed RNA polymerase RRF-3 makes *C. elegans* hypersensitive to RNAi. *Curr Biol* **12**, 1317-1319 (2002).

30 Edgley, M. L., Baillie, D. L., Riddle, D. L. & Rose, A. M. Genetic balancers. *WormBook*, 1-32 (2006).

31 Wicks, S. R., Yeh, R. T., Gish, W. R., Waterston, R. H. & Plasterk, R. H. Rapid gene mapping in *Caenorhabditis elegans* using a high density polymorphism map. *Nat Genet* **28**, 160-164 (2001).

32 Liu, L. X. *et al*. High-throughput isolation of *Caenorhabditis elegans* deletion mutants. *Genome Res* **9**, 859-867 (1999).

33 Shaner, N. C. *et al*. Improved monomeric red, orange and yellow fluorescent proteins derived from *Discosoma* sp. red fluorescent protein. *Nat Biotechnol* **22**, 1567-1572 (2004).

34 Mello, C. C., Kramer, J. M., Stinchcomb, D. & Ambros, V. Efficient gene transfer in *C. elegans*: extrachromosomal maintenance and integration of transforming sequences. *Embo J* **10**, 3959-3970 (1991).

35 Bloom, L. & Horvitz, H. R. The *Caenorhabditis elegans* gene *unc-76* and its human homologs define a new gene family involved in axonal outgrowth and fasciculation. *Proc Natl Acad Sci U S A* **94**, 3414-3419 (1997).

Figures

Figure 1. *n5357* causes symmetry in a normally left-right asymmetric cell lineage. a, The ABaraap cell lineages in the wild type and *n5357* mutants. **b,** Expression of the *D2096.6::pes-10::gfp* and *sams-5::gfp* reporters in a wild type and an *n5357* animal. *D2096.6::pes-10::gfp* reporter was expressed in e3D of the wild type and in e3D and the extra e3D-like cell of the *n5357* mutant (arrowheads). The *sams-5::gfp* reporter was expressed in MI of the wild type (arrow) and was not expressed in the *n5357* mutant. Scale bar, 5 μm. **c, d,** Percentage of animals showing the MI transformation defect. The MI transformation defects in (d) were determined at 15 °C. We noted that the MI transformation defect of *n5357*/*n5357* animals in (d) was less severe than that of *n5357*/*n5357* animals in (c) and found that this difference was caused by a background mutation(s) present in *n5357*/*n5357* strain used in (d) (See Methods for details).

Figure 1.

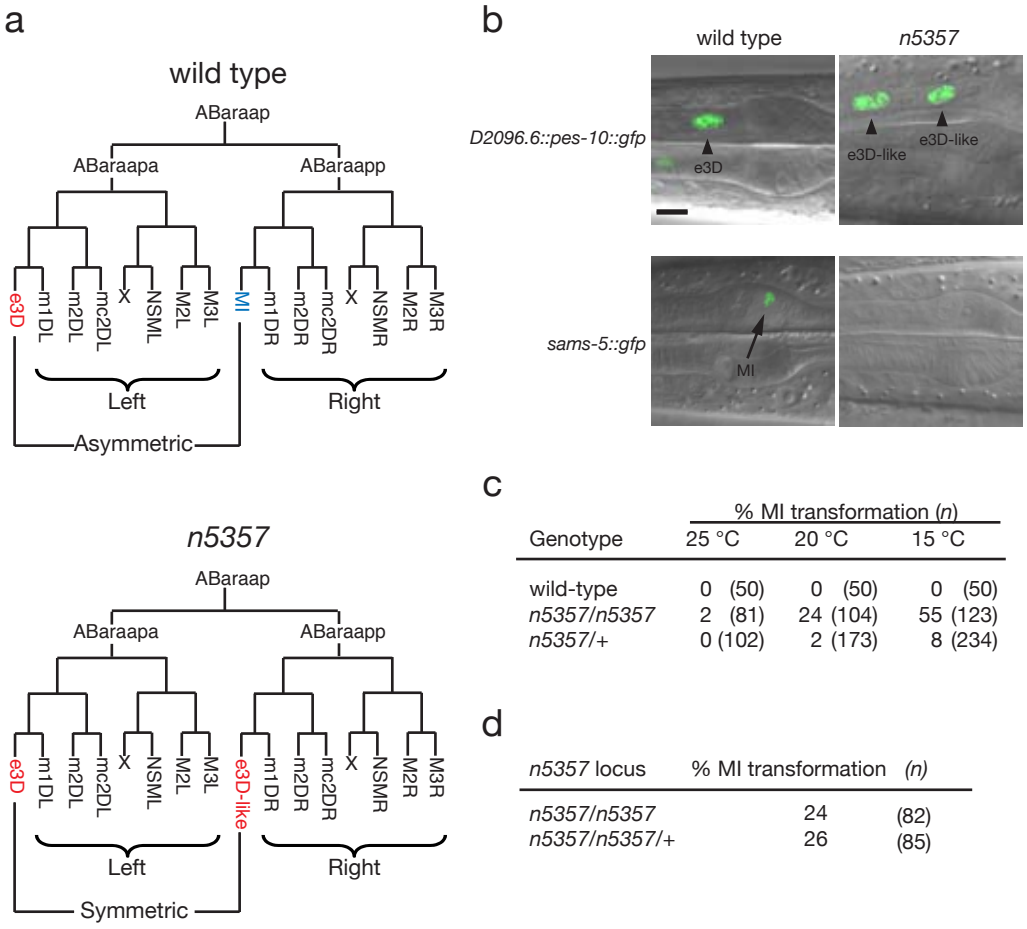

c

Genotype	% MI transformation (*n*) 25 °C	20 °C	15 °C
wild-type	0 (50)	0 (50)	0 (50)
n5357/n5357	2 (81)	24 (104)	55 (123)
n5357/+	0 (102)	2 (173)	8 (234)

d

n5357 locus	% MI transformation	(*n*)
n5357/n5357	24	(82)
n5357/n5357/+	26	(85)

Figure 2. *n5357* is an allele of *his-9*. a, A physical map of the *n5357* region and the location of a mutation in the *his-9* locus of *n5357* animals are shown. The numbers indicate the chromosome coordinates to which the *n5357* mutation was mapped. **b,** Germline transformation experiments using genomic *his-9* clones. The structure of each genomic clone and the percentage of animals showing the MI transformation defect at 15 °C are shown.

Figure 2.

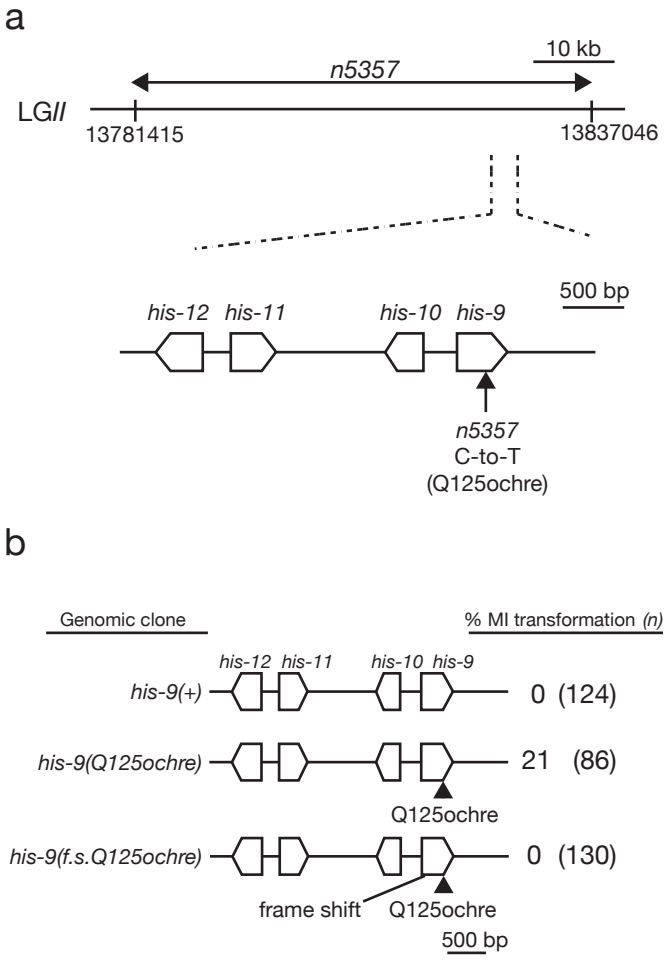
a
10 kb
n5357
LGII
13781415
13837046
500 bp
his-12 his-11 his-10 his-9
n5357
C-to-T
(Q125ochre)
b
Genomic clone
% MI transformation (n)
his-12 his-11 his-10 his-9
his-9(+)
0 (124)
his-9(Q125ochre)
21 (86)
Q125ochre
his-9(f.s.Q125ochre)
0 (130)
frame shift
Q125ochre
500 bp

Figure 3. Alignment of amino acid sequences of HIS-9 protein and human histone H3 proteins. Alignment of the predicted HIS-9 protein (accession no. NP_496894) with *Homo sapiens* histones H3.1 (accession no. NP_003520), H3.2 (accession no. NP_066403) and H3.3 (accession no. NP_002098). Black boxes indicate residues identical among three or more of the four proteins. The site of the *n5357* mutation is shown.

Figure 3.

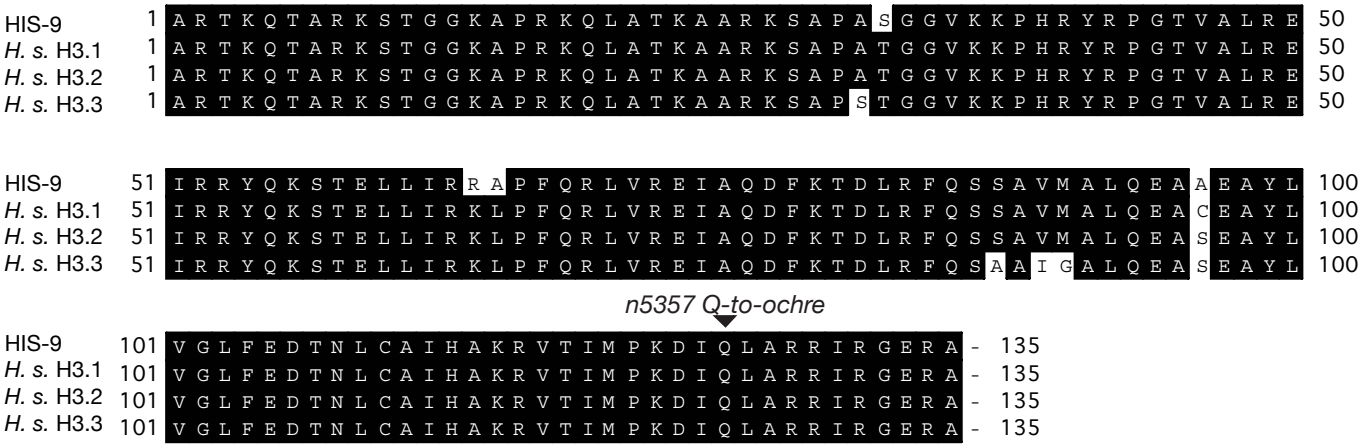
HIS-9 1 ARTKQTARKSTGGKAPRKQLATKAARKSAPASGGVKKPHRYRPGTVALRE 50
H. s. H3.1 1 ARTKQTARKSTGGKAPRKQLATKAARKSAPATGGVKKPHRYRPGTVALRE 50
H. s. H3.2 1 ARTKQTARKSTGGKAPRKQLATKAARKSAPATGGVKKPHRYRPGTVALRE 50
H. s. H3.3 1 ARTKQTARKSTGGKAPRKQLATKAARKSAPSTGGVKKPHRYRPGTVALRE 50
HIS-9 51 IRRYQKSTELLIRRAPFQRLVREIAQDFKTDLRFQSSAVMALQEAAEAYL 100
H. s. H3.1 51 IRRYQKSTELLIRKLPFQRLVREIAQDFKTDLRFQSSAVMALQEACEAYL 100
H. s. H3.2 51 IRRYQKSTELLIRKLPFQRLVREIAQDFKTDLRFQSSAVMALQEASEAYL 100
H. s. H3.3 51 IRRYQKSTELLIRKLPFQRLVREIAQDFKTDLRFQSAAIGALQEASEAYL 100
n5357 Q-to-ochre
HIS-9 101 VGLFEDTNLCAIHAKRVTIMPKDIQLARRIRGERA- 135
H. s. H3.1 101 VGLFEDTNLCAIHAKRVTIMPKDIQLARRIRGERA- 135
H. s. H3.2 101 VGLFEDTNLCAIHAKRVTIMPKDIQLARRIRGERA- 135
H. s. H3.3 101 VGLFEDTNLCAIHAKRVTIMPKDIQLARRIRGERA- 135

Figure 4. Mutations altering the C-terminus of HIS-9 cause MI transformation. a, Genomic region present in *his-9* clones, the amino acid sequence of HIS-9 and the site of the *n5357* mutation are shown. Residues in blue and red are involved in interaction with histones H4 and H3, respectively. **b,** The predicted HIS-9 amino acid sequence of each genomic clone and percentages of animals showing the MI transformation defect are shown. Residues substituted by mutagenesis are shown in green.

Figure 4.

a

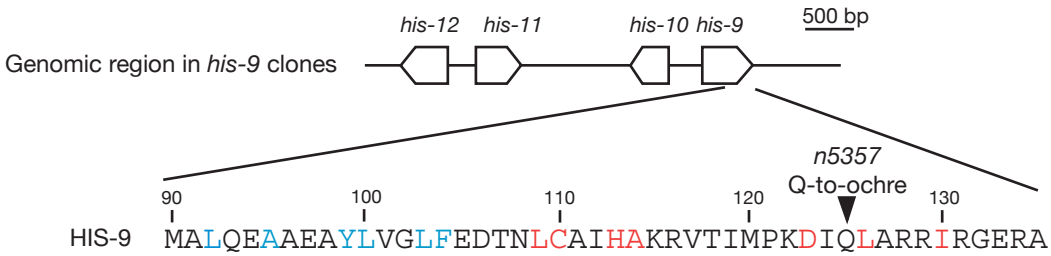

b

Genomic clone		% MI transformation *(n)* 15 °C	20 °C
his-9(+)	MALQEAAEAYLVGLFEDTNLCAIHAKRVTIMPKDIQLARRIRGERA	0 (50)	0 (118)
his-9(ΔQ125-A135)	MALQEAAEAYLVGLFEDTNLCAIHAKRVTIMPKDI	24 (102)	28 (122)
his-9(ΔR116-A135)	MALQEAAEAYLVGLFEDTNLCAIHAK	28 (90)	15 (84)
his-9(ΔD106-A135)	MALQEAAEAYLVGLFED	4 (115)	25 (109)
his-9(ΔL92-A135)	MA	0 (111)	0 (130)
his-9(H113D)	MALQEAAEAYLVGLFEDTNLCAIDAKRVTIMPKDIQLARRIRGERA	22 (73)	43 (102)
his-9(D123H)	MALQEAAEAYLVGLFEDTNLCAIHAKRVTIMPKHIQLARRIRGERA	14 (80)	3 (108)

Figure 5. The CAF-1 complex is required to establish the MI-e3D bilateral asymmetry. a, Expression of the *D2096.6::pes-10::gfp* and *sams-5::gfp* reporters in progeny of animals grown on bacteria expressing double-strand RNA of control (vector) or genes encoding each member of the CAF-1 complex. The arrowheads indicate e3D and the extra e3D-like cell, and the arrow indicates MI. Scale bar, 5 μm. **b,** Percentage of animals showing the MI transformation defect. **c,** Gene structure of *rba-1* and deletion mutations in each mutant are shown. Black boxes indicate exons, and white box an intron. **d,** Percentage of animals showing the MI transformation defect. Each set of *rba-1* deletion homozygotes was derived from their respective heterozygous mothers.

Figure 5.

a

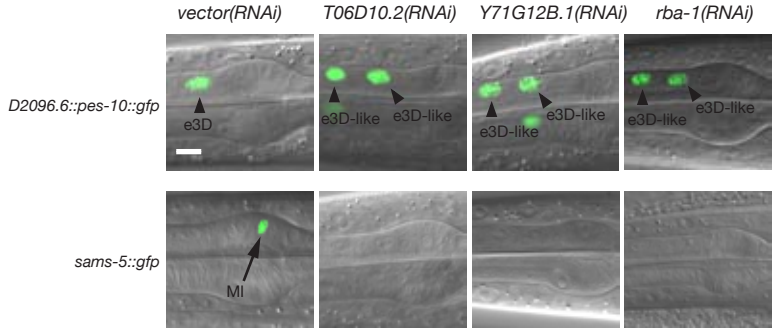

b

RNAi Treatment	% MI transformation	*(n)*
vector	0	(50)
T06D10.2(RNAi)	32	(125)
Y71G12B.1(RNAi)	29	(100)
rba-1(RNAi)	23	(100)

c

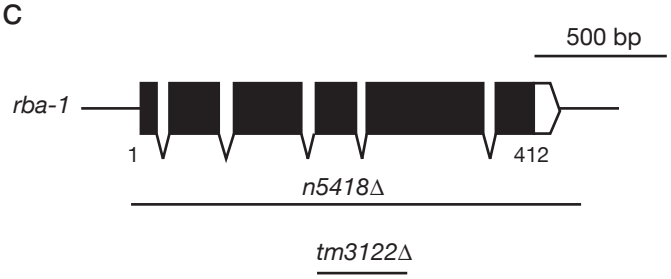

d

	% MI transformation (*n*)			
Genotype	25 °C		20 °C	
wild-type	0	(50)	0	(50)
his-9(n5357)	1	(103)	35	(80)
rba-1(n5418Δ)	0	(50)	0	(50)
rba-1(tm3122Δ)	0	(50)	0	(50)
rba-1(n5418Δ); his-9(n5357)	46	(78)	80	(108)
rba-1(tm3122Δ); his-9(n5357)	43	(84)	73	(90)

Figure 6. Model for inhibition of CAF-1-mediated nucleosome assembly by mutant HIS-9 proteins. In wild type, each CAF-1 complex binds to a histone H3-H4 heterodimer and mediate the deposition of the histone H3-H4 heterotetramer onto a locus required to promote generation of the MI neuron. In *his-9(gf)* mutants, a mutant HIS-9 protein binds to a histone H4 protein to form a mutant HIS-9-H4 heterodimer. CAF-1 bound by a mutant HIS-9-H4 heterodimer cannot complete the deposition of a histone H3-H4 heterotetramer onto a locus required to promote generation of the MI neuron, leading to transformation of MI into an e3D-like cell. See texts for details.

Figure 6.

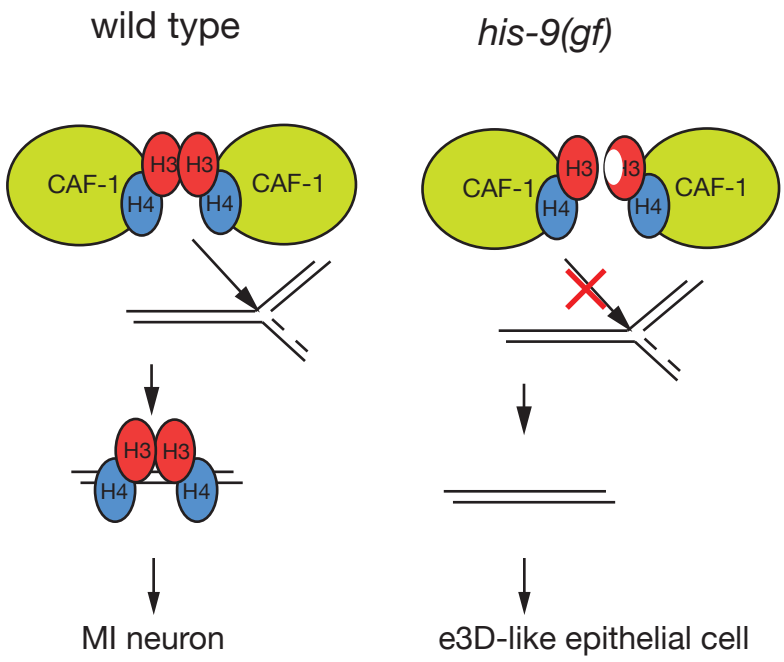
wild type
his-9(gf)
CAF-1
H3
H3
H4
H4
CAF-1
CAF-1
H3
H3
H4
H4
CAF-1
H3
H3
H4
H4
MI neuron
e3D-like epithelial cell

Chapter IV

Chromatin-Remodeling Factors Are Required to Establish a Bilateral Asymmetry of the *C. elegans* Nervous System

Shunji Nakano and H. Robert Horvitz

Introduction

Histone proteins are subject to various post-translational modifications, including phosphorylation, ubiquitination, acetylation and methylation (Kouzarides 2007). The methylation of lysine residues on histone amino-terminal tails is associated with a variety of biological processes, including transcriptional regulation. In particular, the trimethylation of histone H3 lysine 27 (H3K27me3) is associated with transcriptionally repressed loci, while the trimethylation of histone H3 lysine 4 (H3K4me3) is often found at transcriptionally active loci (Sims et al. 2003).

Numerous enzymes that catalyze the methylation or demethylation of specific histone H3 residues have been identified. Many SET-domain containing proteins have been shown to catalyze the methylation of histones. For example, the *Drosophila* E(Z) protein and its mammalian homolog EZH2 protein are histone methyltransferases (HMTs) specific for H3K27 (Cao et al. 2002; Muller et al. 2002), while the mammalian MLL proteins catalyze the methylation of H3K4 (Milne et al. 2002; Nakamura et al. 2002). Recent studies identified JmjC-domain containing proteins that demethylate lysine residues of histones. For example, the mammalian UTX protein is a histone demethylase (HDM) specific for H3K27 (Agger et al. 2007; Lan et al. 2007; Lee et al. 2007), whereas RBP2, also referred to as JARID1A, catalyzes the demethylation of H3K4 (Christensen et al. 2007).

Recently, some promoters in mammalian embryonic stem cells have been observed to carry both H3K4me3 and H3K27me3 (Bernstein et al. 2006; Mikkelsen et al. 2007). The chromatin domain with this combination of methylation marks was termed a "bivalent" domain and was proposed to serve to poise key developmental genes for

lineage-specific activation or repression upon differentiation. A study of zebrafish also provides evidence that the bivalent domain exists *in vivo* (Vastenhouw et al. 2010). In addition to these observations, it has been found that UTX physically interacts with the MLL complex and that this complex catalyzes the methylation of H3K4 and demethylation of H3K27 (Lee et al. 2007). Likewise, RBP2 was found to bind to the EZH2-containing PRC2 complex (Pasini et al. 2008). These findings raised the hypothesis that these complexes, by catalyzing the methylation and demethylation of H3K4 and H3K27, modify the bivalent marks in embryonic stem cells to resolve to active monovalent H3K4me3 and repressive H3K27me3 marks upon the commitment to cell lineages.

We have previously shown that an altered-function mutation of a *C. elegans* histone H3 gene, *his-9,* causes the loss of a single left-right unpaired MI neuron. The MI neuron normally is generated from the right side of an otherwise left-right symmetric cell lineage that on the left generates the e3D epithelial cell (Sulston et al. 1983; Figure 1A). The absence of the MI neuron in *his-9* mutants results from left-right symmetry in this normally asymmetric cell lineage, with the MI neuron transformed into an e3D-like epithelial cell. Inactivation of the *C. elegans* CAF-1 (Chromatin Assembly Factor-1) complex by RNAi treatment also caused transformation of MI into an e3D-like cell, indicating that CAF-1-mediated nucleosome formation is required to establish the bilateral asymmetry in this cell lineage (see Chapter III). In this study, we performed a candidate-gene approach to test whether *C. elegans* HMT and HDM genes are required to establish this MI-e3D bilateral asymmetry. We show that SET-16, a *C. elegans* H3K4 HMT homologous to mammalian MLL, and UTX-1, a *C. elegans* H3K27 HDM

homologous to mammalian UTX, are required for establishing the MI-e3D bilateral asymmetry. In addition, we conduct a genetic screen and recover 12 mutations that cause symmetry in this normally asymmetric cell lineage. We show that two of these 12 mutations are alleles of *egl-27,* which encodes a protein homologous to the mammalian MTA, a member of a chromatin-remodeling complex.

Results

set-16 and *utx-1* Are Required to Establish a Neuronal Bilateral Asymmetry

The *C. elegans* genome contains at least 38 genes that are predicted to encode proteins with a SET domain (Andersen and Horvitz 2007) and at least 11 genes that are predicted to encode proteins with a JmjC domain (WormBase, http://www.wormbase.org). To identify HMTs and HDMs that are involved in generating the bilateral asymmetry of the cell lineage that gives rise on the right to the MI neuron and on the left to the e3D epithelial cell (Figure 1A), we examined previously isolated mutants for 35 of the 49 predicted HMT and HDM genes and performed RNA interference (RNAi) of each of the remaining 14 genes. We asked whether these mutants and animals subjected to RNAi of these genes display symmetry in the normally asymmetric cell lineage by transforming either the MI neuron into an e3D-like epithelial cell or the e3D epithelial cell to an MI-like neuron. We found that mutants for two of the 49 genes, *set-16* and *utx-1,* displayed a defect in generating the bilateral asymmetry in this cell lineage (Table 1).

set-16 encodes a protein homologous to mammalian MLL, which catalyzes the methylation of H3K4. We examined two deletion alleles of *set-16, n4526Δ* and *gk438Δ* (Figure 1F), and found that both mutants displayed larval lethality as previously reported (Andersen and Horvitz 2007) and contained an extra cell that expressed an e3D cell-fate reporter, *D2096.6::pes-10::gfp* (see Chapter II, Figure 1C, D). We also observed that *set-16* mutant animals often lacked the MI neuron (data not shown), indicating that the

MI neuron is transformed into an e3D-like cell in *set-16* mutants, resulting in symmetry in the normally asymmetric cell lineage (Figure 1A, B).

utx-1 encodes a protein homologous to mammalian UTX, which catalyzes the demethylation of H3K27. We examined two deletion alleles of *utx-1, tm3118Δ* and *tm3136Δ* (Figure 1G), and found that both mutants showed larval lethality (data not shown) and contained an extra e3D-like cell (Figure 1C, E), suggesting that *utx-1* is also required to establish the MI-e3D bilateral asymmetry (Figure 1A, B). The *utx-1* mutant phenotype was maternally rescued: whereas *utx-1* homozygous mutant animals derived from *utx-1* homozygous mothers displayed larval lethality and the MI transformation defect, *utx-1* homozygous mutant animals derived from *utx-1* heterozygous mothers did not show lethality or the MI transformation defect (data not shown).

These results indicate that the establishment of the MI-e3D bilateral asymmetry requires two histone-modifying enzymes, SET-16, an H3K4 HMT, and UTX-1, an H3K27 HDM.

An F_3 Non-Clonal Screen Identified 12 Mutations that Cause the MI Transformation

Our observation that the *utx-1* mutant phenotype was maternally rescued suggested that mutants for some *C. elegans* genes might show symmetry in this normally left-right asymmetric cell lineage only when they are derived from homozygous mothers. We could not have isolated such mutants from our previous screen for animals defective in the establishment of the MI-e3D asymmetry, because this screen was designed to seek

mutant animals in the F_2 generation (see Chapter II). To isolate such mutants, we mutagenized wild-type strains carrying an e3D cell-fate reporter, *D2096.6::pes-10::gfp*, and looked for animals in the F_3 generation that contained an extra e3D-like cell or lacked e3D. From this screen, we recovered 12 mutations that caused the presence of an extra e3D-like cell (Table 2): *n5333, n5335, n5336, n5338, n5339, n5340, n5342, n5348, n5351, n5354, n5356* and *n5357*. We observed these mutants using Nomarski optics and found that the MI neuron was missing in all 12 mutants (data not shown), indicating that, like *set-16* and *utx-1* mutations, these mutations transform the MI neuron into an e3D-like cell, causing symmetry in this normally asymmetric cell lineage.

The 12 Mutations that Cause the MI transformation Are Alleles of At Least Six Genes

Based on complementation tests and mapping experiments, we concluded that the 12 mutations are alleles of at least six genes. Three isolates, *n5348, n5354* and *n5356,* failed to complement *ngn-1(n1921)* (see Chapter II) and carry transition mutations in the *ngn-1* locus (Figure 2A), indicating that these mutations are alleles of *ngn-1*. Three allelic mutations, *n5333, n5339* and *n5340,* are alleles of *ceh-36* and are described in Chapter II. Another mutation, *n5357,* is an allele of *his-9* and is described in Chapter III. Two mutations, *n5335* and *n5338,* failed to complement each other and are alleles of *egl-27* (see below). Two mutations, *n5342* and *n5351,* cause or are linked to incompletely-penetrant larval lethality (data not shown) and fail to complement each other for the lethality as well as for the MI transformation defect. Both the lethality and the MI

transformation defect of *n5342* and *n5351* animals were maternally rescued (data not shown). The remaining mutation, *n5336,* causes a strict maternal-effect MI transformation: *n5336* homozygous animals derived from heterozygous mother did not show the MI transformation, whereas *n5336* heterozygous animals derived from a cross between *n5336* homozygous hermaphrodites and wild-type males displayed the MI transformation (data not shown).

n5335 and *n5338* Are Alleles of *egl-27,* a Member of the MTA family

We mapped *n5335* to a 2 m.u. interval of LG *II* that contains the gene *egl-27*. *egl-27* encodes a protein homologous to the mammalian Metastasis-Associated proteins or MTAs (Ch'ng and Kenyon 1999; Herman et al. 1999; Solari et al. 1999), which are components of the mammalian NuRD (Nucleosome Remodeling and Deacetylase) complex (Xue et al. 1998). Given the involvement of MTA proteins in chromatin regulation and of the histone-modifying enzymes SET-16 and UTX-1 in establishing the MI-e3D bilateral asymmetry, we tested whether *n5335* and *n5338* are alleles of *egl-27*. We identified mutations in the *egl-27* locus in each of these mutants (Figure 2B). We also examined other *egl-27* alleles independently isolated previously, including *egl-27(e2394)* (Figure 2B), and found that in all *egl-27* mutants examined, the MI neuron was transformed into an e3D-like cell (Table 3). Furthermore, *egl-27(e2394)* failed to complement *n5335* and *n5338* (data not shown). We concluded that *n5335* and *n5338* are alleles of *egl-27* and that *egl-27* is required to establish the MI-e3D bilateral asymmetry.

The mammalian NuRD complex comprises at least seven proteins, including MTA1, the histone deacetylases HDAC1 and HDAC2, the histone-binding proteins RbAp46 and RbAp48, the ATP-dependent chromatin remodeling enzyme Mi2 and a protein of unknown function p66 (Ahringer 2000). Because the *C. elegans* genome contains genes encoding proteins homologous to the members of the mammalian NuRD complex, including histone deacetylases HDA-1 and HDA-2, histone binding proteins RBA-1 and LIN-53, the Mi2 homologs LET-418 and CHD-3 and the p66 homolog DCP-66, we undertook a candidate-gene approach and tested whether the left-right asymmetric ABaraap cell lineage is disrupted in *C. elegans* mutants for these genes. We reported previously that *rba-1,* a *C. elegans* homolog of the mammalian RbAp46/48, is required for establishing the MI-e3D bilateral asymmetry, likely through interaction with two other components of the *C. elegans* CAF-1 complex (see Chapter III). We observed that mutants for the other genes did not display such a defect (data not shown). We also found that RNAi of *hda-1* or *lin-53* did not cause symmetry in this normally asymmetric cell lineage (data not shown). These results suggest that *egl-27* functions independently of the putative *C. elegans* NuRD complex to establish the MI-e3D bilateral asymmetry.

Discussion and Future Directions

The bilateral asymmetry of the nervous system is a widespread feature both in vertebrates and invertebrates. Despite its importance, the molecular mechanisms that establish neuronal bilateral asymmetry remain largely elusive. Although histone-modifying enzymes have been shown to promote neurogenesis, they have not been shown to act in establishing neuronal bilateral asymmetry. In this study, we demonstrate that the establishment of the left-right asymmetry of the ABaraap cell lineage requires two histone-modifying enzymes, the H3K4 HMT SET-16 and the H3K27 HDM UTX-1. Because the mammalian homologs of these proteins form a complex that activates expression of their target genes by methylating H3K4 and demethylating H3K27, we propose that SET-16 and UTX-1 also form a protein complex that modifies the methylation of H3K4 and H3K27 to promote expression of genes required to establish the bilateral asymmetry of the cell lineage. Our results indicate a novel mechanism of generating a bilateral asymmetry in the *C. elegans* nervous system and reveal that developmental mechanisms establishing the MI-e3D bilateral asymmetry involve histone modifications catalyzed by these enzymes.

What are the target genes of the putative SET-16/UTX-1 complex? Given that the establishment of the MI-e3D bilateral asymmetry requires a CEH-36/NGN-1/HLH-2 transcriptional cascade (see Chapter II) and nucleosome formation mediated by the *C. elegans* CAF-1 complex (see Chapter III), the SET-16/UTX-1 complex might act to impinge upon this transcriptional cascade or nucleosome formation. In the former case, *ceh-36, ngn-1* and *hlh-2* are candidates to be target genes of this SET-16/UTX-1

complex. In mammals, it has been shown that *otx2,* a *ceh-36* homolog, contains a bivalent domain in embryonic stem cells (ESC) and that this bivalent domain resolves to an active H3K4 monovalent domain in neural progenitor cells (NPC) and to a repressive H3K27 monovalent domain in embryonic fibroblasts (MEF) (Mikkelsen et al. 2007). By contrast, *E2A,* an *hlh-2* homolog, is associated with an H3K4 monovalent mark in ESCs, NPCs and MEFs, and *Neurog1* and *Neurog2, ngn-1* homologs, are associated with a bivalent mark in ESCs and NPCs. Thus, it seems plausible that *ceh-36* might be a target of the *C. elegans* SET-16/UTX-1 complex. Like *otx2, ceh-36* might contain a bivalent domain in a precursor cell shared by both the MI neuron and the e3D epithelial cell, such as the ABaraap cell (Figure 1A); upon separation of the left and right branches of the cell lineage, this bivalent domain might resolve to an H3K4 monovalent domain in the MI precursor cell, ABaraapp, and an H3K27 monovalent domain in the e3D precursor cell, ABaraapa, leading to the asymmetric *ceh-36* expression (see Chapter II) that establishes the MI-e3D bilateral asymmetry.

Our survey of *C. elegans* HMTs and HDMs did not identify a role of an H3K27 HMT or an H3K4 HDM. MES-2 and RBR-2 are the *C. elegans* homologs of the mammalian H3K27 HMT, EZH2, and the mammalian H3K4 HDM, RBP2, respectively. We observed that in *mes-2* mutants and *rbr-2(RNAi)* animals, both the MI neuron and the e3D epithelial cell were present (Table 1). If a target gene of the SET-16/UTX-1 complex were truly marked with the bivalent domain, and this bivalent domain were to resolve to a repressive monovalent H3K27 mark in the left branch of the cell lineage that normally gives rise to the e3D epithelial cell, then it would be expected that loss of *mes-2* and *rbr-2* functions would result in transformation of the e3D cell into an MI-like neuron. One

explanation for our observation might be that even though expression of a bivalently marked gene is derepressed in an e3D precursor cell of *mes-2* mutants and *rbr-2(RNAi)* animals, such ectopic expression of the target gene might not be sufficient to transform the e3D cell into an MI-like neuron. It remains to be determined whether ectopic expression of a target gene is sufficient to transform the e3D cell into an MI-like neuron and whether loss of *mes-2* and *rbr-2* function causes derepression of a target gene in the left branch of the cell lineage that normally gives rise to the e3D epithelial cell.

Alternatively, it is possible that a SET-16/UTX-1 complex regulates expression of genes other than *ceh-36, ngn-1* and *hlh-2*. We have shown that an altered-function mutation in a histone H3 gene *his-9* causes transformation of the MI neuron into an e3D-like cell and that this altered-function activity of *his-9* likely impairs the CAF-1-mediated nucleosome formation that might normally acts downstream of or in parallel to the asymmetric expression of CEH-36, NGN-1 and HLH-2. It is plausible that the CAF-1 complex and the SET-16/UTX-1 complex share targets required for establishing the bilateral asymmetry in this cell lineage. If so, the CAF-1 complex might first deposit histones H3-H4 onto its target locus, and the SET-16/UTX-1 complex might then modify histone H3 proteins at that locus. Further studies will be needed to test whether *set-16* and *utx-1* are required for the asymmetric expression of *ceh-36, ngn-1* and *hlh-2*.

The target genes of the CAF-1 complex remain to be determined. Identification of the CAF-1 targets will also help clarify whether the CAF-1 complex acts downstream of or in parallel to the CEH-36/NGN-1/HLH-2 transcriptional cascade: it is possible that the CAF-1 complex acts downstream of the NGN-1/HLH-2 heterodimer where the NGN-1/HLH-2 complex activates expression of its target genes in the MI mother cell and

that the CAF-1 complex mediates the nucleosome formation at these NGN-1/HLH-2 target loci during S-phase of the MI mother cell necessary to maintain expression of these genes in the post-mitotic MI neuron. Additional experiments are required to identify the targets of the CAF-1 complex. Different approaches might be taken to address this question, with success dependent on the number of targets biologically important for establishing the bilateral asymmetry. A biochemical approach might be able to identify multiple loci with altered distribution of nucleosomes in *his-9(n5357)* mutants or *rba-1(n5418Δ)* mutants. Alternatively, given the observation that the zygotic loss of *rba-1* function enhanced the MI transformation caused by the *his-9(n5357)* mutation (see Chapter III), an F_1 clonal enhancer screen to look for mutations that enhance the MI transformation defect caused by *his-9(n5357)* might be able to recover a single target of the CAF-1 complex required to establish the MI-e3D bilateral asymmetry.

Our findings indicate that *egl-27,* a *C. elegans* homolog of the mammalian MTAs, is required to establish the MI-e3D bilateral asymmetry. Although mammalian MTA proteins are known to be members of the NuRD complex, we observed that loss of function of genes encoding other members of the putative *C. elegans* NuRD complex did not cause symmetry in this normally left-right asymmetric cell lineage, suggesting a novel action of EGL-27 in establishing the MI-e3D bilateral asymmetry. We speculate that EGL-27 might interact with the putative SET-16/UTX-1 complex, the CAF-1 complex or an as yet unidentified complex to establish the MI-e3D bilateral asymmetry. Further studies will be needed to determine whether *egl-27* regulates expression of *ceh-36, ngn-1* or *hlh-2* and whether EGL-27 physically interacts with any of the proteins we have identified that are required to establish the MI-e3D bilateral asymmetry.

Identification of the two remaining genes mutated in *n5342* and *n5336* animals should help elucidate the mechanism that establishes the left-right asymmetry in this cell lineage and possibly other cell lineages.

Experimental Procedures

C. elegans Strains

C. elegans strains were cultured at 20 °C as described previously (Brenner 1974). N2 (Bristol) was the wild-type strain. The following mutations were used and have been described (Andersen and Horvitz 2007), except those from this study or otherwise indicated:

LG*I*: *blmp-1(tm548Δ), dcp-66(gk370Δ), dpy-5(e61)* (Riddle et al. 1997), *lin-53(n3368Δ)* (Lu Massachusetts Institute of Technology. PhD Thesis Dept. Biology. 1999), *lin-59(sa489)* (Chamberlin et al. 1999), *met-1(n4337Δ), set-18(gk334Δ).*

LG*II*: *dpy-10(e128)* (Riddle et al. 1997), *egl-27(e2394, n170)* (Herman et al. 1999), *egl-27(n5335, n5338, ok151Δ, ok1670Δ)* (this study, *ok151Δ* and *ok1670Δ* were provided by the *C. elegans* Gene Knockout Consortium), *F43G6.6(hc184Δ)* (this study, provided by the *C. elegans* Gene Knockout Consortium), *hda-2(ok1479Δ)* (Lans et al. 2010), *mes-2(bn11)* (Holdeman et al. 1998), *n5357* (this study), *rol-6(e187)* (Riddle et al. 1997), *set-4(n4600Δ), set-11(n4488Δ), set-13(n5012Δ), set-17(n5017Δ), set-24(n4909Δ), unc-4(e120)* (Riddle et al. 1997).

LG*III*: *met-2(n4256Δ), n5342, n5351* (this study), *set-1(tm1821Δ), set-2(n4589Δ), set-3(n4948Δ), set-16(n4526Δ), set-16(gk438Δ), set-25(n5021Δ), T26A5.5(ok2364Δ)* (this study, provided by the *C. elegans* Gene Knockout Consortium), *unc-32(e189)* (Riddle et al. 1997).

LG*IV*: *dpy-20(e1282)* (Riddle et al. 1997), *eri-1(mg366)* (Kennedy et al. 2004), *n5336* (this study), *psr-1(ok714Δ)* (Zullig et al. 2007), *set-9(n4949Δ), set-21(ok2320Δ), unc-5(e53)* (Riddle et al. 1997).

LG*V*: *dpy-11(e224)* (Riddle et al. 1997), *hda-1(ok1595Δ)* (Matus et al. 2010), *let-418(n3719)* (Ceol et al. 2006), *mes-4(bn73)* (Bender et al. 2006), *set-5(ok1568Δ) set-22(n5015Δ), set-31(ok1482Δ).*

LG*X*: *ceh-36(n5333, n5339, n5340)* (this study), *chd-3(ok1651Δ)* (this study, provided by the *C. elegans* Gene Knockout Consortium), *F18E9.5(gk384Δ)* (Agger et al. 2007), *nIs363[D2096.6::pes-10::gfp, lin-15AB(+)]* (see Chapter II), *lon-2(e678)* (Riddle et al. 1997), *set-6(tm1611Δ), set-8(tm2113Δ), set-12(n4442Δ), set-19(ok1813Δ), set-20(ok2022Δ), set-28(n4953Δ), set-30(gk315Δ), utx-1(tm3118Δ, tm3136Δ)* (this study, provided by Shohei Mitani, Tokyo Women's Medical University).

An F_3 non-clonal screen

We mutagenized wild-type animals carrying an e3D cell-fate reporter, *D2096.6::pes-10::gfp,* with ethyl methanesulfonate, and observed their F_3 progeny using a fluorescence-equipped dissecting microscope. From screens of approximately 100,000 F_3 mutagenized animals, we recovered 12 independent mutations that caused the presence of an extra e3D-like cell.

Mapping of *egl-27(n5335)*

We allowed hermaphrodites of genotype *dpy-10(e128) unc-4(e120)/n5335* to self-fertilize and observed that one of eight Dpy non-Unc progeny segregated *n5335* and that seven of eight non-Dpy Unc progeny segregated *n5335*.

Mapping of *n5336*

We allowed hermaphrodites of genotype *unc-5(e53) dpy-20(e1282)/n5336* to self-fertilize and observed that eight of nine Unc non-Dpy progeny segregated *n5336* and that one of nine non-Unc Dpy progeny segregated *n5336*.

Mapping of *n5342*

To map *n5342,* we followed the maternal embryonic lethality that is linked to *n5342*. We crossed *n5342* hermaphrodites with males of genotype *dpy-5(e61)/+; rol-6(e189)/+; unc-32(e189)/+* or *unc-5(e53)/+; dpy-11(e224)/+; lon-2/0* and observed that four of 20 *dpy-5*, seven of 20 *rol-6*, zero of 20 *unc-32*, four of 20 *unc-5*, four of 20 *dpy-11* and six of 20 *lon-2* F_2 progeny segregated the maternal lethal mutation.

Acknowledgments

We thank Shohei Mitani for *utx-1* mutants; Xiaowei Lu for isolating *lin-53(n3368Δ)* mutants; the *Caenorhabditis* Genetics Center, which is funded by the NIH National Center for Research Resources (NCRR), for strains; Na An, Rita Droste and Tove Ljungars for technical assistance; and Nicolas Paquin and David Harris for critical reading of this chapter. H.R.H is an Investigator of the Howard Hughes Medical Institute and the David H. Koch Professor of Biology at MIT.

References

Agger K, Cloos PA, Christensen J, Pasini D, Rose S, Rappsilber J, Issaeva I, Canaani E, Salcini AE, Helin K. 2007. UTX and JMJD3 are histone H3K27 demethylases involved in HOX gene regulation and development. *Nature* 449: 731-734.

Ahringer J. 2000. NuRD and SIN3 histone deacetylase complexes in development. *Trends Genet* 16: 351-356.

Andersen EC, Horvitz HR. 2007. Two *C. elegans* histone methyltransferases repress *lin-3* EGF transcription to inhibit vulval development. *Development* 134: 2991-2999.

Bender LB, Suh J, Carroll CR, Fong Y, Fingerman IM, Briggs SD, Cao R, Zhang Y, Reinke V, Strome S. 2006. MES-4: an autosome-associated histone methyltransferase that participates in silencing the X chromosomes in the *C. elegans* germ line. *Development* 133: 3907-3917.

Bernstein BE, Mikkelsen TS, Xie X, Kamal M, Huebert DJ, Cuff J, Fry B, Meissner A, Wernig M, Plath K et al. 2006. A bivalent chromatin structure marks key developmental genes in embryonic stem cells. *Cell* 125: 315-326.

Brenner S. 1974. The genetics of *Caenorhabditis elegans*. *Genetics* 77: 71-94.

Cao R, Wang L, Wang H, Xia L, Erdjument-Bromage H, Tempst P, Jones RS, Zhang Y. 2002. Role of histone H3 lysine 27 methylation in Polycomb-group silencing. *Science* 298: 1039-1043.

Ceol CJ, Stegmeier F, Harrison MM, Horvitz HR. 2006. Identification and classification of genes that act antagonistically to *let-60* Ras signaling in *Caenorhabditis elegans* vulval development. *Genetics* 173: 709-726.

Ch'ng Q, Kenyon C. 1999. *egl-27* generates anteroposterior patterns of cell fusion in *C. elegans* by regulating Hox gene expression and Hox protein function. *Development* 126: 3303-3312.

Chamberlin HM, Brown KB, Sternberg PW, Thomas JH. 1999. Characterization of seven genes affecting *Caenorhabditis elegans* hindgut development. *Genetics* 153: 731-742.

Christensen J, Agger K, Cloos PA, Pasini D, Rose S, Sennels L, Rappsilber J, Hansen KH, Salcini AE, Helin K. 2007. RBP2 belongs to a family of demethylases, specific for tri-and dimethylated lysine 4 on histone 3. *Cell* 128: 1063-1076.

Herman MA, Ch'ng Q, Hettenbach SM, Ratliff TM, Kenyon C, Herman RK. 1999. EGL-27 is similar to a metastasis-associated factor and controls cell polarity and cell migration in *C. elegans*. *Development* 126: 1055-1064.

Holdeman R, Nehrt S, Strome S. 1998. MES-2, a maternal protein essential for viability of the germline in *Caenorhabditis elegans*, is homologous to a *Drosophila* Polycomb group protein. *Development* 125: 2457-2467.

Kennedy S, Wang D, Ruvkun G. 2004. A conserved siRNA-degrading RNase negatively regulates RNA interference in *C. elegans*. *Nature* 427: 645-649.

Kouzarides T. 2007. Chromatin modifications and their function. *Cell* 128: 693-705.

Lan F, Bayliss PE, Rinn JL, Whetstine JR, Wang JK, Chen S, Iwase S, Alpatov R, Issaeva I, Canaani E et al. 2007. A histone H3 lysine 27 demethylase regulates animal posterior development. *Nature* 449: 689-694.

Lans H, Marteijn JA, Schumacher B, Hoeijmakers JH, Jansen G, Vermeulen W. 2010. Involvement of global genome repair, transcription coupled repair, and chromatin remodeling in UV DNA damage response changes during development. *PLoS Genet* 6: e1000941.

Lee MG, Villa R, Trojer P, Norman J, Yan KP, Reinberg D, Di Croce L, Shiekhattar R. 2007. Demethylation of H3K27 regulates polycomb recruitment and H2A ubiquitination. *Science* 318: 447-450.

Lu X, Massachusetts Institute of Technology. PhD Thesis. Dept. Biology. 1999. Molecular analyses of the class B synthetic multivulva genes of *Caenorhabditis elegans*. p. 170.

Matus DQ, Li XY, Durbin S, Agarwal D, Chi Q, Weiss SJ, Sherwood DR. 2010. In vivo identification of regulators of cell invasion across basement membranes. *Sci Signal* 3: ra35.

Mikkelsen TS, Ku M, Jaffe DB, Issac B, Lieberman E, Giannoukos G, Alvarez P, Brockman W, Kim TK, Koche RP et al. 2007. Genome-wide maps of chromatin state in pluripotent and lineage-committed cells. *Nature* 448: 553-560.

Milne TA, Briggs SD, Brock HW, Martin ME, Gibbs D, Allis CD, Hess JL. 2002. MLL targets SET domain methyltransferase activity to Hox gene promoters. *Mol Cell* 10: 1107-1117.

Muller J, Hart CM, Francis NJ, Vargas ML, Sengupta A, Wild B, Miller EL, O'Connor MB, Kingston RE, Simon JA. 2002. Histone methyltransferase activity of a *Drosophila* Polycomb group repressor complex. *Cell* 111: 197-208.

Nakamura T, Mori T, Tada S, Krajewski W, Rozovskaia T, Wassell R, Dubois G, Mazo A, Croce CM, Canaani E. 2002. ALL-1 is a histone methyltransferase that assembles a supercomplex of proteins involved in transcriptional regulation. *Mol Cell* 10: 1119-1128.

Pasini D, Hansen KH, Christensen J, Agger K, Cloos PA, Helin K. 2008. Coordinated regulation of transcriptional repression by the RBP2 H3K4 demethylase and Polycomb-Repressive Complex 2. *Genes Dev* 22: 1345-1355.

Riddle DL, Blumenthal T, Meyer BJ, Priess J. 1997. *C. elegans II*. Cold Spring Harbor Laboratory Press, Plainview, N.Y.

Sims RJ, 3rd, Nishioka K, Reinberg D. 2003. Histone lysine methylation: a signature for chromatin function. *Trends Genet* 19: 629-639.

Solari F, Bateman A, Ahringer J. 1999. The *Caenorhabditis elegans* genes *egl-27* and *egr-1* are similar to MTA1, a member of a chromatin regulatory complex, and are redundantly required for embryonic patterning. *Development* 126: 2483-2494.

Sulston JE, Schierenberg E, White JG, Thomson JN. 1983. The embryonic cell lineage of the nematode *Caenorhabditis elegans*. *Dev Biol* 100: 64-119.

Vastenhouw NL, Zhang Y, Woods IG, Imam F, Regev A, Liu XS, Rinn J, Schier AF. 2010. Chromatin signature of embryonic pluripotency is established during genome activation. *Nature* 464: 922-926.

Xue Y, Wong J, Moreno GT, Young MK, Cote J, Wang W. 1998. NURD, a novel complex with both ATP-dependent chromatin-remodeling and histone deacetylase activities. *Mol Cell* 2: 851-861.

Zullig S, Neukomm LJ, Jovanovic M, Charette SJ, Lyssenko NN, Halleck MS, Reutelingsperger CP, Schlegel RA, Hengartner MO. 2007. Aminophospholipid translocase TAT-1 promotes phosphatidylserine exposure during *C. elegans* apoptosis. *Curr Biol* 17: 994-999.

Table 1.

set-16 and *utx-1* are required to establish the MI-e3D left-right asymmetry

Genotype	(%) MI transformation[a]	*n*
wild-type	0	30
set-16(n4526Δ)[b]	8	100
set-16(gk438Δ)[b]	1	100
utx-1(tm3118Δ)[c]	20[e]	100
utx-1(tm3136Δ)[c]	18[e]	100

[a] The percentage of the MI transformation defect was determined using an e3D cell-fate reporter, *nIs363[D2096.6::pes-10::gfp]* (see Chapter II).

[b] We allowed animals of genotype *set-16/eT1[nIs267];nIs363* to self-fertilize and examined *myo-2::gfp*-negative progeny to determine the presence and absence of the MI neuron and the e3D epithelial cell.

[c] We allowed animals of genotype *dpy-6 utx-1 nIs363 unc-3/szT1* to self-fertilize and isolated Dpy Unc progeny. We then allowed these Dpy Unc animals to self-fertilize and examined their progeny to determine the presence and absence of the MI neuron and the e3D epithelial cell.

We observed that the MI neuron and the e3D epithelial cell were present in the following animals (n=30): *blmp-1(tm548Δ), lin-59(sa489), mes-2(bn11), mes-4(bn73), met-1(n4337Δ), met-2(n4256Δ), set-1(tm1821Δ), set-2(n4589Δ), set-3(n4948Δ), set-4(n4600Δ), set-5(ok1568Δ), set-6(tm1611Δ), set-8(tm2113Δ), set-9(n4949Δ), set-10(RNAi), set-11(n4488Δ), set-12(n4442Δ), set-13(n5012Δ), set-14(RNAi), set-15(RNAi), set-17(n5017Δ), set-18(gk334Δ), set-19(ok1813Δ), set-20(ok2022Δ), set-21(ok2320Δ), set-22(n5015Δ), set-23(RNAi), set-24(n4909Δ), set-25(n5021Δ), set-26(RNAi), set-27(RNAi), set-28(n4953Δ), set-29(RNAi), set-30(gk315Δ), set-31(ok1482Δ), C29F7.6(RNAi), F18E9.5(gk384Δ), F23D12.5(RNAi), F29B9.2(RNAi), F43G6.6(hc184Δ), jmjd-2(RNAi), psr-1(ok714Δ), rbr-2(RNAi), T07C4.11(RNAi),* and *T26A5.5(ok2364Δ).*

Table 2. Twelve mutations that cause the MI transformation are alleles of at least six genes.

Group	Gene	Allele	LG	Notes
1	*ngn-1*	*n5348* *n5354* *n5356*	N.D.	Show zygotic effects. Carry transition mutations in the *ngn-1* locus.
2	*ceh-36*	*n5333* *n5339* *n5340*	XR	Show zygotic effects. Carry mutations in the *ceh-36* locus.
3	*his-9*	*n5357*	IIR	Shows zygotic effect. Carries a transition mutation in the *his-9* locus
4	*egl-27*	*n5335* *n5338*	IIC	Show zygotic effects. Carries transition mutations in the *egl-27* locus.
5	N.D.	*n5342* *n5351*	IIIC	Both display incomplete penetrant embryonic lethality. Both the MI transformation and lethality are maternally rescued.
6	N.D.	*n5336*	IVR	Shows strict maternal effect.

Table 3. *egl-27* is required to establish the MI-e3D bilateral asymmetry.

Genotype	% MI transformation[a]	*n*
wild-type	0	50
egl-27(e2394)	29	100
egl-27(n170Δ)	7	100
egl-27(n5335)	24	100
egl-27(n5338)	29	100
egl-27(ok151Δ)	32	100
egl-27(ok1670Δ)	6	100

[a] The penetrance of the MI transformation was determined using an e3D cell-fate reporter, *D2096.6::pes-10::gfp* (see Chapter II).

Figures

Figure 1. *set-16* and *utx-1* Are Required to Establish the MI-e3D Bilateral Asymmetry. (A) The left-right asymmetric ABaraap cell lineage in wild type. The left-right asymmetry is seen in the different cell fates of the MI neuron and the e3D epithelial cell. (B) In *set-16* and *utx-1* mutants, left-right asymmetry in the cell lineage is lost as a result of the cell-fate transformation of the presumptive MI neuron into an e3D-like cell. (C) *D2096.6::pes-10::gfp* reporter expression in the wild type. The *D2096.6::pes-10::gfp* reporter was expressed in the e3D epithelial cell (arrowhead). (D, E) *D2096.6::pes-10::gfp* reporter expression in (D) *set-16(n4526Δ)* and (E) *utx-1(tm3118Δ)* mutants. The *D2096.6::pes-10::gfp* reporter was expressed in the e3D epithelial cell and the extra e3D-like epithelial cell (arrowheads). Scale bar, 5 μm. (F) Gene structure of *set-16* and mutations associated with each mutant are shown. (G) Gene structure of *utx-1* and mutations associated with each mutant are shown. The black boxes indicate exons, and white boxes untranslated regions.

Figure 1.

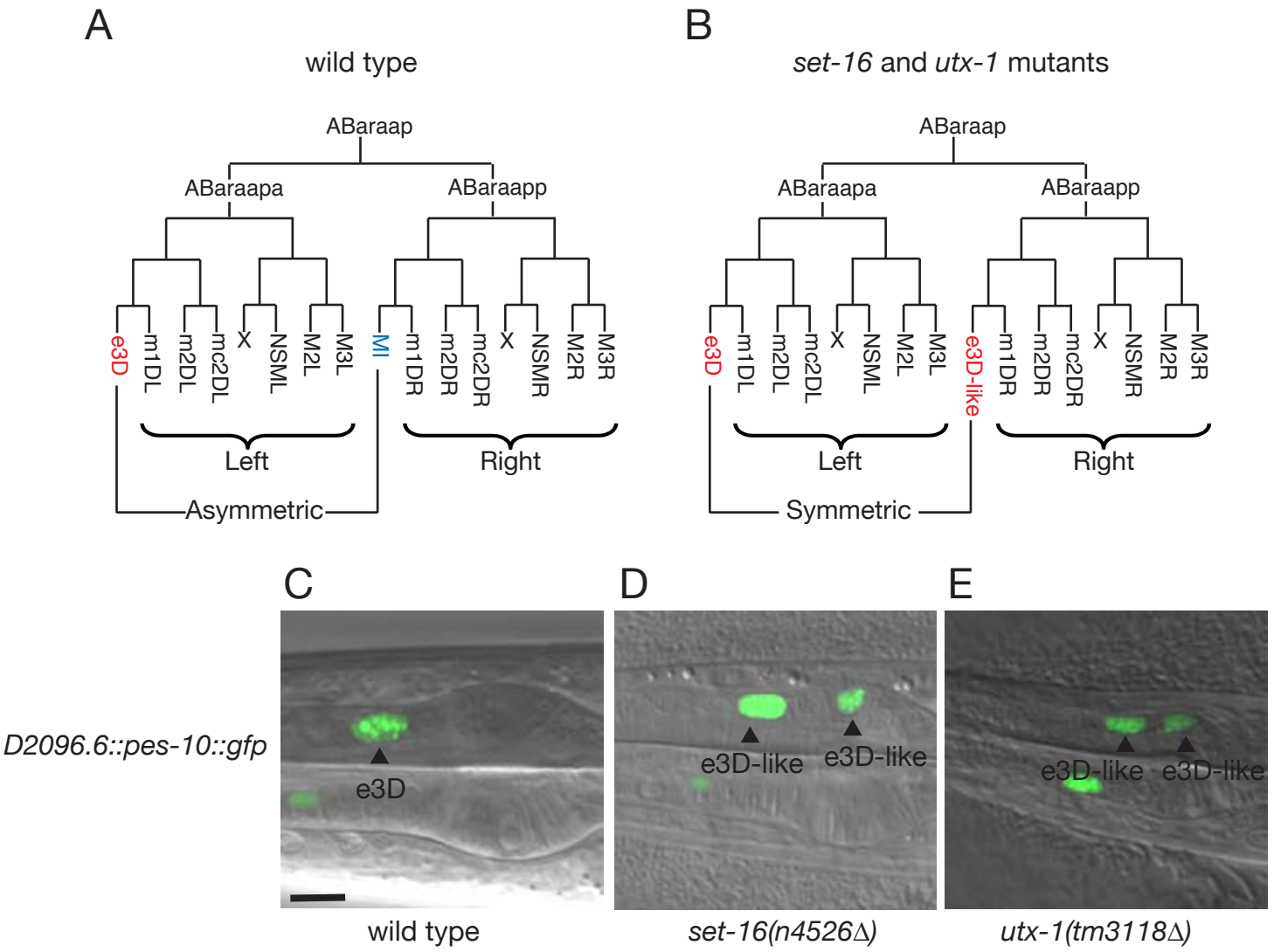
A
wild type
ABaraap
ABaraapa
ABaraapp
e3D
m1DL
m2DL
mc2DL
X
NSML
M2L
M3L
MI
m1DR
m2DR
mc2DR
X
NSMR
M2R
M3R
Left
Right
Asymmetric
B
set-16 and utx-1 mutants
ABaraap
ABaraapa
ABaraapp
e3D
m1DL
m2DL
mc2DL
X
NSML
M2L
M3L
e3D-like
m1DR
m2DR
mc2DR
X
NSMR
M2R
M3R
Left
Right
Symmetric
C
D
E
D2096.6::pes-10::gfp
e3D
e3D-like
e3D-like
e3D-like
e3D-like
wild type
set-16(n4526Δ)
utx-1(tm3118Δ)
F
1 kb
set-16
1
2475
gk438Δ
n4526Δ
G
1 kb
utx-1
1
1168
tm3136Δ
tm3118Δ

Figure 2. Mutations in *ngn-1* and *egl-27* Cause MI Transformation. (A) Gene structure of *ngn-1* and mutations associated with each mutant are shown. The black boxes indicate exons, and white boxes untranslated regions. (B) Gene structure of *egl-27* and mutations associated with each mutant are shown. The black boxes indicate exons.

Figure 2.

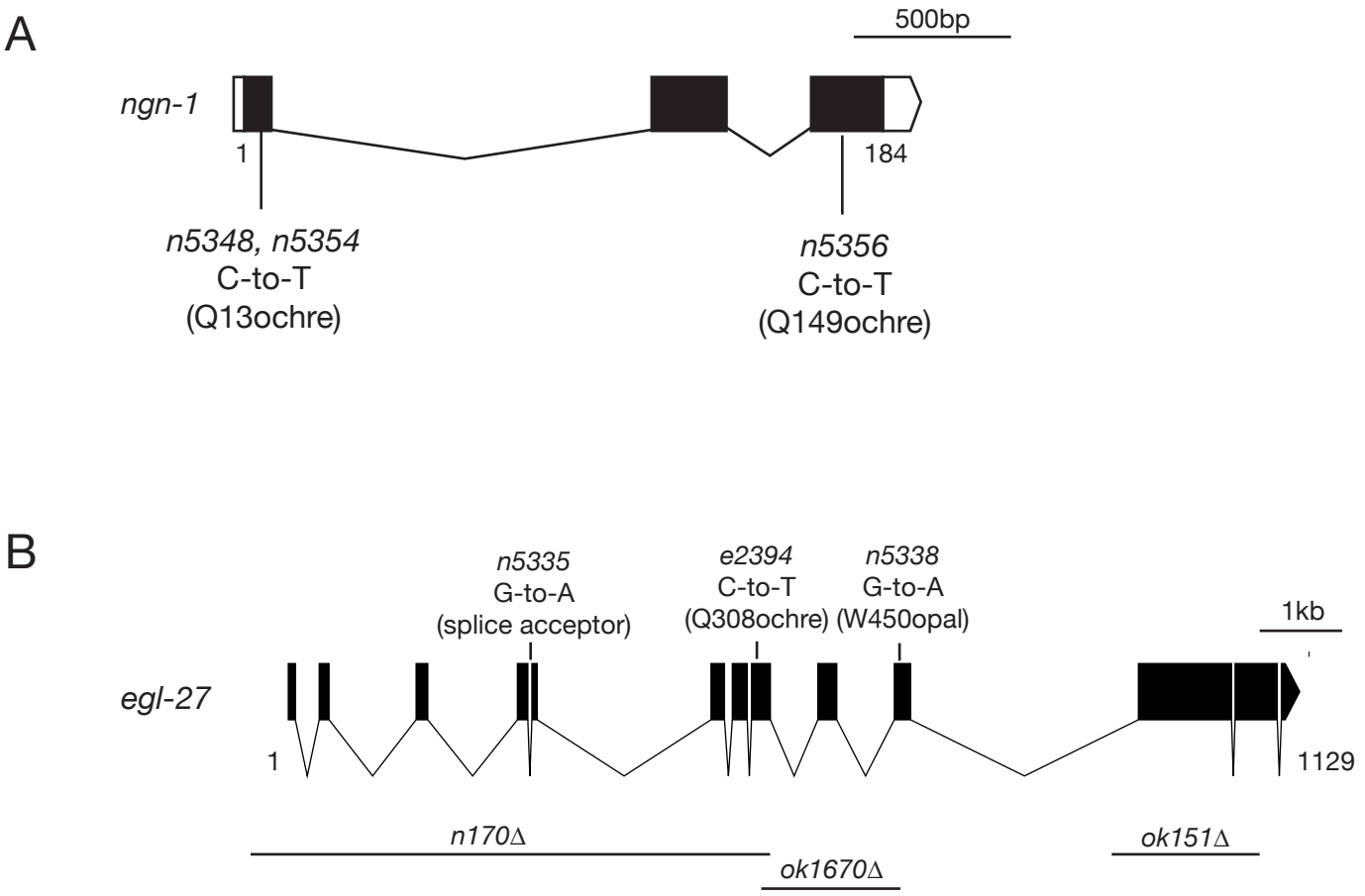
A
500bp
ngn-1
1
184
n5348, n5354
C-to-T
(Q13ochre)
n5356
C-to-T
(Q149ochre)
B
n5335
G-to-A
(splice acceptor)
e2394
C-to-T
(Q308ochre)
n5338
G-to-A
(W450opal)
1kb
egl-27
1
1129
n170Δ
ok1670Δ
ok151Δ